

# UNIVERSITÀ DEGLI STUDI DI TORINO



Dipartimento di Scienza e Tecnologia del Farmaco

*Corso di Laurea Magistrale in Chimica e Tecnologia Farmaceutiche*

## GPR21 inverse agonists: a binary approach from *in silico* to *in vitro* for the identification of new antidiabetic compounds

**Agonisti inversi del GPR21: un approccio binario *in silico* ed *in vitro* per l'identificazione di nuovi composti antidiabetici**

Relatrice:  
Dott.ssa Elisa Benetti

Candidato:  
Simone Girardi

Co-relatrice:  
Dott.ssa Gemma Kinsella

Anno Accademico 2020-2021

*To my family.*

# INDEX

<b>1. INTRODUCTION.....</b>	<b>1</b>
<b>1.1 Diabetes overview .....</b>	<b>1</b>
1.1.1 Type two diabetes aetiology .....	2
<b>1.2 Insulin signalling pathway .....</b>	<b>4</b>
1.2.1 Canonical insulin pathways .....	5
1.2.2 Principal players .....	6
1.2.3 Negative feedbacks and block signals .....	7
1.2.4 Current main diabetes treatments .....	8
<b>1.3 GPCRs overview .....</b>	<b>10</b>
1.3.1 GPCRs as targets for T2D treatment.....	13
<b>1.4 GPR21 overview .....</b>	<b>14</b>
<b>2. Study aim.....</b>	<b>22</b>
<b>3. Materials and methods .....</b>	<b>25</b>
<b>3.1 Compounds preparation .....</b>	<b>25</b>
<b>3.2 Cell cultures identification and definition.....</b>	<b>25</b>
3.2.1 Cell type description .....	25
3.2.2 Cells reconstitution .....	25
3.2.3 Cells transfer and count .....	26
<b>3.3 MTT testing .....</b>	<b>27</b>
3.3.1 Method's description.....	27
3.3.2 Test preparation .....	27
3.3.3 Test results and analysis .....	28
<b>3.4 Protein extraction and protein concentration determination.....</b>	<b>28</b>
3.4.1 Extraction .....	28
3.4.2 Concentration determination .....	29
<b>3.5 Western blot.....</b>	<b>29</b>
3.5.1 Rationale of the test.....	29
3.5.2 Polyacrylamide gel preparation .....	30
3.5.3 Sample preparation and loading.....	30
3.5.4 Electrophoretic run .....	31
3.5.5 Transfer (immunoblotting).....	31
3.5.6 Photographic development .....	32
3.5.7 Stripping.....	33
3.5.8 Ponceau S staining solution .....	34
<b>3.6 Ca<sup>2+</sup> release assay .....</b>	<b>34</b>
3.6.1 Rationale of the assay .....	34
3.6.2 Basal conditions assessment.....	34
3.6.3 Compounds activity evaluation .....	35
3.6.4 Maximum Ca <sup>2+</sup> release determination.....	36
3.6.5 Results analysis .....	36
<b>3.7 Insulin resistance states generation .....</b>	<b>37</b>
3.7.1 High glucose.....	37
3.7.2 High insulin .....	38
<b>3.8 Statistics .....</b>	<b>39</b>

<b>3.9 Solutions .....</b>	<b>39</b>
<b>4. Results .....</b>	<b>42</b>
<b>4.1 Homology modelling.....</b>	<b>42</b>
<b>4.2 Docking studies.....</b>	<b>48</b>
4.2.1 ADME analysis.....	48
4.2.2 Binding pocket .....	50
4.2.3 Interactions analysis .....	52
4.2.4 Analogues docking .....	55
4.2.5 Tautomers docking .....	58
4.2.5 Compounds screening .....	58
<b>4.3 In vitro testing .....</b>	<b>60</b>
<b>4.4 MTT testing on HepG2 cells treated with -160 and -399 .....</b>	<b>60</b>
<b>4.5 Ca<sup>2+</sup> release assay .....</b>	<b>62</b>
<b>4.6 Insulin resistance states generation: prolonged insulin exposure .....</b>	<b>65</b>
4.6.1 GPR21 expression in IR states.....	65
4.6.2 Insulin pathway activation in IR states.....	67
<b>4.7 Insulin pathway activation in IR states with 10 minutes insulin chase .....</b>	<b>68</b>
<b>5. DISCUSSION .....</b>	<b>72</b>
<b>5.1 Preliminary remarks.....</b>	<b>72</b>
<b>5.2 In silico studies.....</b>	<b>73</b>
<b>5.3 In vitro studies .....</b>	<b>75</b>
<b>5.4 Future studies.....</b>	<b>79</b>
<b>6. BIBLIOGRAPHY.....</b>	<b>81</b>



# 1. INTRODUCTION

## 1.1 Diabetes overview

Diabetes is a disease in which the insulin signalling pathway is impaired, the body is either not able to respond to the hormone insulin or not able to produce it anymore, resulting in abnormal metabolism of carbohydrates and high levels of glycaemia. In the following image (*fig. 1*) the glycaemia values are reported as diagnostic reference: glucose readings and the percentages of A1C test, also known as HbA1c test, able to measure the average blood sugar levels over the previous three months, are indicated for both healthy subjects and diabetic patients.

TIME	WITHOUT DIABETES	WITH DIABETES
Fasting	70–99 mg/dL	80–130 mg/dL
1–2 hours after meals	< 140 mg/dL	< 180 mg/dL
A1C test	< 5.7%	< 7%

Source: American Diabetes Association INSIDER

**Figure 1** Glycaemia values of reference in healthy subjects and diabetic patients (<https://www.insider.com/normal-blood-sugar-levels>)

According to the data reported by the International Diabetes Federation (IDF)<sup>1</sup>, in 2021 537 million adults (20 to 79 years old) and 1.2 million children and adolescents had diabetes and it was correlated to 6.7 million deaths due to diabetes complications, seventh leading cause of death in the US (*Sapra A. et al., 2021*)<sup>2</sup>. The complications related to diabetes are several, well described by *Cole J.B. et al. (2020)* in their review<sup>3</sup>, and can be divided between acute complications, requiring an immediate medical intervention, and chronic complications, further distinguished in microvascular and macrovascular complications. Among the most common acute complications are counted the ketoacidosis, caused by an incremented use of fats and ketone bodies as energy source by the cells resulting in unconsciousness and death if not treated, and the Hyperosmolar Hyperglycemic Nonketotic Syndrome (HHNS), increased urination due to high glycaemia that can lead to dehydration.

Major microvascular complications are diabetic kidney disease, diabetic retinopathy, diabetic neuropathy whereas the macrovascular ones include brain stroke, ischemic attacks, cognitive impairments, coronary heart disease and peripheral vascular disease due to narrowed blood vessels and slower healing of feet wounds contributing to gangrene and other complications. All the complications are related to the degree and the duration of poorly controlled diabetes but the most relevant are on the cardiovascular system; the diabetic condition is associated from a twofold to a tenfold increased risk of a cardiovascular event compared with individuals without diabetes: approximately two-thirds of the patients affected by diabetes mellitus will die from a myocardial infarction or stroke<sup>2</sup>.

Two main types of diabetes can be identified, main differences are that type 1 is an autoimmune disorder, with a genetic predisposition, that often shows up early in life because the immune system attacks and destroys pancreatic  $\beta$  cells whereas type 2 is largely diet-related and has a later onset. People over 45 years old, with family history of diabetes or overweight are more likely to develop the latter diabetes type.

### **1.1.1 Type two diabetes aetiology**

Type two diabetes (T2D) is a multifaceted disease (*Riddy D.M. et al., 2018*)<sup>4</sup> related to an insulin resistance state and involves many body districts:  $\alpha$  and  $\beta$  pancreatic cells, adipose tissue, skeletal muscles, liver, intestine, kidney and the central nervous system (CNS).

In healthy people there is a balance between glucagon and insulin actions, strictly regulating the glucose homeostasis. During fasting periods  $\alpha$ -pancreatic cells produce glucagon that increases glycogenolysis and gluconeogenesis until a food intake stimulates the release of insulin from  $\beta$  cells; insulin promotes glycogen synthesis, glucose uptake (mediated by the glucose transporters) and inhibits hepatic glucose production (HGP).

This homeostasis happens to be impaired in different insulin-resistance states and this imbalance can be the result of different genetical and environmental causes, in T2D obesity plays an important role in the outbreak of the disease.

Obesity triggers a low-grade chronic inflammation (*Osborn O. et al., 2012*)<sup>5</sup> that promotes macrophages and other immune cells infiltration into adipose tissue and liver.

<sup>4</sup>Under normal conditions adipocytes are surrounded by M<sub>2</sub> macrophages that have an anti-inflammatory action secreting anti-inflammatory mediators such as interleukin 4 (IL4) and interleukin 13 (IL13). The action of these macrophages contributes to maintain an insulin-sensitive environment.

Obesity, and so an increase in fat and free fatty acids (FFAs), leads to adipocyte hypertrophy, lipolysis and endoplasmic reticulum (ER) stress causing M<sub>1</sub> macrophages to infiltrate and M<sub>2</sub> to differentiate and polarize into M<sub>1</sub> proinflammatory macrophages associated to an uncontrolled expansion of adipose tissue. M<sub>1</sub> macrophages start to produce cytokines, as TNF $\alpha$ , that sustain the inflammatory process and reduce insulin-sensitivity.

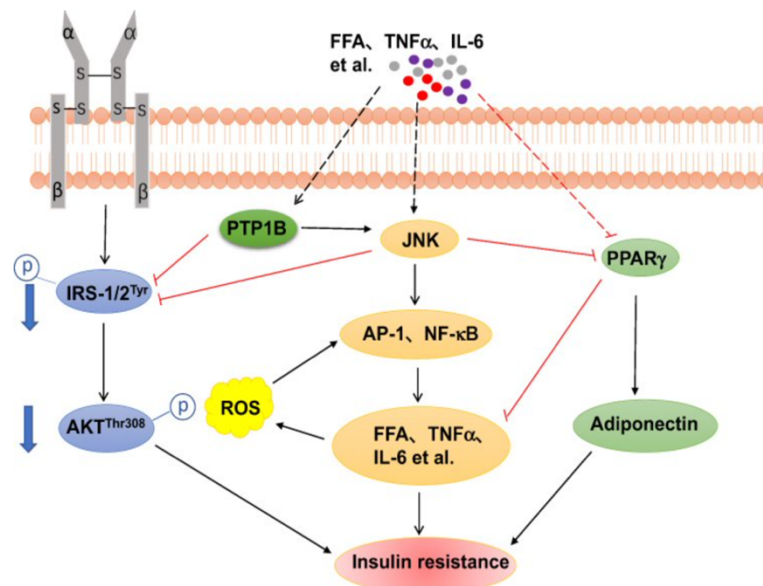


**Figure 2** Cytokines and free fatty acids molecular pathway associated to insulin resistance onset (Feng et al. "The Role of JNK Signaling Pathway in Obesity-Driven Insulin Resistance". *Diabetes Metab Syndr Obes.* 2020;13:1399-1406)

Activation of inflammatory pathways leads to a direct impairment of insulin action through the phosphorylation of insulin receptor substrate (IRS1) and so to negative feedback on the insulin pathway, in which IRS1 is actually the first step of the mediators cascade.

The increased secretion of FFAs and cytokines further contributes to the augmented hepatic glucose production and reduced glucose uptake by skeletal muscle.



The insulin pathway impairment, and the resulting reduced functionality of insulin-sensitive tissues, determines an increased insulin production and  $\beta$  cells proliferation. This adaptation mechanism can overcome the higher demand in first stages of the disease but over time  $\beta$  cells can not cope anymore resulting in  $\beta$  cells disfunction and exacerbated insulin resistance. Beta cells disfunction is further determined by the excess of FFAs and hyperglycaemia that cause ER stress trough the activation of the apoptotic unfolded protein response (UPR) pathways.

Obesity, T2D and hyperglycemia also lead to morphological modifications (Stuart CA et al., 2013)<sup>6</sup> in different glucose-sensitive tissues such as skeletal muscles (SKM). SKM consist in an association of different types of muscular fibers: slow-contracting oxidative fibers that preferentially utilize fatty acids as fuel and fast-contracting fibers that use more glucose. T2D patients are characterized by a slow-to-fast switch with a subsequent decrease in muscular resistance.

### 1.2 Insulin signalling pathway

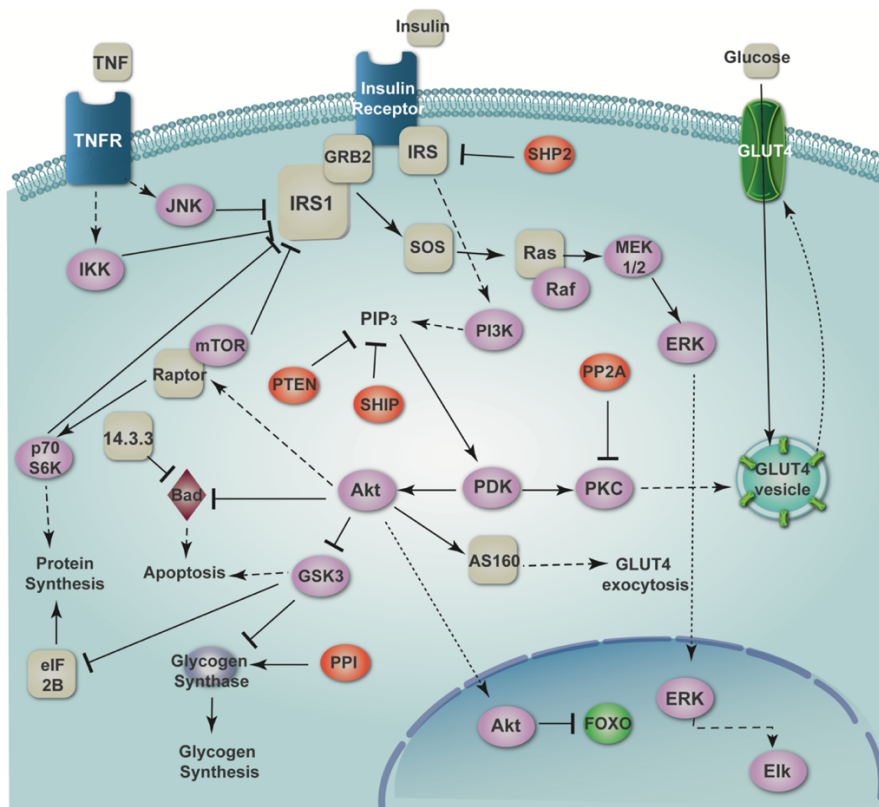


Figure 3 Insulin signalling pathway (<https://www.tocris.com/pathways/insulin-signaling-pathway>)

Insulin is an anabolic peptide (*De Metys P. et al., 2016*)<sup>7</sup> hormone secreted by pancreatic  $\beta$  cells, located in the inner part of Langerhans islets, with low basal levels that increase significantly as a result of different stimuli<sup>8</sup> such as glucose, mannose, amino acids (as leucine and arginine), hormones as GLP-1, high fatty acids concentrations and  $\beta$ -adrenergic activity.

Insulin acts in the target cells through a membrane receptor that belongs to the tyrosine kinase receptors superfamily and has orthologues in all metazoans. The insulin receptor presents an important crosstalk with insulin-like growth factors receptor (IGF<sub>1</sub>R), forming hybrids that modulate the selectivity and the affinity for insulin and insulin-like growth factors (IGFs) (*White F. et al., 2003*)<sup>9</sup>.

Two subtypes of IGFs can be identified (*Akhtar A. et al., 2020*)<sup>10</sup>, they are both structurally very similar to insulin and thus can bind insulin receptors (IRs) besides IGF receptors. IGFs and insulin, by activating IRs, play a direct role in cell differentiation, metabolic activities and growth regulation. The primary role of insulin is the systemic glucose homeostasis but to a further extent it is also involved in the dementia-like symptoms of Alzheimer disease, by competition of  $\beta$ -amyloid protein molecules with insulin for brain IRs and the subsequent deregulated glucose metabolism.

Insulin receptor belongs to tyrosine kinase superfamily receptor and exerts its functions by acting through insulin receptor substrates (IRSs) that are divided in six subtypes IRS1, IRS2, IRS3, IRS4, IRS5 and IRS6. All these substrates contain a phosphotyrosine binding-domain and IRS1 is the most important player in the insulin signalling mechanism.

### **1.2.1 Canonical insulin pathways**

After the insulin binds the outer portion of the receptor it undergoes a tri-phosphorylation of its activation loop, in particular on tyrosine residues situated on the carboxy-terminal region. Insulin receptor phosphorylates IRS1 on tyrosine residues which will be now bound by Growth Factor Receptor Bound Protein 2's (Grb2) src-homology 2 (SH2) domain. Son of sevenless (Sos) factor now binds Grb2 and then a Ras protein, promoting the release of guanosine diphosphate (GDP) from Ras and the guanosine triphosphate (GTP) bond. Ras activates Raf-1

which phosphorylates the mitogen-activated protein kinase kinase (MEK) on two serine residues and MEK activates the extracellular-signal-regulated kinase (ERK) by phosphorylating a threonine and a tyrosine residues. ERK (member of the MAPKs, mitogen-activated protein kinases) moves to the nucleus and activates different nuclear transcription factors, such as ETS Like-1 protein (Elk1).

IRS1 phosphorylation also leads to phosphatidylinositol-3 kinase (PI3K) activation (as Grb2 this mediator presents a SH2 domain); this enzyme that converts phosphatidylinositol 4,5-bisphosphate (PIP2) in phosphatidylinositol 3,4,5-trisphosphate (PIP3). PIP3 binds a protein kinase B (PKB, also referred to as Akt), phosphorylated by 3-Phosphoinositide-dependent kinase 1 (PDK1). Once activated PKB promotes the inactivation of glycogen synthase kinase-3 (GSK3) that usually inactivates the glycogen synthase (GS), so the glycogen synthesis from glucose is accelerated. PKB also promotes the translocation of the glucose transporter GLUT4 from cytoplasmatic vesicles to the membrane, increasing the glucose uptake.

### 1.2.2 Principal players

Grb2: an adapter protein, critical in linking cell surface growth factor receptors and the Ras signalling pathway. This protein contains one src homology 2 (SH2) domain and two SH3 domains, the SH2 domain allows the linkage with tyrosine phosphorylated IRS1 while the SH3 domains are involved in the interaction of this protein with Sos.

Sos: a guanine nucleotide exchanging factor for Ras, it determines the Ras switch from inactive to active form initiating the MAPK pathway activation.

MAPK: a class of mitogen-activated protein kinases that includes ERK1 and ERK2 that are involved in cell proliferation and differentiation. The linking of these proteins with transcription factors such as the cAMP response element binding protein (CREB) or Elk1 determines an increase in specific genes transcription.

PI3K: a serine/threonine protein kinase involved in several cellular processes including protein synthesis, proliferation, migration and survival and alterations in its enzymatic activity have associated to the onset of different pathologies from chronic inflammation to cancer. Its activity in the described insulin pattern is critical for PKB activation mediated by PIP3.

PKB/Akt: a serine/threonine protein kinase presenting three subtypes and regulating a large number of cellular activities including growth, proliferation, motility, adhesion and death. This protein also exerts regulatory functions on proapoptotic factors such as Bcl2 and BAD, targeting the transcription factors of apoptotic agents resulting in being classified as a potential oncogene.

GSK-3: a serine/threonine protein kinase presenting two subtypes, GSK-3 $\beta$  is more important in several signaling pathways than the alpha isoform, including the insulin's one. Both the isoforms undergo a phosphorylation on the N-terminal regulatory site performed by Akt and leading to the inactivation of this enzyme that, otherwise, would inhibit the GS.

AS160: a protein that connects the activation of the Akt pathway with the increment of GLUT4 glucose transporters at the cell surface observed in fat and muscle cells after insulin treatment. *Mîinea C.P. et al.*<sup>11</sup> described this protein having a functional Rab GTPase-activating protein (GAP) domain and its GAP activity is blocked when phosphorylated by Akt leading to an increase of the GTP form of Rab(s) needed for GLUT-4 translocation.

GLUT: <sup>8</sup>five different isoforms of GLUT can be identified with specific tissue distributions in humans: GLUT-1 has a wide distribution in all tissues, especially in erythrocytes and brain; GLUT-2 is important in  $\beta$ -pancreatic cells, liver, kidneys and intestine; GLUT-3 in brain, placenta and kidneys; GLUT-4 in muscles and adipose tissue; GLUT-5 in intestine and kidneys.

### 1.2.3 Negative feedbacks and block signals

The *figure 3* also shows different possible pathways operating a signal block, especially by a direct impairment of IRS1.

TNF: tumor necrosis factor, the first factor acting as an inhibitor of the insulin pathway in the *figure 3* and, to a further extent, representing the influence of various inflammation states on the insulin pathway. TNF is both a cytokine, so used by the immune system for cell signalling purposes, and an adipokine, thus a cytokine secreted by the adipose tissue. In particular the alpha subtype of the TNF receptor is well known for its role in lipid metabolism in acute inflammation states and identified as a causative factor in obesity associated insulin resistance and type 2 diabetes (T2D) onset (*Moller D.E. et al., 2000*)<sup>12</sup>. In the image (*fig. 3*) it is possible

to see its action through a membrane receptor recruiting JNK (Jun N-terminal Kinase) and IKK (I $\kappa$ B kinase), enzymes that inactivate IRS1.

mTOR: mammalian target of rapamycin, is a protein kinase and a nutrient sensor (*Leibowitz G. et al., 2008*)<sup>13</sup> involved in several cellular processes such as growth, proliferation, metabolism and apoptosis. In the insulin pathway mTOR explicates a negative feedback, following Akt activation, on IRS1 action. mTOR can be found in two different complexes and in particular in the insulin pathway the mTOR complex 1, associated with raptor (regulatory associated protein of mTOR), acting through ribosomal protein S6 kinase beta-1 (S6K1) inhibits IRS1 activity.

SHP2: Src homology-2 domain containing protein tyrosine phosphatase-2, is a protein phosphatase controlling biological activities and involved in pathways related to several growth factors and cytokines (*Qu C.K. et al., 2000*)<sup>14</sup>. The sh2 domain allows this enzyme to bind IRS, once that is phosphorylated, dephosphorylating this substrate exerting in a diminished local signalling flow.

This whole signalling pathway results in an increased glucose uptake and a suppressed glucose production; it can be impaired on different levels and so there are different possible therapeutic targets.

#### **1.2.4 Current main diabetes treatments**

At the moment the only treatment for type 1 diabetes (T1D) is the administration of exogenous insulin, available in different releasing rates according to its formulation, an interruption in this replacement therapy may be putting the patient in a life-threatening danger causing diabetic ketoacidosis (DKA). DKA is due to an excessive release of fatty acids (FAs) and the subsequent formation of ketoacids at toxic levels.

The main available types of insulin formulations are distinct from one another in four categories<sup>8</sup> according to their pharmacokinetics: rapid acting insulin, short acting insulin, intermediate acting insulin and long acting insulin.

*Rapid acting insulin*: insulin formulations that allow a very rapid and short-lasting glycaemic control. Lispro and aspart insulins are the main members of this class, obtained with recombinant DNA techniques they do not self-aggregate resulting immediately available.

*Short acting insulin*: the effect starts after 30 minutes following the administration and lasts 5 to 8 hours. It is the regular type and, obtained with recombinant DNA techniques, it is identical to the human insulin, zinc-crystalline and soluble.

*Intermediate acting insulin*: formulations resulting in retarded uptake and action, onset after 2 to 5 hours and lasting for 4 to 12 hours. The main exponent of this class is the isophane or neutral protamine Hagedorn (NPH) insulin, the association of the insulin with protamine allows the effect to start after the action of proteolytic enzymes.

*Long acting insulin*: formulations resulting in retarded uptake and action, effect starting after 1 to 2 hours and duration of about 24 hours. Examples of insulin formulations belonging to this class are glargine insulin, precipitating at physiological pH, and detemir insulin, whose long life is due to an augmented autoaggregation and the reversible binding with the albumin. Belonging to this class there also is an ultra-long acting insulin in which the alteration on the aminoacidic sequence allows the formation and accumulation of stable and soluble multi-hexamers in the subcutaneous tissue: dulgludec insulin.

Type two diabetes (T2D) presents instead several treatment possibilities because of its more complex aetiology. Currently most used treatments in therapy are the following:

*Biguanides*: metformin is the only compound belonging to this class and represents the first-line treatment in T2D. This class presents a not yet fully assessed mechanism of action, it reduces the endogenous glucose production and increase body sensitivity to insulin probably acting through both AMP-activated protein kinase (AMPK)-dependent and AMPK-independent mechanisms. Metformin is used in several associations with other antidiabetic drugs.

*Sulfonylureas*: a class of compounds that induce insulin release from  $\beta$  pancreatic cells by closing ATP-dependent  $K^+$  ( $K_{ATP}$ ) channels, miming glucose intake. Exponents of this class are glimepiride, glipizide and glyburide.

Meglitinides: similarly to sulfonylureas they bind the  $K_{ATP}$  channels inducing insulin release. Most common compounds belonging to this class are nateglinide and repaglinide.

Thiazolidinediones: they decrease the insulin resistance regulating gene expression by acting through peroxisome proliferator-activated receptors gamma (PPARs- $\gamma$ ). Commonly used drug belonging to this class is pioglitazone.

Glucagon-like peptide-1 receptor agonists (GLP-1 receptor agonists): exenatide, dulaglutide and liraglutide are compounds that acts miming the natural hormone incretin increasing  $\beta$  pancreatic cells growth, slowing stomach emptying, increasing insulin glucose-mediated production and reducing appetite.

Dipeptidyl peptidase-4 (DPP-4) inhibitors: they inhibit the enzyme that degrades GLP-1, increasing the activity of this hormone. Examples are sitagliptin, alogliptin and linagliptin.

Sodium-glucose cotransporter-2 (SGLT2) inhibitors: canagliflozin, dapagliflozin, and empagliflozin are marketed drugs belonging to this class; they lead to a reduced resorption and higher renal clearance of sugar.

Alpha glucosidase inhibitors: inhibiting this class of intestinal enzymes they lower the uptake of monosaccharides. Examples are acarbose and miglitol.

Unfortunately, despite these different therapeutical options almost half of the patients do not achieve treatment goals leading to a still intensive research activity.

### 1.3 GPCRs overview

G-protein coupled receptors (GPCRs) are membrane receptors that, combining with an extracellular signal, are able to transduce the signal across the membrane (*Gardner J. et al., 2012*)<sup>15</sup>. These receptors can detect different kinds of extracellular signal such as light energy, lipids, peptides, sugars and proteins.

GPCRs represent the largest family of proteins encoded by the human genome (*Yang D. et al., 2021*)<sup>16</sup> and are known to be related to a substantial number of diseases such as type 2 diabetes mellitus (T2DM), obesity, depression, cancer, Alzheimer's disease, and many others. Considering the total of 826 GPCRs present in the human species over 40% are considered as druggable and 165 are now confirmed drug targets. The increasing comprehension of their

structure and activity is leading a switch in their study from a random ligand screening to a knowledge-driven drug design, making this protein class even more important in the pharmacological research and development field.

GPCRs consist of a single polypeptide chain folded in seven transmembrane domains forming loops both inside and outside the cell. The extracellular loops contribute to form the pockets where the external signal binds to the GPCR.

G-proteins associated to GPCRs are heterotrimeric, having three different subunits: alpha subunit, beta subunit and gamma subunit.

<sup>17</sup>Once that the receptor is activated by the ligand it undergoes a conformational change that can lead to the exchange of guanosine diphosphate (GDP) for guanosine triphosphate (GTP) on the alpha subunit of the heterotrimeric complex or the activation of beta-arrestins pathway.

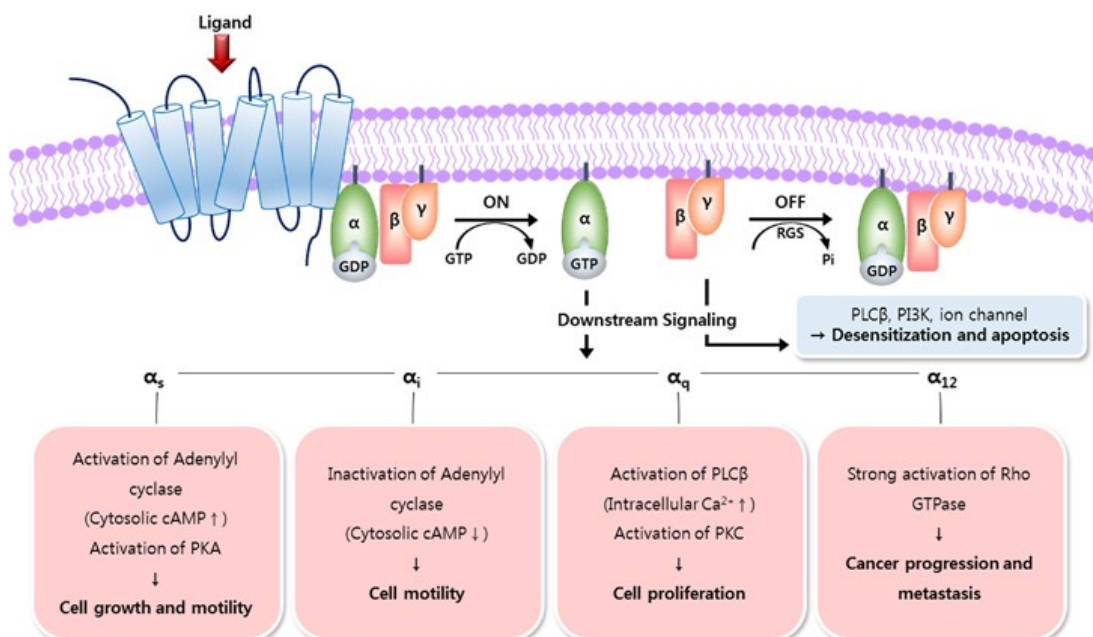


**Figure 4** GPCRs associated G-proteins subunits and the different pathways activated by the alpha-subunits (Jo, M. Jung, S. Engineering therapeutic antibodies targeting G-protein-coupled receptors. *Exp Mol Med* 48, e207, 2016)

Following the activation of a GPCR the alpha subunit separates from the other subunits, both parts are still anchored to the plasma membrane, but no longer bound to the GPCR and can diffuse laterally in order to interact with other membrane proteins.



Once the signal stops and the GTP is hydrolysed back to GDP the different subunits go back in place forming again the heterotrimeric complex and coupling with the GPCR, now inactive. In this way extracellular signals can switch on and off the G-protein signalling pathway.

Human GPCRs family can be subdivided into different classes (*Hoque M. et al., 2018*)<sup>18</sup> according to their aminoacidic sequences: A (rhodopsin), B (secretin and adhesion), C (glutamate) and F (frizzled).

Another division can be made according to the functional properties of the alpha-subunit (*Barella L.F. et al., 2021*)<sup>19</sup> identifying four major families of G-proteins.

The activation of G $\alpha$ -s stimulates adenylate cyclase leading to an increase of cyclic adenosine monophosphate (cAMP) levels, whereas adenylate cyclase activity is inhibited by the stimulation of G $\alpha$ -i/ G $\alpha$ -0, which is also responsible of regulating the activity of several ion channels. G $\alpha$ -q activation determines an increase in intracellular calcium levels due to the activation of phospholipase-C $\beta$  that acts on the membrane phosphatidylinositol 4,5-biphosphate releasing inositol 1,4,5-trisphosphate (IP3) together with diacylglycerol (DAG). G $\alpha$ -12/13 protein stimulation promotes the activity of different types of Rho and MAP kinases.

Analysing the superfamily of GPCRs it is necessary to briefly describe a class of small proteins having different roles related to GPCRs signal transduction: beta-arrestins.

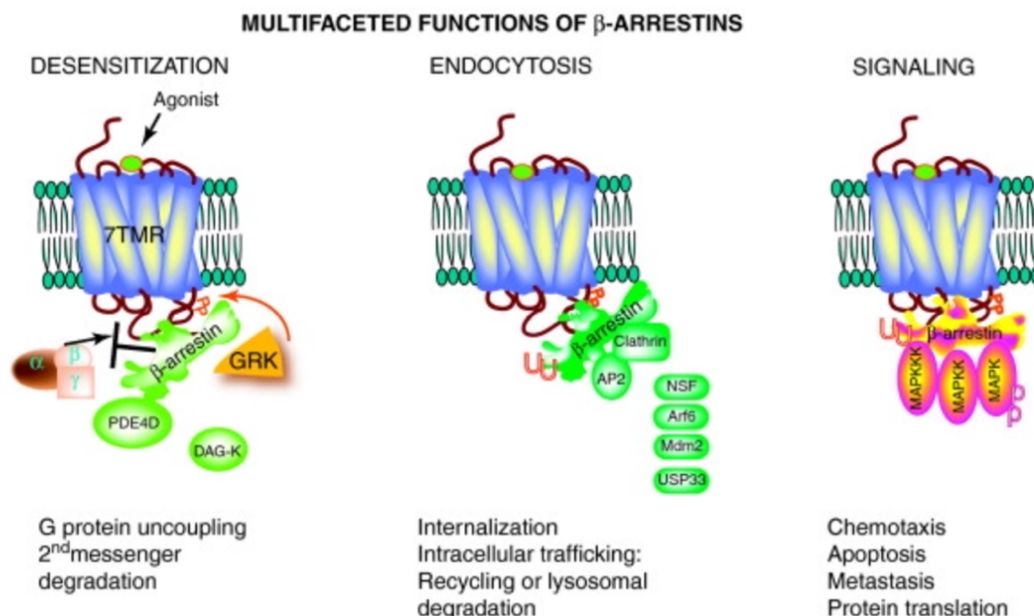


*Figure 5 Multifaceted functions of beta-arrestins: desensitization, endocytosis and signalling (S.K.Shenoy et al., REVIEW/ VOLUME 32, ISSUE 9, P521-533, SEPTEMBER 01, 2011 "beta-arrestin-mediated receptor trafficking and signal transduction", Published: June 15, 2011)*

Beta-arrestins have different roles in regulating GPCRs functionality and signalling pathway (*Jean-Charles PY et al., 2017*)<sup>20</sup>. For long time after their discovery beta-arrestins were considered just as inhibitors of GPCR signalling due to their ability to deactivate and desensitize these kinds of receptors by promoting the uncoupling with the G-proteins and causing the degradation of secondary messengers.

Beta-arrestins are also critical adaptors for agonist-induced ubiquitination and endocytosis of GPCRs, governing the trafficking itinerary of internalized GPCRs. Beta-arrestins play an important role in GPCRs activity also as scaffolds for mitogen activated protein kinases (MAPKs) and they are able to promote these pathways even when the G protein is not activated.

From here emerges the bimodal nature of GPCRs signalling and the possibility to activate these receptors to favour either G proteins or beta-arrestins pathway.

### **1.3.1 GPCRs as targets for T2D treatment**

Given the large number of GPCRs expressed in both islets of Langerhans and enteroendocrine cells (EECs) (*Ghislain J. et al., 2021*)<sup>21</sup>, that control insulin secretion, they are an interesting target for developing new antidiabetic drugs.

<sup>4</sup>Among the many different types of GPCRs expressed in human islets, or more in general possible GPCRs targets for T2D treatment, the best characterized is the glucagon-like peptide 1 (GLP1) receptor, the only one actually used in therapy at the moment. GLP1 is a member of incretins system, the activation of its receptor leads to an increase of cAMP in beta cells and therefore an increase in insulin secretion and  $\beta$ -cells proliferation. Examples of drugs targeting GLP1 receptor are exenatide and liraglutide. A long-term treatment with these drugs can also promote satiety and weight loss by inhibiting gastric emptying.

Another important class of GPCRs expressed in islets are free fatty acids (FFAs) receptors. FFA1r or GPR40 activation leads to the activation, via  $G\alpha$ -q protein, of the phospholipase C and a consequent increase in calcium concentration that finally leads to insulin secretion and

hormonal release of GLP1. This G $\alpha$ -q signalling pathway, with a positive role in maintaining the glucose homeostasis, is very different in hepatic cells where G $\alpha$ -q pathways are correlated with an impaired glucose tolerance (Li J.H. et al., 2013)<sup>22</sup>.

Another FFA receptor that may be an interesting target for new antidiabetic drugs is FFA4 or GPR120 whose activation in obese mice can improve glucose tolerance and insulin sensitivity. Improvements in insulin resistance states mediated by FFA4 are probably also attributable to a reduction in somatostatin secretion.

Adrenoceptors GPCRs have an important role in glucose homeostasis, in particular  $\alpha$ 1 adrenoceptors, by acting through a G $\alpha$ -q protein, promote an insulin-independent glucose uptake in SKMs and adipose tissue.

#### 1.4 GPR21 overview

In screening GPCRs as potential targets for T2D treatment, a specific receptor has appeared as an important player in the outbreak of the insulin resistance state that characterize this disease: GPR21<sup>5</sup>.

GPR21 is an orphan receptor belonging to the A family of GPCRs (rhodopsin-like receptors), its endogenous ligand has not yet been identified and its structure not yet been crystalized. A model of the receptor is available but, being just a prediction automatically produced by AlphaFold, further modelling studies are required in order to better define its tridimensional structure.

<sup>15</sup>GPR21 encoding gene is located on chromosome 9, region q33 in humans and on chromosome 2 in the mouse. GPR21 has a high aminoacidic sequence homology with GPR52 (71%), another orphan GPCR, and it has been identified along with GPR20 to GPR23.

A comparison of the receptor encoded by GPR21 and other GPCRs was performed by *O'Dowd B.F. et al. (1997)*<sup>23</sup> finding relevant similarities with  $\beta$ 1-adrenergic receptor (33% of TM region similarities), adenosine A3 receptor and histamine H2 receptor, both with 32% of analogies in the TM region. A similar analysis, on phylogenetic basis, is described by *Kakarala K.K. et al. (2014)*<sup>24</sup> placing GPR21 in a receptors cluster with Q6NWM5 HUMAN, Q8BX79 MOUSE, GPR52

HUMAN. In particular Q6NWM5 HUMAN, Q8BX79 MOUSE are closer in structure and function to GPR21 whereas GPR52 has a more distant relationship with GPR21, but yet related to obesity, inflammation and glucose metabolism.

Several hypotheses have been formulated about GPR21's possible ligands, by most accounts it has been suggested being a member of FFAs family and it could be found within the serum. The endogenous presence of a GPR21 ligand in the serum is supported by a reduced Akt phosphorylation in serum-starved GPR21-overexpressing cells when compared with similar cells in presence of serum and after stimulation of this pathway administrating exogenous insulin<sup>4</sup>.

It also has been hypothesized that GPR21's ligand could be of a peptide nature, in fact GPR21 contains a lysine residue in an analogous position as the endothelin receptor, crucial residue in binding its peptide agonist.

GPR21 has been suggested to couple with a  $G\alpha$ -q protein by *Bresnick et al. (2003)*<sup>25</sup> and afterwards confirmed by the work of *Xiao et al. (2008)*<sup>26</sup> that were able to identify the subtype of Gq protein that more activated the PLC pathway when interacting with GPR21:  $G\alpha$ 15/16.

GPCR	Fold Stimulation Over Vector Control*, #							
	No G Protein	Gqi5	Gqi9	Gqo5	Gqo3	$\alpha$ 16	$\alpha$ 15	Gmyri5
GPR21	1.2	1.9	1.5	1.7	1.6	2.5	2.7	1.2

**Figure 6** GPR21 signalling pathway activation when coupled with different types of alpha subunits (*Xiao et al., High throughput screening for orphan and liganded GPCRs. Comb Chem High Throughput Screen. 2008 Mar;11(3):195-215*)

*Leonard S. et al. (2016)*<sup>27</sup> further analysed the GPR21 signalling pathway reporting constitutive activity of this receptor that showed an increase in endogenous inositol phosphate (IP1) in the absence of a ligand, in HEK293T cells overexpressing this receptor, increment that became more evident when the receptor was coupled with  $G\alpha$ 15/16.

For what concerns GPR21 constitutive activity it has been confirmed by different studies such as *Adam L. Martin et al. (2015)*<sup>28</sup> GPR21, together with its closely related GPR52, showed a constitutive stimulation of baseline cAMP dependent signalling, stimulation that was not affected by the presence of forskolin. They also have related this response with the one that characterizes a mutant M3 human muscarinic acetylcholine receptor.

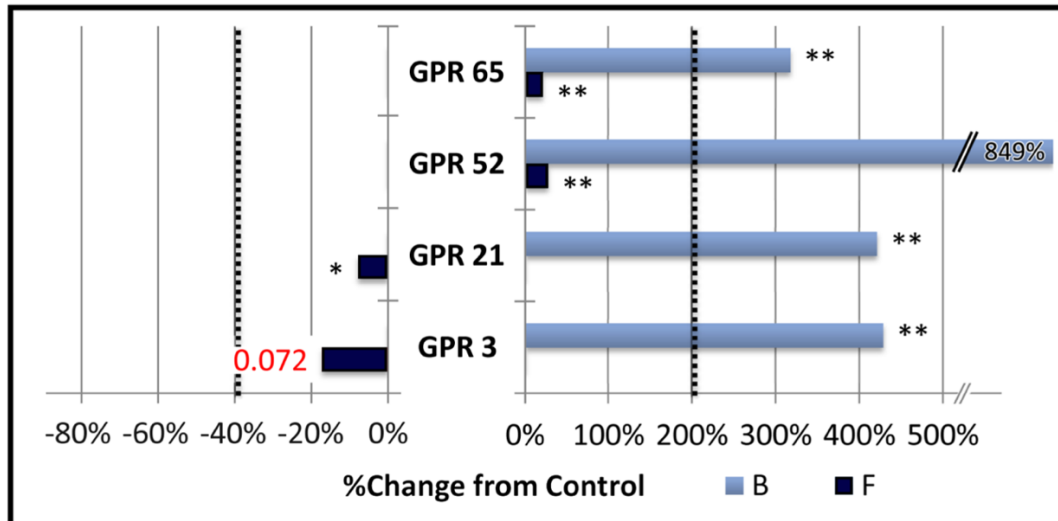


**Figure 7** GPCRs comparison for constitutive activity assessment vs control (Martin AL et al., Constitutive Activity among Orphan Class-A G Protein Coupled Receptors. PLoS One. 2015 Sep 18)

Despite this study would seem to indicate a differ pathway correlated to GPR21’s activity a possible correlation between a  $G\alpha$ -q activation and cAMP release (usually generated following a  $G\alpha$ -s activation) could be supposed basing on the work of White A.D. et al. (2020)<sup>29</sup> that shows a beta-arrestins mediated endosomal cAMP production following the activation of a Gq pathway.

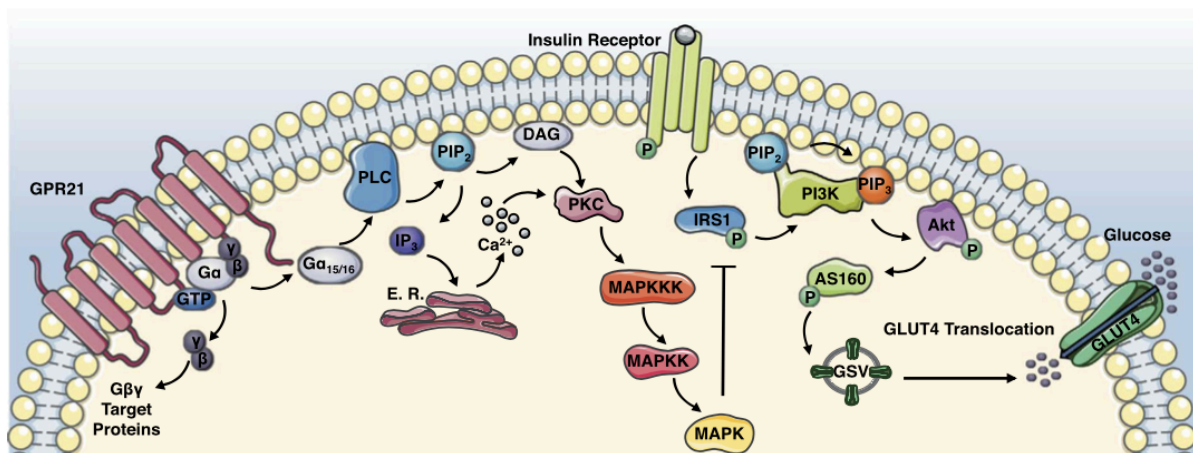


**Figure 8** GPR21 signalling pathway: PLC activation, calcium release and IRS1 inactivation (Leonard S., et al. Regulating the effects of GPR21, a novel target for type 2 diabetes. Scientific Reports. 2016, 6: 27002. PubMed ID: 27243589)

As previously said,  $G\alpha$ -q protein activation leads to PLC activation and so to IP3 (of which IP1 represents the most stable metabolite) and DAG liberation, calcium release and the subsequent activation of MAPK cascade that includes Erk, p38 and JNK.

JNK plays a central role in insulin resistance onset because of the phosphorylation of IRS1 at a serine residue. This phosphorylation operated by JNK prevents the insulin-induced phosphorylation of a tyrosine residue that would lead to the activation of insulin signalling pathway. JNK activation also promotes HFD-induced accumulation of macrophages in adipose tissue.

In physiological conditions GPR21 activity is supposedly strictly regulated by an endogenous ligand, this control becomes insufficient in case of deregulation of the insulin pathway.

<sup>5</sup>GPR21 is widely expressed in various organs involved in energy balance regulation such as the CNS but, what becomes relevant in its expression pattern for T2D treatment, is its high expression in temperature-sensing hypothalamic neurons and in macrophages.

<sup>30-32</sup>Given that both obesity and low-grade inflammation states are emerging as key etiologic factors in insulin-resistance states being able to target with specificity GPR21 could represent a new important tool in T2D treatment.

In order to evaluate GPR21's role in diabetes outbreak and progression a knockout (KO) of its encoding gene has been made in mice.

KO mice showed an improved phenotype than their wild-type littermate<sup>5</sup>, both normal chow fed mice and the ones on a high-fat diet. KO of GPR21 gene led to a reduction in tissue inflammation due to a decreased macrophages cytoskeletal reorganization and subsequent chemotaxis to adipose tissue and liver.

GPR21 KO mice on HFD diet displayed an improved glucose tolerance and systemic insulin sensitivity, increased energy expenditure, increased brown portion of adipose tissue (BAT) mass and modest body weight (BW) reduction.

An increment in the BAT rather than in the white one is important because of its role in burning fat to generate energy and heat while WAT is important as fat storage. The novel BAT mass also expresses high level of uncoupling protein 1 (Ucp1, also known as thermogenin), marker of BAT's role in generating heat by non-shivering thermogenesis.

<sup>15</sup>Another important evidence is that several inflammatory markers as the monocyte chemoattractant protein 1 (MCP-1), c-reactive protein (CRP), serum amyloid protein (SAP) and Interferon gamma inducible protein-10 (IP-10) were decreased in mutant GPR21 KO animals,

suggesting that GPR21 may also mediate its effect through anti-inflammatory mechanisms. In particular, CRP and SAP are members of pentraxin family, produced by hepatocytes and known to be involved in autoimmunity and acute phase inflammatory response so their reduction is an important achievement in T2D treatment.

To be noted that the results arising from a KO in the only hematopoietic compartment were consistent with the ones in whole-body GPR21 knock-out, which outlines the GPR21 deletion in macrophages as the dominant cause of the metabolic aspects of the improved phenotype.

A possible complication (*Wang J. et al., 2016*)<sup>33</sup> to the previous considerations is that mouse GPR21 gene is located on chromosome 2 within the intron of Rabgap1 gene and there is evidence that indicated that the genetic modifications in the original KO line modified Rabgap1 mRNA expression levels. When a different technique is used to knock out the GPR21 gene, in a way that does not affect Rabgap1 expression, there is no evidence of an improved insulin sensitivity, glucose tolerance or blood insulin level in GPR21 KO mice compared to their wildtype littermates.

Rabgap1 is a coding gene, according to *Samarelli A. et al. (2020)*<sup>34</sup>, correlated to  $\beta$ 1-integrins activity and trafficking. Integrins are heterodimeric transmembrane receptors for extracellular matrix proteins and cell counter receptors that link the extracellular environment to the intracellular actomyosin cytoskeleton. They have a crucial role in cell adhesion and migration. They confirmed an interaction between Rabgap1 and  $\beta$ 1-integrin cytoplasmatic domain and its colocalization with integrins in early and recycling endosomes promoting the recycling of active  $\beta$ 1-integrins. Rabgap1 regulates the GTPase activity of several Rab proteins, in particular it controls Rab11 activation that, if not controlled would affect  $\beta$ 1-integrins recycling process to the membrane.

Given that leucocytes (*Brown E.J. et al., 2003*)<sup>35</sup> actually express integrins, a silencing of Rabgap1 gene it is not to be excluded as cause of the reduced macrophages mobility and the subsequent improved phenotype previously described.

GPR21 is the only GPCR receptor that clearly has an antagonistic influence on the glucose uptake pathway, unlike all the other GPCRs related to glucose homeostasis. Therefore, pharmacological research for new antidiabetic compounds targeting this receptor focused on antagonists and inverse agonists screening.

The only known compound related to GPR21 is the inverse agonist GRA2<sup>27</sup> and it's being tested at the moment in preclinical research phase.

The use of GRA2 in cells overexpressing GPR21 showed a decreased concentration of IP1, a stable metabolite deriving from the IP3 liberated following the receptor activation. The reduction in GPR21's signalling pathway activation led to restoration of the insulin pathway and phosphorylation of Akt and AS160 (following insulin administration), mediators with a critical role in GLUT-4 translocation to cell membrane. Nevertheless, if the insulin-stimulated Akt phosphorylation improvement was observed in liver and adipose tissue, no significant difference was registered in muscle.

In order to further evaluate GPR21 role in diabetes outbreak and progressing recent studies were carried on HepG2 cells (*Kinsella G. et al., 2021*)<sup>36</sup>, in which the expression of GPR21 was previously assessed by Western Blot analysis. As previously said IP1 concentration is a useful marker of GPR21's signalling pathway activation, when a siRNA against GPR21 or the inverse-agonist GRA2 were used IP1 levels significantly decreased in HepG2 determining the constitutive activity of GPR21 in these cells and allowing this cell line to be considered a suitable model in evaluating GPR21 role in hepatocytes.

Liver plays a fundamental role in maintaining glucose homeostasis by hepatic glucose production (HPG) and by glucose uptake and, especially the uptake, these actions have been seen to be impaired in insulin resistance states. To assess the role of GPR21, and if its activity actually leads to a compromised glucose homeostasis, its gene has been silenced and its receptor activity blocked by GRA2. Glucose *in vitro* uptake was significantly increased by both siRNA and inverse-agonist treatment whereas HPG remained unaltered suggesting that GPR21 activity affects mainly the glucose uptake in hepatocytes.

The correlation between the gene silencing or the blockage of GPR21 and the augmented glucose uptake was found to be related to GLUT-2 translocation to hepatocyte membrane. GLUT transporters are a membrane proteins family that allows a facilitate diffusion of glucose trough membranes, in particular GLUT-2 isoform in liver is the more expressed one whereas GLUT-1 and GLUT-4 have a higher expression in adipose tissue and muscle. A treatment with either siRNA against GPR21 or GRA2 (30  $\mu$ M) have shown an increased GLUT-2 translocation to HepG2 membrane, consistent with the higher glucose uptake. Improved GLUT-2 translocation is due to an augmented phosphorylation of both Akt and GSK-3 $\beta$ . In particular,



GSK3 $\beta$  inhibition resulting from Ser9 phosphorylation is associated with an increased GLUT2 expression.

Important implication of the role of GPR21 in GLUT2 expression is related to the impact that this expression has on beta cell function, suggested by recent studies (*Seyer et al., 2013*)<sup>37</sup>. Beta pancreatic cells functionality could be improved by inhibition of GPR21 in liver, but an inhibition of this receptor in islets themselves is to be investigated.

Other studies (*Bordano V. et al., 2022*)<sup>38</sup> have further explored how GPR21 is involved in inflammatory responses and in particular its expression pattern in macrophages. It has been shown that GPR21 expression levels increased in M<sub>1</sub> when compared to M<sub>0</sub> levels and lowered instead in M<sub>2</sub> anti-inflammatory macrophages.

When exposed to increasing concentration of GRA2 macrophages growth rate, both M<sub>1</sub> and M<sub>2</sub>, was not affected but when IP1 levels were evaluated lower concentrations of GRA2 were able to significantly reduce IP1 levels in M<sub>1</sub> than M<sub>2</sub>, confirming the higher expression of GPR21 in M<sub>1</sub> pro-inflammatory macrophages. The diminished signalling of GPR21 in M<sub>1</sub> has resulted in a reduced cytokines release (as TNF- $\alpha$  and IL-1 $\beta$ , important in maintaining inflammation states) from this cell type whereas no change was seen in anti-inflammatory cytokines release (such as IL-10) from M<sub>2</sub> macrophages.

Further confirmation of *Osborn et al.* work come from chemotactic assay using CCL7 (C-C Motif Chemokine Ligand 7) and treating macrophages with GRA2: M<sub>1</sub> cells migration was inhibited whereas M<sub>2</sub>'s one was increased. M<sub>2</sub> macrophages activity is not merely anti-inflammatory but they are cells known to promote insulin sensitivity, incrementing the value of GPR21 as new pharmaceutical target in T2D treatment.

As further confirmation of GPR21's role in diabetes pathogenesis and as potential therapeutic target *Riddy D.M. et al. (2021)*<sup>39</sup> performed a KO of the gene using the CRISPR-Cas9 technique, assessing the integrity of Rabgap1 expression. They confirmed a leaner phenotype in GPR21 KO mice, a better glucose handling after 12 weeks of HFD compared with controls and a reduction in Ccr2 expression in epididymal white adipose tissue (eWAT) and liver. In this study is again underlined the role of GPR21 in relation to inflammation and macrophages chemotaxis assessing a delayed polarization of Gpr21<sup>-/-</sup> CD11b<sup>+</sup> Bone Marrow-derived Macrophages (BMMs) in response to MCP-1 and a downregulation of genes with key roles in

the adhesion cascade, such as Itgb3 and VCAM. Of particular relevance is the expression of MCP1 and GPR21 in diabetic patients, both significantly higher than relative controls, and the correlation in the expression pattern of GPR21 and CCR2 in CD14+ peripheral blood mononuclear cells (PBMCs). When a GPR21's KO is made on CD14+ PBMCs an impaired chemotaxis is observed, linking GPR21 to the MCP-1/CCL2-CCR2 axis.

This study not only makes the possibility of pharmacologically blocking GPR21, in order to obtain an anti-inflammatory activity, become even more relevant in T2D patients but suggests GPR21 as possible target in other diseases in which CCR2-driven inflammation is a cardinal feature.

GPR21 is also expressed and has a relevant role in the CNS. *Hossain M.S. et al. (2016)*<sup>40</sup> showed to be a correlation between different neuronal orphan GPRs, among which GPR21, and glycerophospholipids plasmalogens (PIs) pathway. PIs are enriched in the brain and reported to prevent neuronal cell death by enhancing phosphorylation of Akt and Erk signalling in neuronal cells. By using an inhibitor able to block all the GPCRs they found out that PIs pathway was reduced and, by screening GPRs expression in those areas of CNS, that was due to the inhibition to the blockage of specific GPRs including GPR21. This study suggests so that this receptor could be actually involved in a neuronal protective pattern in CNS enhancing PIs pathway. Given the supposed protective role in the SNC, opposed to the detrimental ones previously described, it could be of clinical interest to design inverse agonists that are not able to pass through the blood-brain barrier.

Another paper (*Rodrigo R. Nava et al., 2020*)<sup>41</sup> suggests the possibility of a relation between GPR21 expression and some of the phenotypes that characterize the metabolic syndrome (MS). They confirmed GPR21 to be expressed ubiquitously in the brain, heart, aorta, liver and kidney of the rats used in their tests.

As previously stated, GPR21's signalling pathway is mediated by a Gq protein that leads to PLC activation and calcium release. The activation of this pathway generates vasoconstriction in smooth muscle, NO release in endothelium, promotes cardiac hypertrophy and is related to glomerular filtration rate in the kidney. All these actions in different districts of the body are so supposed to be involved in hypertension observed in MS thus supporting the inhibition of GPR21 having a potentially wider role in ameliorating metabolic-related disorders.

## 2. STUDY AIM

Diabetes is a disease correlated to an impairment in the insulin physiologic signalling pathway and it is clearly becoming a relevant pathology both for the epidemiological and mortality-related aspects.

Two main types of this disease can be identified: the first one has autoimmune bases, and originates from a genetic predisposition, whereas the second one, most widespread in the population, is largely diet-related and has a later onset.

Although type two diabetes (T2D) is a multifaceted disease in the last years obesity conditions have taken on a central role in the understanding of the correlation between a low-grade chronic inflammation state and the development of diabetic pathology.

Several modifications, triggered by obesity and the generalized inflammatory state associated, in the immune system and in different glucose-sensitive tissues have been described resulting, among others, in a direct impairment of the insulin's pathway, reduced glucose uptake and pancreatic  $\beta$ -cells failure.

As the understanding of their functioning improves, so increase the interest on the vast class of receptors that are the G-proteins associated receptors (GPCRs). Given the large number of GPCRs expressed in cells responsible for both secretion and insulin's activity, the GPCRs have recently been widely investigated as possible new targets in diabetes treatment.

As the moment there are several therapeutic possibilities available for T2D's treatments but only a few successfully exploiting the GPCRs class (GLP1R) and almost half of the patients do not achieve treatment goals.

In this scenario in the last few years a novel GPCR has been investigated as new possible target for anti-diabetic compounds: GPR21.

In precedent works GPR21 has been proved to be constitutively active but its activity can become detrimental for the insulin's pathway if deregulated. Different approaches have been investigated to reduce this receptor's activity, in particular it was silenced both *in vivo* and *in vitro* successfully improving glucose handling and homeostasis.

A pharmacological inhibition of GPR21 became possible with the development of a lead compound: GRA2.

From GRA2 testing emerged an acceptable toxicological profile (toxicity detected over 100  $\mu\text{M}$ ) but the minimum effective concentration (MEC) remained too high.

The aim of the present work is to better determine GPR21's tridimensional structure, not yet crystalized, creating a three-dimensional model based on homologues structure.

The best models of GPR21 will be used to study the active site and consequently the interactions occurring between the binding site's residues and different ligands, GRA2 among them.

The next step will be to compare the affinity values of the interaction between GPR21 and GRA2 with the values deriving from the interactions among GPR21 and five GRA2's analogues searching for compounds that showed higher affinity for this receptor.

Using the models generated will be also performed a structure-based research and a delineation of new GRA2's potential analogues with higher affinity values for the binding site.

Completed the *in silico* analyses, the analogues are to be tested *in vitro* to assess their toxicity values, working in the same range previously used for GRA2, performing a MTT assay.

Once assessed the concentrations interval at which it is safe to use the compounds, they will be screened conducting a  $\text{Ca}^{2+}$ -release assay on HepG2 cells treated with the analogues versus GRA2. Analysing the  $\text{Ca}^{2+}$ -release decrease following the compounds administration it should be possible to define which compounds can reduce more the activation of GPR21 pathway and, therefore, the insulin's pathway impairment. The compounds that are able to inhibits GPR21 at lower concentration than 30  $\mu\text{M}$  will undergo further tests because potentially more potent drugs than GRA2.

At the same time different models of insulin resistance states are to be defined and induced on HepG2 cells to determine how changes GPR21's expression compared to physiological conditions. These induced pathological states are also to be used to determine if same concentrations of GRA2 and analogues entail major responses in IR states.

Insulin resistance states in this work are induced using two different methods: high glucose medium for different periods of time and high concentrations of insulin.

The GPR21 expression and levels of insulin signaling pathway activation on IR cells is tested by performing a western blot, with and without GRA2 and its analogues administration.

To summarize, the following aspects and techniques are investigated in this work:

- In silico:
  - Homology modelling to define a GPR21's tridimensional model
  - Docking studies of GRA2 and five analogues
  - Informatic protein analysis to refine the binding site
  - Compounds screening and design for more affine molecules
  
- In vitro:
  - Determination of cell viability after treatments with GRA2 analogues
  - Screening of the analogues on a potency base by a Ca<sup>2+</sup>-release assay
  - Induction of insulin resistance states using two different approaches:
    - High glucose prolonged exposure
    - High glucose and high insulin prolonged exposure
  - Definition of GPR21 expression in HepG2 presenting induced insulin resistance
  - Evaluation of the insulin signaling pathway activation and potential insulin resistance reversion after treatment with new inverse agonists

### 3. MATERIALS AND METHODS

#### 3.1 Compounds preparation

The compounds tested were kindly provided by Dr. Gemma Kinsella of TU Dublin and bought from SPECS (PB, The Netherlands) in the following amounts of powder:

██████████160: 10,2 mg

██████████399: 10,4 mg

All the compounds were solubilized in dimethyl-sulfoxide (DMSO) in different final volumes in order to generate the same concentration of 0,05 mol/L.

#### 3.2 Cell cultures identification and definition

##### 3.2.1 Cell type description

In the following part of the work the aim was to identify a cell culture's type involved in the glucose homeostasis and that was proved to express a functional GPR21 protein in order to test the compounds identified, in the previous part, as possible new anti-diabetic agents.

HepG2 is a cell line isolated from a hepatocellular carcinoma of a 15-years-old, white, male with liver cancer and it exhibits an epithelial-like morphology<sup>42</sup>.

The utilisation and the representativity of this cell type for the GPR21's activity and functions studies are legitimated by the previous work by *Kinsella et al. (2021)*<sup>36</sup>, in which GPR21's expression was assessed.

##### 3.2.2 Cells reconstitution

The cells used for the experiments were preserved in a DMSO 10% solution and at the temperature of -80°C at Pharmacology laboratories of the Pharmaceutic Science and Technology Department, University of Turin and, previously, generously donated by the Clinical and Biological Sciences Department of the University of Turin.

Once thawed the aliquot, the cells were plated in a 25 cm<sup>2</sup> flask with Dulbecco's Modified Eagle Medium Low glucose (DMEM, Sigma-Aldrich, St Louis, MO, USA), as culture medium, added with 10% of Fetal Bovine Serum (FBS), 100 U/mL of penicillin, 100 µg/mL of streptomycin, 2 mM of L-glutamine (Aurogene Srl, RM, Italy) and incubated at 37°C, 5% CO<sub>2</sub> atmosphere.

Through the following days their growth was monitored and the medium was changed and renewed several times to ensure the complete DMSO removal and provide optimal culture conditions.

When the flask presented an 80% of cells confluence, and the cells showed the distinctive cluster formation, a transfer to a 75 cm<sup>2</sup> flask was performed in order to allow a further growth.

The described reconstitution and maintenance processes were performed for every cell aliquot and all the procedures involving this cell line were carried out in sterile conditions, allowed by laminar flow hoods with HEPA filters, to prevent microorganisms' contaminations.

### 3.2.3 Cells transfer and count

When at 80% confluence the cells were plated for experimental reasons and, the remaining amount, transferred to a different flask with new medium to allow the growth under the best conditions.

The first step in this protocol was the separation of the cells from the culture flask, performed removing the medium, washing with PBS 1X and by adding 5 mL of a trypsin solution (Trypsin-EDTA 1X in PBS, Aurogene, RM, Italy) in the 75 cm<sup>2</sup> flask and let act for approximately 5-10 minutes in incubator. Afterwards the flask was checked at the microscope to assess that all the cells were now in suspension and the trypsin was neutralized with double the amount of medium.

The suspension was then transferred to a falcon and the clusters broken.

In order to transfer or use a specific number of cells a volume of 10 µL was collected and placed in a Bürker chamber, a device that permits the manual count of cells in suspension using a microscope.



Figure 9 Bürker chamber

The number of cells present in 10  $\mu\text{L}$  was related in proportion to the number present in the total volume of the suspension and then a specific volume, corresponding to a specific number of cells, was transferred in a new flask with new medium.

### **3.3 MTT testing**

#### **3.3.1 Method's description**

The first step in the process of assessing the therapeutic potential of the new compounds was to determine their effect on HepG2 cells viability at various concentrations.

The test of choice was a MTT test, capable of measuring metabolic activity as indicator of cell viability, proliferation and cytotoxicity.<sup>43</sup> This is a colorimetric assay based on the reduction of a yellow tetrazolium salt (3-(4,5-dimethylthiazol-2-yl)-2,5-diphenyltetrazolium bromide or MTT) (Sigma-Aldrich, St Louis, MO, USA) to purple formazan crystals by metabolically active cells, carried out by NAD(P)H-dependent oxidoreductase enzymes. The results were quantified by solubilizing the formazan crystals using DMSO and analyzing the resulting-colored solution's absorbance with a spectrophotometer at 570 nm wavelength.

#### **3.3.2 Test preparation**

In previous works<sup>36</sup> the toxicity values of the lead compound GRA2 were evaluated and assessed starting at concentration of 80  $\mu\text{M}$  and better described at 100  $\mu\text{M}$  with the identification of precipitates in the culture medium and a reduction in cells growth rate.

All the five compounds were plated in 96-wells plates using cells cultured in the exact same conditions (37°C and 5%  $\text{CO}_2$ ) to grant an appropriate level of representativeness and repeatability of the data subsequently collected.

Cells were plated ( $1 \cdot 10^4$  cells/well) in 96-well culture plates and then stored in an incubator at 37°C for 24 hours.

On the next day the cells were exposed to the five different compounds at the following concentrations, working in quadruplicate: 0, 1, 10, 30, 100  $\mu\text{M}$ .

Subsequently, 5 mg/mL of the MTT solution were added to each well and the plates were incubated at 37°C for one hour. After the incubation hour the medium was removed and 90



$\mu\text{L}$  per well of the DMSO solubilizing solution was added; the plates are ready for the absorbance's measurement.

The absorbance values of each condition were compared to control's absorbance.

### **3.3.3 Test results and analysis**

All the absorbance values collected were analyzed studying their mean and standard dispersion using GraphPad (by Dotmatics, GraphPad Software, San Diego, California, USA) and  $p$  values  $< 0.05$  were considered as significant.

Data are presented as mean $\pm$ SD. Statistical significance was evaluated by a one-way analysis of variance (ANOVA) with a Dunnett's post-hoc test.

## **3.4 Protein extraction and protein concentration determination**

### **3.4.1 Extraction**

In order to obtain the protein extract the HepG2 cells, plated and cultivated in small Petri's plates, were extracted with RIPA lysis buffer containing:

- TRIS-HCl 50 mM, pH 7.4
- Nonidet P40 1%
- Sodium deoxycholate 0.5%
- SDS 0.1%
- NaCl 150 mM
- EDTA 2 mM
- NaF 50 mM
- Water for injections

At the RIPA buffer were contextually added proteases inhibitors (PIC, 1  $\mu\text{L}/\text{mL}$ ), a serine protease inhibitor (phenylmethylsulphonyl fluoride, PMSF, 10  $\mu\text{L}/\text{mL}$ ) and a phosphatase inhibitor (sodium orthovanadate 10  $\mu\text{L}/\text{mL}$ ).

The solution and all the described and following steps are to be performed maintaining the plates in ice.

At first the cells, in non-sterile conditions, were washed with a cold PBS solution then 40  $\mu\text{L}$  of the RIPA buffer were added and left to act for 20 minutes.

The cellular lysate was now scraped obtaining the extract and collected in eppendorfs. The eppendorfs were centrifugated for 20 minutes at 13000 rotations per minute and at the controlled temperature of 4°C.

The supernatant, containing the proteins, was now collected and preserved at -80°C.

### **3.4.2 Concentration determination**

The protein concentration of the extracts was therefore assessed using the *Pierce<sup>TM</sup> BCA Protein Assay Kit* (Thermo Fisher Scientific Inc., Rockford, IL, USA), a colorimetric assay. The assay was performed on 96-wells plates and each sample was double tested.

The assay mechanism is based on the reduction of copper ions ( $\text{Cu}^{2+}$  to  $\text{Cu}^{+}$ ) catalyzed by the proteins in the alkaline medium (Biuret reaction) and in presence of the bicinchoninic acid, BCA.

The BCA is needed for the colorimetric detection of the  $\text{Cu}^{+}$  ion: two BCA molecules chelate a  $\text{Cu}^{+}$  ion forming a violet water-soluble complex, which intensity is proportional to the protein concentration.

The plate was incubated at 37°C for 30 minutes and then the absorbance at 570 nm was measured using a spectrophotometer.

Samples protein concentration was determined using known concentrations of albumin in order to set a calibration line.

## **3.5 Western blot**

### **3.5.1 Rationale of the test**

A western blot is a laboratory method<sup>44</sup> used to identify a specific protein molecule from among a mixture of proteins, often deriving from a specific tissue or cell type, using an antibody capable of recognizing an antigen of that protein. This test involves an electrophoretic run on a polyacrylamide gel, so it is also able to evaluate the size of the protein of interest and to measure the amount of protein expression in a semi-quantitative manner.

### 3.5.2 Polyacrylamide gel preparation

The first step of this technique is an electrophoretic run on a gel made of an acrylamide polymer that allows the separation of the proteins according to their molecular weight: higher the weight shorter will be the run.

The gel can present different specifics, it can have the thickness of 1 mm or 1,5 mm and disparate mesh widths according to the acrylamide's percentage. In this study slim gels (1 mm) were used with 8% or 10% of acrylamide.

The gel consists of two portions presenting different pH values and acrylamide concentrations:

- *Stacking gel*: the upper part of the gel presenting the wells for the sample's loading; this portion has lower pH and wider meshes to allow the samples to align.
- *Separating gel*: in this portion, the bigger one, the proteins will separate according to their molecular weight during the running phase of the process.

Once that the separating gel's solution (*cf. solution b.*) has been prepared it is poured between two slides of a specific support structure. On the top of the solution was added a SDS 0.1% solution, to prevent drying, and then the gel was let to polymerize for 30 minutes at 4°C. The stacking gel solution (*cf. solution a.*) was prepared and, once that the first part was ready and the SDS solution removed, it has been added on the separating gel. A small brush was added in order to generate the wells during the polymerization, that requires 15 minutes at 4°C.

### 3.5.3 Sample preparation and loading

Once that the protein concentration of the extracts has been determined it possible to calculate the sample volume that is needed to load in order to obtain the same amount of protein in each well and so loading homogeneity. In the experiments described in this work 15-30 µg of protein per sample were loaded in a final volume of 15 µL; to this solution 3 µL of sample buffer 15X (*cf. solution c.*) were added, previously diluted down to a 6X concentration with dithiothreitol (DTT, PanReac – AppliChem, ITW Reagents).

The samples thus prepared were put in thermoblock for 5 minutes at 70°C and briefly centrifuged to promote protein denaturation.

It then proceeds with sample loading in the stacking gel's wells, previously cleaned of any residual. One of the wells was always reserved for the loading of 2-4  $\mu$ L of the reference molecular weights (Opti-Protein XL Marker - Abm, Applied Biological Materials Inc., Canada) and any empty wells are filled with 5  $\mu$ L of sample buffer and water.

### **3.5.4 Electrophoretic run**

The loaded gels were transferred on specific holders for the electrophoretic run and the latter are filled with *Running buffer (cfr. solution d.)*, a solution that stabilizes the pH and allows the electric conduction between the electrodes.

The protein migration was conducted by applying a potential difference of 70 V for the first 10-15 minutes, subsequently incremented up to 100 V until the end of the electrophoretic run.

### **3.5.5 Transfer (immunoblotting)**

Once that the electrophoretic run was complete the proteins were transferred on a polyvinylidene fluoride (PVDF) membrane (Millipore Corporation, MA, USA) using a transfer support and a *Transfer buffer (cfr. solution e.)*. For the transfer, a potential difference of 100V for 60 minutes was used.

The membrane was treated with a blocking buffer (*cfr. solution i.*), a solution of 5% bovine serine albumin (BSA) in PBS 1X Tween 20-0.1%, needed to saturate any not-specific binding site for the antibodies. The incubation time can go from 20 minutes up to 2 hours, under agitation. Once this phase is over the filter undergoes three rapid washes with PBS 1X Tween 20-0.1%.

The filter was then incubated overnight with the primary antibody at 4°C, under constant agitation.

Primary antibodies are meant to detect and recognize the target protein and are prepared in a PBS 1X Tween 20-0.1% with a 5% of BSA. The primary antibodies used in this work are the following: Ph-AS160 (1:2000, Rabbit),  $\beta$ -actin (1:1000, Rabbit), Ph-GSK-3 $\beta$  (1:1000, Rabbit), Ph-Akt (1:1000, Mouse) from Cell Signaling Technology (Inc., MA, USA), Tubulin (1:5000, Mouse) from Abcam (Cambridge, UK) and GPR21 (1:500, Rabbit) from Origene Technologies (MD, USA).

Once that the incubation period was over the filter undergoes three washes with T-PBS 1X in order to remove the antibody's excess, each wash has a duration of 5 minutes.

The filter was incubated with the secondary antibody for 1 hour, at room temperature. This second antibody targets the first one because it recognizes the immunoglobulins specifically derived from the animal species of the primary.

Secondary antibodies are prepared on different dilution indexes, according to the primary's performances, in a PBS 1X Tween 20 0.1% solution with a 5% of BSA. In this study the following secondary antibodies were used:  $\alpha$ -Mouse (from 1:5000 to 1:10000),  $\alpha$ -Rabbit (from 1:2000 to 1:10000) both from Cell Signaling Technology (Inc., MA, USA).

The filter was once again washed three times with a T-PBS solution for a total duration of 15 minutes.

### 3.5.6 Photographic development

The filter was treated for 2 minutes, at room temperature but protected from direct light, with an ECL (Enhanced ChemiLuminescence) (WesternBright™, Advansta, San Jose, CA, USA) solution, a luminol-based chemiluminescence detection system.

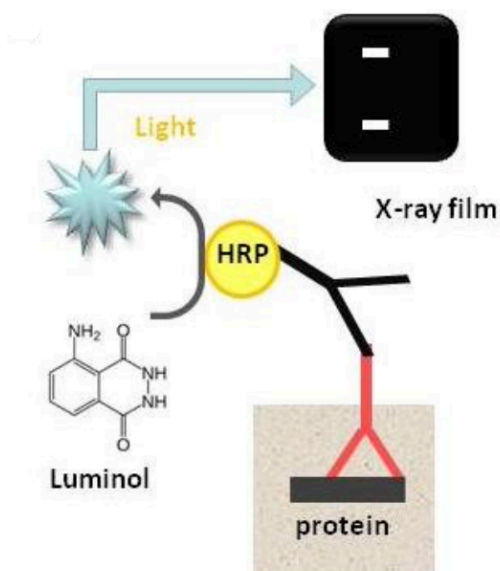


**Figure 10** Secondary antibody coupled with horseradish peroxidase and luminol oxidation (Characterization of potential modulators of the intestinal peptide transporter PEPT1 in *Caenorhabditis elegans* and human colon carcinoma cells - Scientific Figure on ResearchGate)

The secondary antibody is conjugated with an enzyme which catalyze a chemiluminescence reaction when incubated with its substrate, easily detected. This enzyme is usually a peroxidase (horseradish peroxidase, HRP) that cleaves the hydrogen peroxide into water and superoxide radical, the latter will oxidize the luminol in the ECL solution. Luminol oxidation cause an electrons shift from the basal to the excited state; the electrons, because of the instability of the excited state, will return to the basal state emitting photons, able to impress the photographic plate, on which the proteins bands can eventually be visualized.

After the ECL treatment the on-plate development starts in the darkroom. The filter enters in contact with a photographic plate (Cytiva, Amersham™ Hyperfilm™ MP) for a variable period of time in order to obtain a clean image; the plate is now put for few seconds, from 5 seconds up to 10 seconds, in a development solution (GBX Developer and Replenisher - Aurogene) and then immersed in a fixative solution (GBX Fixer and Replenisher - Aurogene). If the protein is present, and it has been correctly recognized, a band will appear at the level of the molecular weight of that protein.

Some of the development reported in the present work were performed using a ChemiDoc Imagers machine (BioRad, USA), an instrument able to detect fluorescence and chemiluminescence. The ChemiDoc was used along with a different ECL solution: Clarity™ Western ECL (BioRad, USA).

On each filter a control of the loading's homogeneity is necessary: the filter is incubated with an antibody that targets the tubulin (1:5000 dilution) and then with a secondary antibody that targets mouse's immunoglobulins (1:10000 dilution).

Tubulin is a structure cytoskeletal protein not affected by the treatments to which the cells have been exposed and, therefore, a reference for the loaded proteins amount.

Bands analysis is then performed with a densitometric-based method using the ImageJ (by the National Institute of Health, USA) software and the proteins expression is determined as optic density, normalized with the tubulin's values.

### **3.5.7 Stripping**

In case of multiple developments of the same membrane these were stripped in order to remove the bonded antibodies that could interfere with the subsequent ones. In this work a ready to use stripping solution (Western Blot Strip-it Buffer, Advansta, San Jose, CA, USA) was applied for 5 minutes under agitation at dark.

This protocol is required in case primary antibodies require the same secondary antibody or two proteins of interest presents very close molecular weights.

After stripping the membranes were washed 3 times with T-PBS 1X (*cfr. solution h.*) for 5 minutes each wash and then they underwent again a blocking protocol.

### **3.5.8 Ponceau S staining solution**

When necessary to visually assess the proteins transfer on the analyzed membrane a Ponceau S staining solution (Sigma, Sigma-Aldrich, St Louis, MO, USA) was used. This ready to use solution is able to stain protein bands on nitrocellulose or PVDF membranes in 5 minutes. In order to effectively perform the test, the membrane needs to be washed from any PBS-Tween 20 residue using distilled water. Another wash with water is required after the staining to clear the background and leaving only the protein bands stained.

## **3.6 Ca<sup>2+</sup> release assay**

### **3.6.1 Rationale of the assay**

As described in the “GPR21 overview” (*cf.* 1.4) section GPR21 is a G-protein coupled receptor which activates the PLC-IP<sub>3</sub>/DAG pathway and therefore leads to Ca<sup>2+</sup> release.

The aim of the present study was to assess basal levels of intracellular Ca<sup>2+</sup> of healthy HepG2 cells and then using this assay to screen our five compounds to see at what concentrations they were able to reduce the Ca<sup>2+</sup> release and, therefore, the GPR21-related pathway.

Given that the general aim of this project is to find compounds with a higher potency, as inverse-agonists of GPR21, than the lead compound GRA2 we also tested GRA2 to obtain reference values, not yet reported in literature for this assay.

### **3.6.2 Basal conditions assessment**

HepG2 cells were plated in a black 96-wells culture plate, leaving the whole first row (12 wells) without cell as a control, at two different per well concentrations, 20000 cells per well in the first half and 40000 cells in the second half plate. The plate was then incubated at 37°C and 5% of CO<sub>2</sub> for 24 hours in order to allow the cells to adhere and stabilize.

Once the 24 hours have passed the plate was treated as following.

	1	2	3	4	5	6	7	8	9	10	11	12
A	NO CELLS											
B	CONTROL						CONTROL					
C	60 minutes of probe treatment			60 minutes of probe treatment			60 minutes of probe treatment			60 minutes of probe treatment		
D	NO PLURONIC			WITH PLURONIC			NO PLURONIC			WITH PLURONIC		
E												
F	30 minutes of probe treatment			30 minutes of probe treatment			30 minutes of probe treatment			30 minutes of probe treatment		
G	NO PLURONIC			WITH PLURONIC			NO PLURONIC			WITH PLURONIC		
H												
	20000 CELLS						40000 CELLS					

*Figure 11 Schematic refiguration of the plate used to assess the method and the basal conditions of the calcium release assay*

Six wells per cell concentration were used as secondary control then each half plate was treated with the calcium probe Fluo-8<sup>®</sup> AM (AAT Bioquest, Inc., CA, USA), the upper part for 60 minutes whereas the bottom one for 30 minutes.

In order to treat the cells with the probe the medium was removed in sterile conditions, the wells gently washed with 100  $\mu$ L of PBS 1X, at room temperature, then the calcium probe was added at 5  $\mu$ M concentration in DMEM low glucose, without serum. A medium without serum is needed because of the supposed presence in the serum of a GPR21's ligand with regulatory activity, regulation that is impaired in insulin resistance states.

The probe was added at different times according to the described plate scheme and the washes were performed being extremely cautious not to removing the cells.

As further condition to test a 0.04% of Pluronic (AAT Bioquest, Inc., CA, USA) was added, together with the probe, in half of the wells per cell concentration. Pluronic is a poloxamer, an amphiphilic copolymer composed of a central hydrophobic chain of polyoxypropylene (poly-propylene oxide) flanked by two hydrophilic chains of polyoxyethylene (polyethylene oxide) and is here used to enhance the cell permeability.

### 3.6.3 Compounds activity evaluation

HepG2 were plated ( $4 \cdot 10^4$  cells/well) in black 96-well culture plates and then stored in an incubator at 37°C for 24 hours.

After the 24 hours the medium was removed using an aspirator, paying extreme attention to stay near the wells walls to not damage or detach the adherent cells. A wash with 100  $\mu$ L of



sterile PBS 1X, at room temperature, was performed and then the DMEM low glucose medium, without serum, but containing the probe Fluo-8® AM at the concentration of 5 µM, was added.

The probe was let acting for 1 hour in incubator and afterwards was removed at the cells washed again once with 100 µL of sterile PBS 1X, at room temperature.

Then 100 µL per well of HHBS (Hank's Buffer Solution with HEPES, *cfr. solution k*) were added leaving some wells as no-probe controls (thus adding the same solution without probe) and the plate was read using the EnSight microplate reader (PerkinElmer, Waltham, MA, USA) using the protocol specified by the Fluo-8® AM product information sheet provided by AAT Bioquest.

Now the five different compounds and GRA2 were added at the final concentration of 10 µM, repeating the same conditions six times per compound and leaving some wells for the only-probe control. The plate was read once again applying the same protocol.

All the readings were performed in kinetic mode, evaluating the absorbance values at 30 seconds time intervals for a total of five minutes.

#### **3.6.4 Maximum Ca<sup>2+</sup> release determination**

In order to better determine the effect of the compounds tested, after the readings previously described, a Triton X solution (*cfr. solution j.*) was added to all the wells.

Triton X is a nonionic surfactant able to permeabilize the membranes of living cells allowing a massive entrance of the extracellular calcium that, once inside of the plated cells, is detected by the probe giving the maximal value of intracellular calcium concentration.

#### **3.6.5 Results analysis**

The readings for each experiment were obtained in kinetic mode, each compound was evaluated six times for reading and for six consecutive readings. For our purposes of screening the mean of the six wells per compound were related to the mean of the control wells at the same time and the best mean value deriving from the kinetic reported to the mean value deriving from the readings with triton in those same wells.

### 3.7 Insulin resistance states generation

In order to evaluate if there are changes in GPR21's expression or activity following the onset of insulin resistance states those were induced in HepG2 cells using two parallel approaches involving the exposure of the cells to high concentrations of glucose for different periods of time and to insulin with both low and high glucose mediums.

#### 3.7.1 High glucose

Following previous studies such as *Herrera I. et al. (2014)*<sup>45</sup>, that have shown an impairment of the insulin pathway in HepG2 cells after their exposure to high concentrations (over 20 mM for at least 24 hours) of L-glucose we treated our cells cultures with DMEM High Glucose (4500 mg/L, Sigma, Sigma-Aldrich, St Louis, MO, USA) medium for different periods of times starting with a 24 hours exposure up to 10 days.

The HepG2 cells were plated in 6-wells culture plates and left to settle in 3 mL DMEM Low Glucose (1000 mg/L) medium for 24 hours. The next day a change of medium was performed using 3 mL DMEM High Glucose (4500 mg/L) medium, left acting for 24 hours, 72 hours, 5 days and 10 days.

We started with a  $1 \cdot 10^6$  cells per well for the 24 hours exposure reducing the amount of cells plated to  $6 \cdot 10^5$  cells per well for the 72 hours exposure and to  $4 \cdot 10^5$  cells per well for the 5 and 10 days experiments.

For the longer periods the medium was partially (1.5 mL) renewed every 3 days.

In each experiment low glucose controls were present to validate the results.

After the different experiments the cells have been lysed in order to extract the proteins and their concentration in the extracts was determined. With a western bolt technique was then assessed the expression of GPR21 and the activation of the insulin mediators cascade.

As further validation of these models a final chase with 100 nM of insulin (Sigma-Aldrich, St Louis, MO, USA) for 10 minutes was performed before the extraction in order to better establish any possible variation of the canonical insulin pathway, better determinable when activated rather than in basal conditions.

### 3.7.2 High insulin

In order to determine an efficient protocol able to produce an insulin resistance model following insulin administration to HepG2 the work of *Huang Q. et al. (2002)*<sup>46</sup> was used as reference. In this paper they tested different concentrations of insulin on HepG2 cultures followed by an analysis of their glucose consumption, defining 100 nM as the most efficient exposure concentration to induce an insulin resistance state.

	Concentration of insulin (mol/L)	Glucose consumption (mmol/L)	Glucose consumption ratio (%)
Control	0	3.97 ± 0.04 <sup>c</sup>	
Insulin	5 × 10 <sup>-5</sup>	2.94 ± 0.08 <sup>b</sup>	25.95
	5 × 10 <sup>-6</sup>	3.04 ± 0.30 <sup>b</sup>	23.43
	5 × 10 <sup>-7</sup>	2.29 ± 0.09 <sup>a</sup>	42.32
	5 × 10 <sup>-8</sup>	2.85 ± 0.02 <sup>b</sup>	28.21
	5 × 10 <sup>-9</sup>	3.13 ± 0.07 <sup>b</sup>	21.16

**Figure 12** Insulin concentration and glucose uptake in HepG2 cells (*Huang et al., Phenolic compounds ameliorate the glucose uptake in HepG2 cells' insulin resistance via activating AMPK: Anti-diabetic effect of phenolic compounds in HepG2 cells, Journal of Functional Foods, Volume 19, Part A, 2015, Pages 487-494*)

Therefore, in our work the cells were plated in 6-wells culture plates at the concentration of 1\*10<sup>6</sup> cells per well in DMEM low glucose medium for 24 hours and then the medium was changed in order to have some wells continuing with a low glucose medium and others presenting a high glucose DMEM medium, both the conditions were then added with insulin at the final concentration of 100 nM and let act for 24 hours. In all the experiments we preserved a percentage of the wells as controls for both high and low glucose conditions. After the different experiments the cells have been lysed in order to extract the proteins and their concentration in the extracts was determined. With a western bolt technique was then assessed the expression of GPR21 and the activation of the insulin mediators cascade.

As further validation of these models a final chase with 100 nM of insulin for 10 minutes was performed before the extraction in order to better establish any possible variation of the

canonical insulin pathway, better determinable when activated rather than in basal conditions.

### 3.8 Statistics

Statistical analysis was performed by two-tailed Student's t test or by a one-way analysis of variance (ANOVA) followed by a Dunnett's post-hoc test using GraphPad (by Dotmatics, GraphPad Software, San Diego, California, USA). *P* values < 0.05 were considered as significant. Data, when applicable, are presented as mean±SD

### 3.9 Solutions

#### a. Stacking gel

- 60% distilled water
- 25% Tris-HCl (pH 6.8)
- 1% SDS 10%
- 13% Acryl/BIS
- 1.6% APS 10%
- 8% TEMED (Tetramethylethylenediamine)

#### b. Running gel (10%)

- 40.8% distilled water
- 24.5% Tris-HCl (pH 8.8)
- 0.98% SDS
- 32.7% Acryl/BIS
- 0.65% APS 10%
- 0.33% TEMED (Tetramethylethylenediamine)

#### c. Sample buffer 15X

- 70% Tris-HCl (pH 6.8)
- 1% SDS
- 0.001% Bromophenol blue

- 30% glycerol

**d. Running buffer 1X**

- 3.02 g/L Tris-HCl
- 14.4 g/L glycine
- 1 g/L SDS
- Up to volume with milliQ water

**e. Transfer buffer 1X**

- 3.02 g/L Tris-HCl
- 14.4 g/L glycine
- 15% methanol
- Up to volume with milliQ water

**f. PBS 10X (Phosphate Buffered Saline 10X)**

To prepare 1 liter of PBS 10X the following amounts of substances, final pH of 6.9:

- 80g NaCl (sodium chloride)
- 14.4 g Na<sub>2</sub>HPO<sub>4</sub> (Sodium phosphate dibasic)
- 2 g KCl (potassium chloride)
- 2.40 g KH<sub>2</sub>PO<sub>4</sub> (Potassium dihydrogen phosphate)
- Up to volume with milliQ water

**g. PBS 1X (Phosphate Buffered Saline 1X)**

Perform a 1:10 dilution of the of the PBS 10x, final pH of 7.4.

**h. PBS 1X – Tween 20-0.1%, washing solution:**

Solution used to wash PVDF filters, prepared as following:

- PBS 10X, diluted 1:10 (Phosphate Buffered Saline 1x)
- 0.1% Tween 20

**i. Blocking buffer**

- PBS 10X, diluted 1:10 (Phosphate Buffered Saline 1x)

- 0.1% Tween 20
- 5% BSA

**j. PBS 1X – TRITON**

- PBS 10X, diluted 1:10 (Phosphate Buffered Saline 1x)
- 0.5% TRITON

**k. HHBS (Hank's Buffer Solution with HEPES)**

- 140 mg/L  $\text{CaCl}_2$
- 100 mg/L  $\text{MgCl}_2 - 6 \text{H}_2\text{O}$
- 100 mg/L  $\text{MgSO}_4 - 7 \text{H}_2\text{O}$
- 400 mg/L KCl
- 60 mg/L  $\text{KH}_2\text{PO}_4$
- 350 mg/L  $\text{NaHCO}_3$
- 8000 mg/L NaCl
- 48 mg/L  $\text{Na}_2\text{HPO}_4$
- 1000 mg/L D-Glucose
- 4760 mg/L Hepes

## 4. RESULTS

### 4.1 Homology modelling

Despite all the pharmacological works here reported, in order to discover new compounds able to target GPR21 and represent a new tool in T2D treatment more homology modelling studies are required to identify GPR21's structure.

GPR21 structure has not yet been crystalized, some predictive models are available so far but more work is required to improve these models and, in particular, to better establish GPR21's structure when bound to an antagonist/inverse agonist. In order to predict the structure and the conformational features of antagonist coupled GPR21 some crystalized proteins with different grades of homology were used as templates.

An alignment of GPR21 FASTA sequence with the other receptors first cloned and studied along with it, shows several similarities between different receptors of the same family and can be used to outline the seven trans-membrane segments:

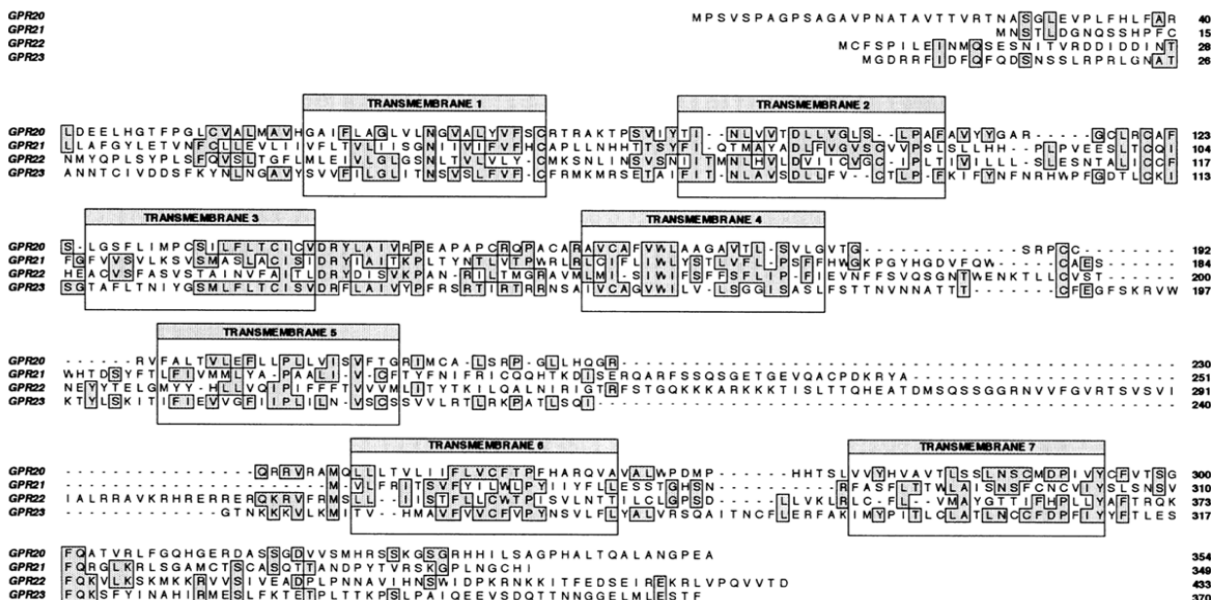


Figure 13 GPRs 20,21,22 and 23 FASTA sequences alignment and transmembrane segments identification (B.F. O'Dowd et al. Gene 187 (1997) 75-91)

Different templates (present on the RCSB, Protein Data Bank site) were used to build several models, the ones able to produce the best models are reported below. All the templates were chosen according to different important parameters: identity, query cover, resolution of the

template model and presence of an antagonist/inverse-agonist. After that a model was generated using SWISS-MODEL<sup>α</sup> online tools, it was evaluated with SAVES<sup>β</sup>. The evaluation of a model goodness takes in consideration different factors, here priority was given to the Ramachandran plot (that gives a report of the stereochemical problems) and to the ERRAT value.

Template	Resolution	Identity&Positivities	Coverage	Ligand
<b>5mzj</b> – A2R	2.00 Å	33% - 43%	42%	NSAt
<b>4gbr</b> – β2R	3.99 Å	24% - 45%	78%	NSAt
<b>5zhp</b> – M3R	3.10 Å	31% - 50%	37%	SAt
<b>6li1</b> – GPR52	2.90 Å	67% - 82%	89%	-

*Figure 14* Resumptive table the template used to create a GPR21 tridimensional model and their main parameters

The best model generated with SWISS has been built using 5MZY as template, a crystallised structure of a human A2 adenosine receptor in association with theophylline, a non-selective antagonist. The template presents an identity of 33.12% with GPR21 and covers the 42% of the target sequence with a resolution of 2.0 Å.

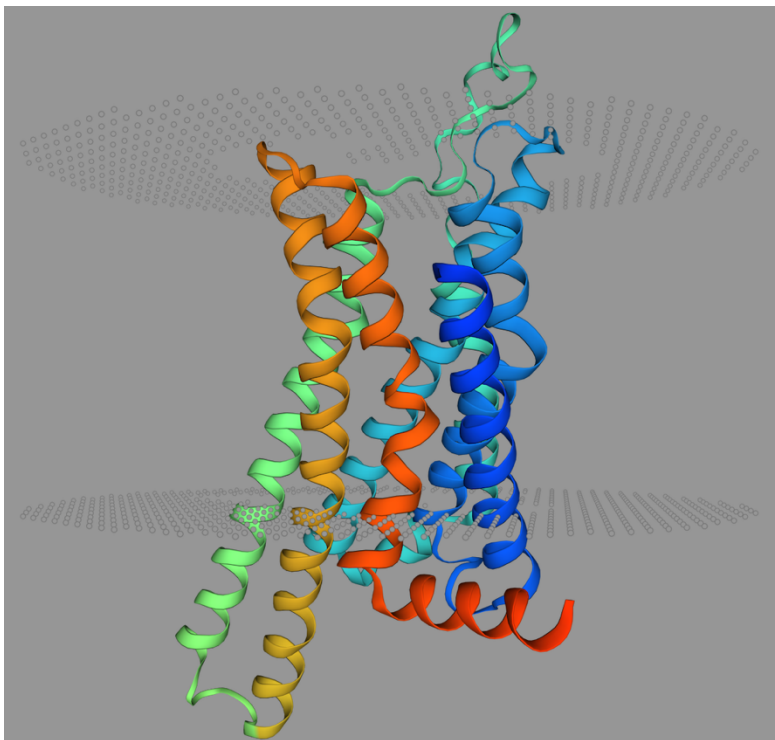


*Figure 15* Model-5mzj

This model presents an overall quality factor of 96.83. Some potentially problematic aminoacids can be identified between the residues 59-64, 164-165, 167, 187, 234 and 278. Verifying the location of these residues in the structure of the protein they are all in the loops with the exception of residues 164 and 165 that are situated at the very end of TM4.

Another good model was generated with SWISS using 4GBR.1 as template, a crystallised structure of a beta2 adrenergic receptor bound to a non-selective antagonist. This template



presents an identity a little lower than the precedent (23.76%) but the query cover is higher, 78%.

As it is possible to see, the template presents a N-terminal lysozyme fusion, to stabilize the structure, that was subsequently manually removed from the model.

This model presents an overall quality factor of 94.64. There are different potentially problematic residues but, as in the precedent model, they are mostly in the loops so they should not affect the predictivity quality of the model.

Using Schrodinger Maestro<sup>v</sup> tools, a model based on both 4GBR and 6LI1 was generated. 6LI1 is a crystal structure of GPR52 ligand free form and

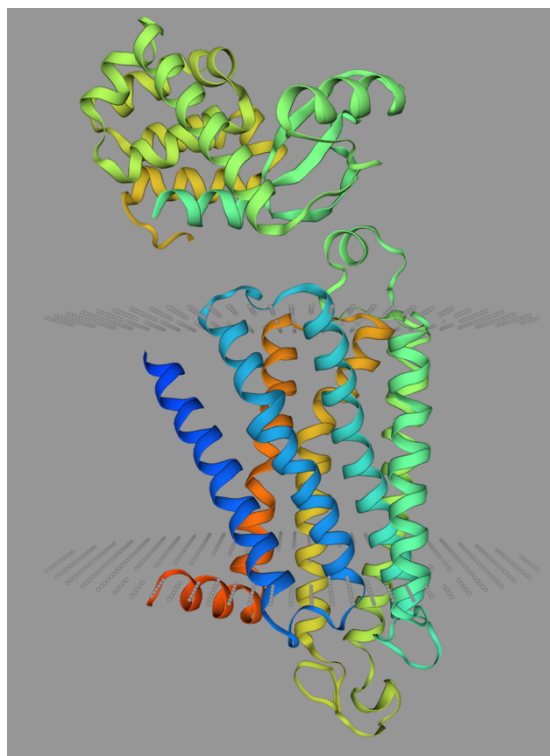


*Figure 16 Model-4gbr*

was used due to the high homology between GPR21 and GPR52. It presents an overall quality factor of 90.91 but could represent a good tool.

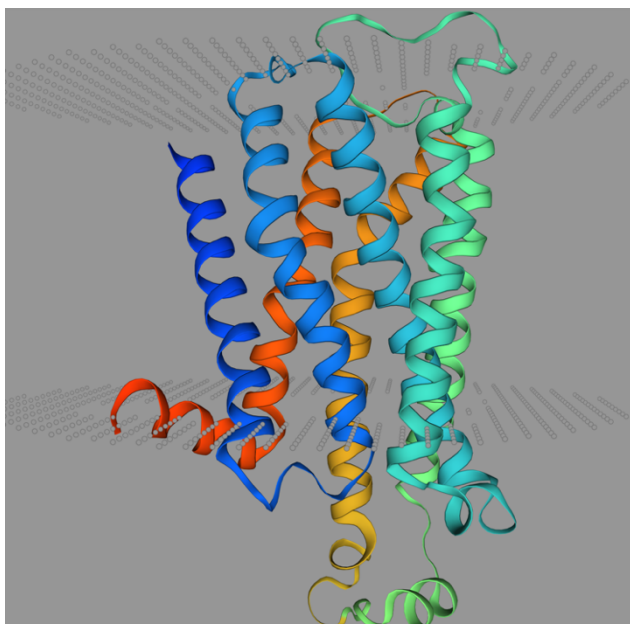


*Figure 17 Model-5zhp*

Here is shown a model of GPR21 obtained with SWISS using 5ZHP as template, M3 muscarinic acetylcholine receptor in complex with a selective antagonist. It has a good overall score, 95.76, with problematic residues all situated far from the supposed binding region. This model could represent a good predictive tool even if the template is a crystalized non-human protein.

These models will be used in docking studies together with model-2014, a model of GPR21 generated using 2RH1 and 4GBR, two  $\beta$ 2-adrenergic receptors in association with antagonists,

as templates. This model has a good overall quality factor, 96.24, and valid templates so will be used too in the subsequent studies here reported.

Model	Overall quality - ERRAT	Ramachandran
model-2014	96.24	8 residues warnings
model-5mzj	96.83	5 residues warnings
model-zhp	95.76	4 residues warnings

Figure 18 Table of GPR21 models evaluation

An alignment of the different models with GPR21's sequence and the ones deriving from the different templates was performed in order to check if there were gaps in TMs sequences and if specific segments were conserved.

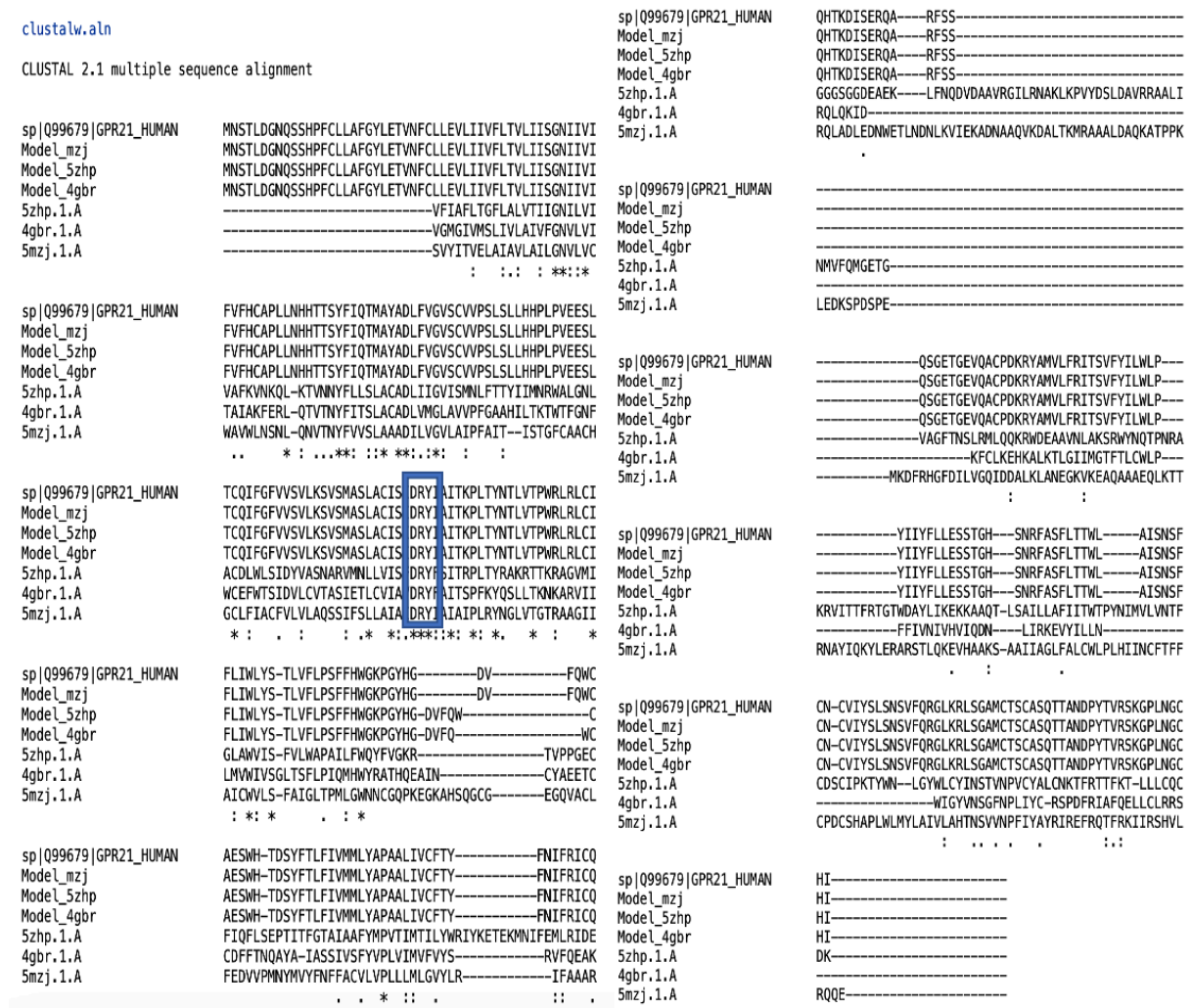


Figure 19 Multiple alignment: GPR21, model-mzj, model-5zhp, model-4gbr, 5zhp, 4gbr and 5mzj (performed using Clustalw online tools: <https://www.genome.jp/tools-bin/clustalw>)

It is possible to see how the DRY motif is conserved in all the different sequences whereas the NPXXY motif was only partially conserved because it was slightly different already in GPR21's sequence.

Gaps in TMs sequences of the generated models were found in the middle of the fourth one (157<sup>th</sup> residue), two gaps in the fifth one (195 and 208) and at the very beginning of the sixth (251).

Using Pymol<sup>6</sup> tools is possible to align different models so an alignment between the first model, model-5mzj, and the model predicted by AlphaFold<sup>47, 48</sup> was made and affinity of 1.39 (*fig. 20*) was found. Another useful alignment has been made with a model-2014, founding a similarity of 1.97.

Same alignments have been made with mode-5zhp obtaining as results similarity values of 1.27 (*fig. 21*) with model-2014 and 1.84 with model-Alphafold.

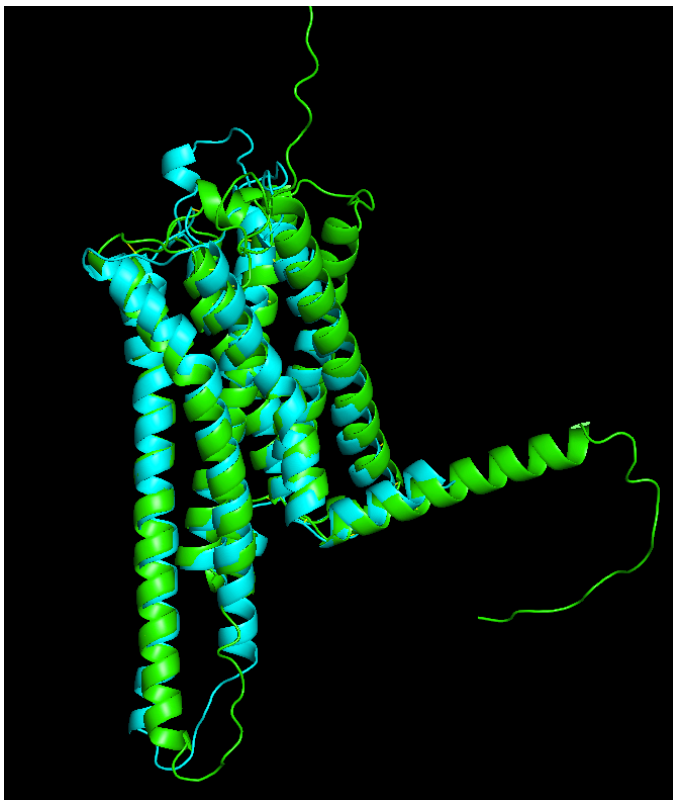


**Figure 20** Model-5mzj and model-Alphafold structures alignment; affinity of 1.39



**Figure 21** Model-5zhp and model-2014 structures alignment; affinity of 1.27

To be noted that the two structures are abundantly overlapping but presenting relevant differences in the loop portion that appeared to be problematic when analysed with Saves.

The relevance of the problematic portion in the models is to be assessed by determining where the aminoacidic residues forming the binding pocket of the receptor are.

X. Lin et al. (2020)<sup>49</sup> in their work determined the residues forming the binding pocket of GPR52, work that, given the high identity percentage between GPR52 and GPR21, is a fundamental starting point to determine GPR21's binding pocket.

In this paper they were able to define the orthosteric region of binding and crystalize the receptor in association with c17, a surrogate agonist.

The alignment between GPR52 and GPR21 sequences shows that there is a shift of 12 residues between the preserved amino acids of the two proteins.

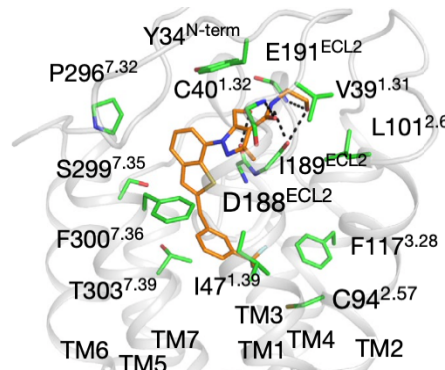


Figure 22 Aminoacids responsible for c17, a surrogate agonist, docking in GPR52 (X. Lin et al., Structural basis of ligand recognition and self-activation of orphan GPR52. Nature 579, 152–157 (2020)

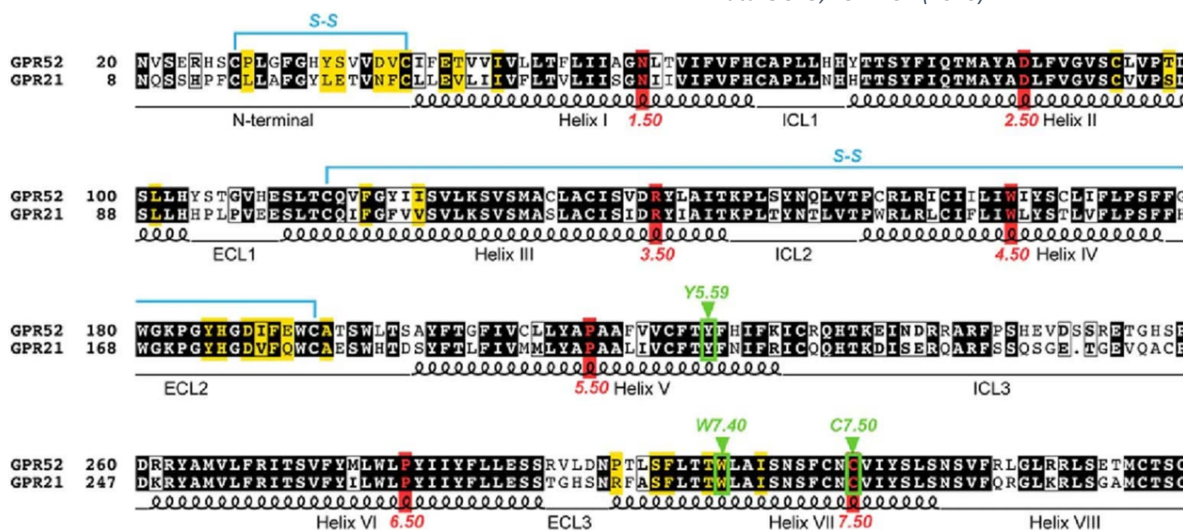


Figure 23 Alignment between GPR52 and GPR21 with the identification of main secondary and tertiary structure features (X. Lin et al., Structural basis of ligand recognition and self-activation of orphan GPR52. Nature 579, 152–157 (2020)

This alignment from the previously cited X. Lin et al. paper also shows the disulphide bonds granting the right conformation of the protein. The disulphide bond between cys114 and cys193 in particular is responsible for the position of the ECL2 in the binding pocket. Checking our model of choice is possible to see that these bonds are preserved.

## 4.2 Docking studies

The aminoacidic residues which constitute the binding pocket in GPR52 are the following, located 12 positions before but conserved in GPR21: Y34, V39, C40, I47, C94, L101, D188, I189, E191, P296, S299, F300 and T303.

By defining the binding pocket of our models, it is possible to perform docking studies with molecules that bind our structures as GRA2 and its analogues. As reported in section 1.4 "GPR21 overview", GRA2 is an inverse-agonist of GPR21, proven to being able of stopping its intrinsic activity. Optimization studies and analogues screenings are needed in order to improve its effective dose, now around 30  $\mu\text{M}$ , that should be in the nanomolar range to represent a good starting point for *in vivo* studies and for a possible use in clinical practice.

### 4.2.1 ADME analysis

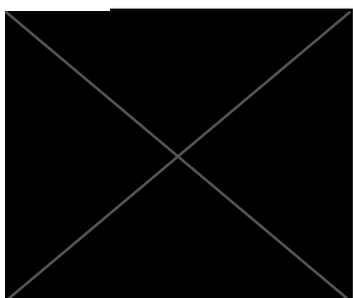
Before to start docking studies it is necessary to perform a chemical analysis of these compounds:

1. **GRA2:** O=C



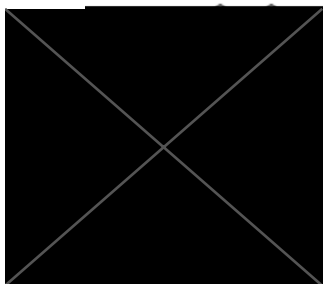
This molecule presents an iLOGP of 3.45 that confers a high GI absorption, good values of absorption and penetration confirmed by the absence of violations of Lipinski's rules. Problematic aspects of this molecule are due to being a P-gp substrate and an inhibitor of several cytochromes<sup>450</sup> such as CYP1A2, CYP2C19, CYP2C9 and CYP2D6.

2.  366: C



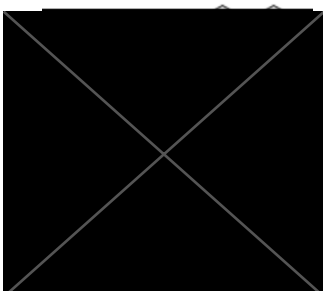
This molecule presents an iLOGP of 3.17 but, despite it presents no Lipinski's rules violations, has a low GI absorption. It does not permeate the blood-brain barrier (BBB), it is a P-gp substrate and inhibits different cytochromes.

3. [REDACTED] 041: [REDACTED]



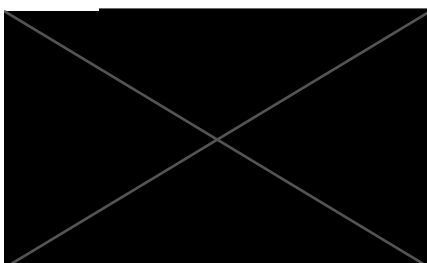
This compound has an iLOGP of 3.49 and even if not all Lipinski's rules are respected (MLogP over 4.15) it presents an high GI absorption and permeates the BBB. As the other analogues it inhibits several cyp450.

4. [REDACTED] 160: [REDACTED]



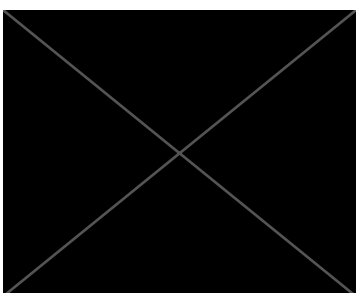
This compound has an iLOGP of 3.30 and even if not all Lipinski's rules are respected (MLogP over 4.15) it presents an high GI absorption and permeates the BBB. As the other analogues it inhibits several cyp450.

5. [REDACTED] 399: [REDACTED]



This molecule presents an iLOGP of 3.59 that confers an high GI absorption, good values of absorption and penetration confirmed by the absence of violations of Lipinski's rules. It is a P-gp substrate, permeates the BBB and inhibits different cyp450.

6. [REDACTED] 582: [REDACTED]



This compound has an iLOGP of 3.53 and even if not all Lipinski's rules are respected (MLogP over 4.15) it presents an high GI absorption and permeates the BBB. As the other analogues it inhibits several cyp450.

50

<i>Compound</i>	<i>MW (g/mol)</i>	<i>MLOGP</i>	<i>Solubility</i>	<i>GI</i>	<i>CYP inhibition</i>	<i>Lipinski</i>
GRA2	369.41	3.99	-5.77	high	yes	yes
-866	462.58	4.04	-6.02	low	yes	yes
-041	339.39	4.63 (!)	-5.73	high	yes	yes (!)
-160	353.41	4.57 (!)	-5.68	high	yes	yes (!)
-399	369.41	3.99	-5.77	high	yes	yes
-582	353.41	4.57 (!)	-5.68	high	yes	yes (!)

Figure 24 GRA2 and analogues ADME analysis summary table

#### 4.2.2 Binding pocket



Figure 25 GRA2 docked in model-2014; grid: -7.91, -9.44 and 17.6.

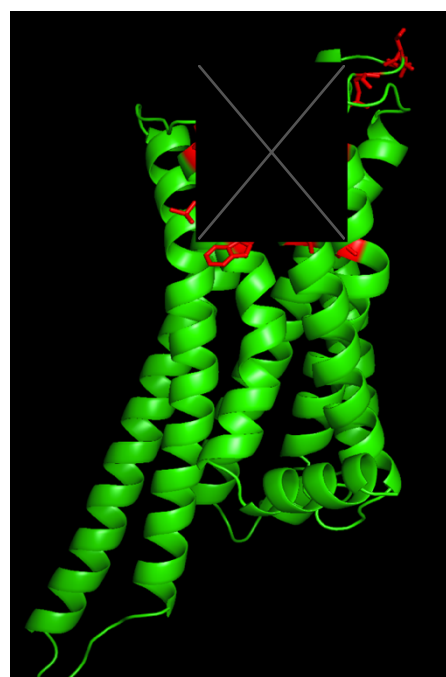


Figure 26 GRA2 docked in model-5mzj; grid: -25.28, 9.51 and 13.74.

The first image (fig. 25) shows the docking of GRA2 in the Model-2014 of GPR21. The docking, knowing the aminoacidic residues of the binding pocket, was possible by defining a docking grid using Schrödinger's Maestro and Mcule<sup>ε</sup> tools. The affinity was assessed with a value of -9.1, goodness of the binding improves with negatives values. Using Pymol is possible to color

the amino acids of the binding pocket highlighting them and showing the main interactions with the compound.

The same docking has been done with GRA2 bonding model generated from 5mzj (*fig. 26*), the result shows a similar affinity (-8.4) between the compound and the binding site. Important difference between the two dockings is the binding site position, central in model-5mzj and lateral in model-2014.

Binding affinity was assessed for GRA2 binding the AlphaFold predicted model and a lower affinity was found, -7.0.

To further understand the binding pocket an analysis of our models was carried out with PrankWeb<sup>7</sup> binding site predicting tools.

The model-5mzj's binding pocket responsible for the described docking of GRA2 has a pocket percentage score of 8.11%, 0.27 as probability score and it is shown in image (*fig 27*), and it represents one of the most probable binding sites for this model.

Analyzing the clusters in detail it is possible to find that all the residues responsible for the potential binding, predicted by *X. Lin et al.* or not, are possible sites of binding.

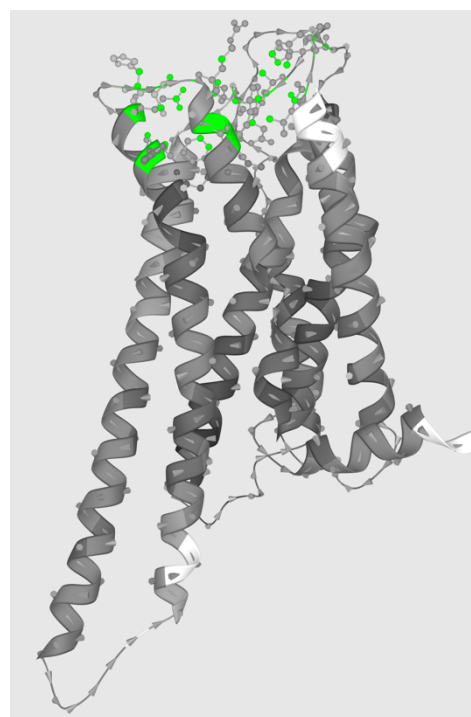


**Figure 27** Model-5mzj's binding pocket defined with PrankWeb

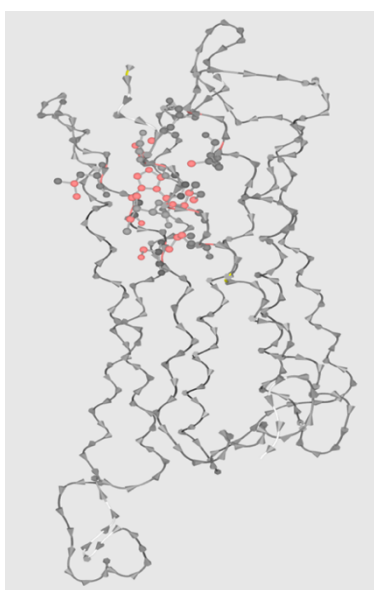


**Figure 28** First model-2014 binding site identified with PrankWeb

Same analysis has been made on model-2014 (*fig. 28 and 31*) finding two noteworthy binding sites.

The first one matches the one involved in the binding of GRA2 represented in figure (*fig. 25*) and presents a score of 4.41% and a probability score of 0.098.

Even if this binding pocket is the one that better includes the residues described by *X. Lin et al.* the low probability value of this analysis requires a further search for better docking sites, possibly in a similar position to the one described in the model-5mzj.





Figure 29 Schematic representation of fig. 28 binding pocket on GPR21 sequence

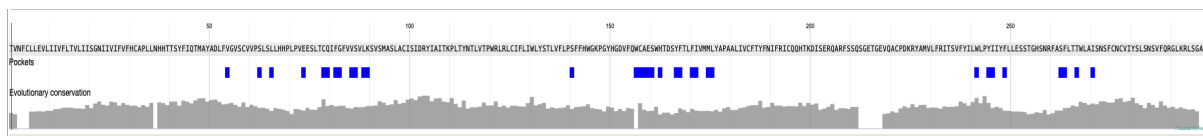


Figure 30 Schematic representation of fig. 31 binding pocket on GPR21 sequence

The second binding site identified in model-2014 and relevant in this work is the one reported in figure (fig. 31.).

Presenting a score of 40.52%, a probability score of 0.915 and a central position it is possible to assume that this binding pocket represents the orthosteric binding site for this model and the first one (fig. 28) describes a side binding site.

The presence of a side pocket was already observed by X. Lin *et al.* in GPR52. In GPR52 the formation of a side pocket, different from the canonical orthosteric binding site, was due to the N-terminal loop and ECL2 that pushed the ligand towards one site.

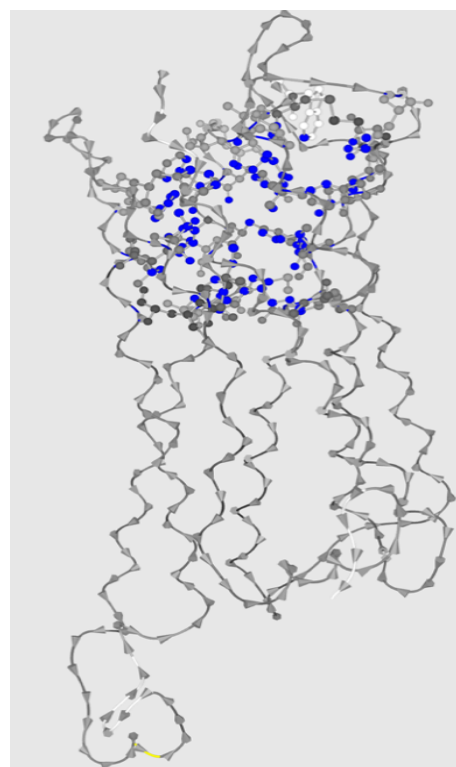
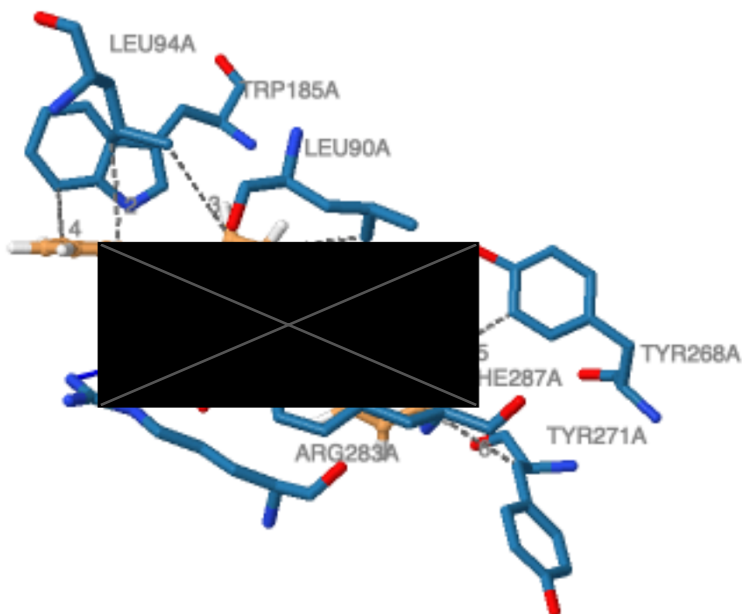


Figure 31 Second model-2014 binding site identified with PrakWeb

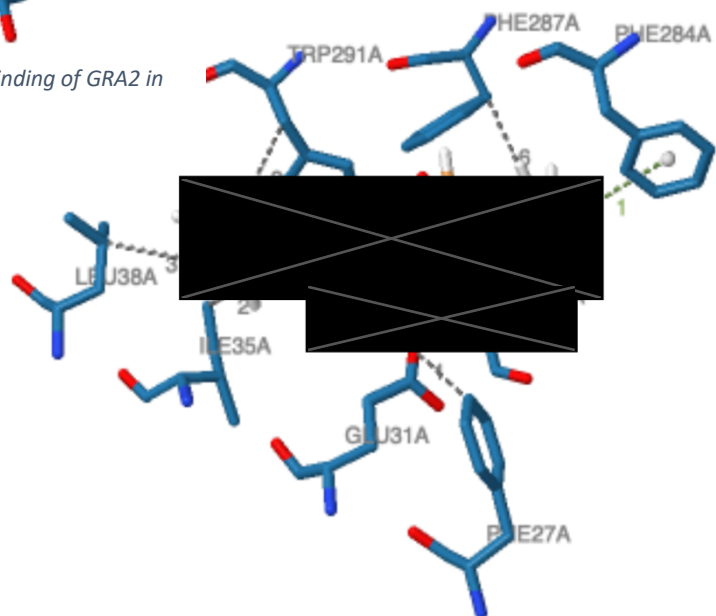
#### 4.2.3 Interactions analysis

To better understand the affinity values given for the different models and compounds it is necessary to further investigate the interactions that take place in the binding pocket. Starting with the binding between our main compound GRA2, model-5mzj (fig. 32) and model-2014 (fig. 33) the following interactions can be identified:



- Hydrophobic interactions: Leu90, Leu94, Trp185, Tyr268, Tyr271 and Phe287.
- Hydrogen bonds: Arg283.

Figure 32 Analysis of the interactions occurring in the binding of GRA2 in model-5mzj



- Hydrophobic interactions: Phe27, Ile35, Leu38, Leu90, Phe287 and Trp291.
- Hydrogen bonds: Glu31.
- $\pi$ -stacking: Phe284.

Figure 33 Analysis of the interactions occurring in the binding of GRA2 in model-2014



Figure 34 Binding of GRA2 in model-2014; grid - 5.45, -9.0 and 17.57

In order to force the docking in the orthosteric pocket it was performed with a smaller grid obtaining a conformation in which the predicted interactions are observed even if the affinity was lower, -7.9. To be noted that there are no interactions with TM1, as in model-5mzj confirming that is the N-terminal region that may have a role in forcing the ligand in a secondary side pocket.

- Hydrophobic interactions: Leu89, Leu90, Ala182, Phe284, Phe287.
- Hydrogen bonds: Ser184 and Phe287.

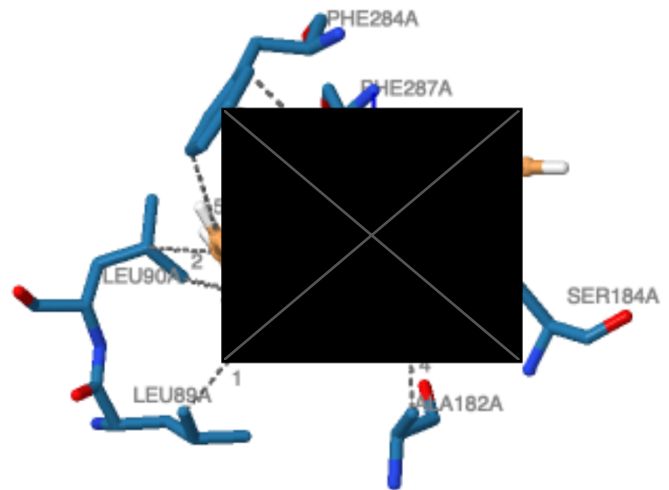


Figure 35 Analysis of the interactions occurring in the binding of GRA2 in model-2014; grid -5.45, -9.0 and 17.57

Analyzing which aminoacidic residues are responsible for the interactions it is possible to discriminate between the ones expected to play a key role in binding and the ones not. Identifying the amino acids previously assumed by *X. Lin et al.* to characterize the bond (green) and the ones that are very close to them in the aminoacidic sequence (orange) seems that model-2014 presents more of the predicted interactions, in both the docking models.

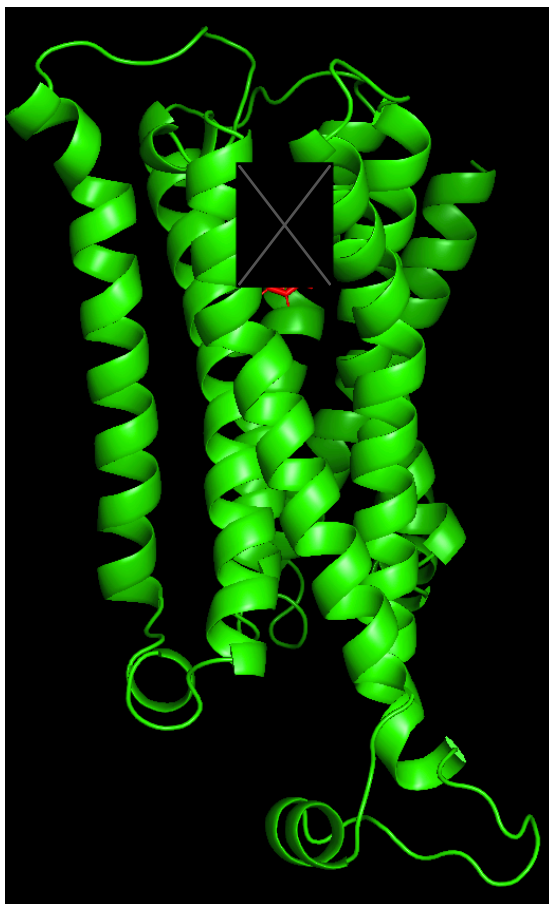


Figure 36 Binding of GRA2 in model-5zhp

To further asses the location of the orthosteric binding pocket, a docking was performed in model-5zhp and the interactions between GRA2 and the receptor were analyzed.

As shown in the picture the central position of the binding site is quite similar to the one identified in the previous models and the interactions are in the predicted regions with an affinity score of -7.7.

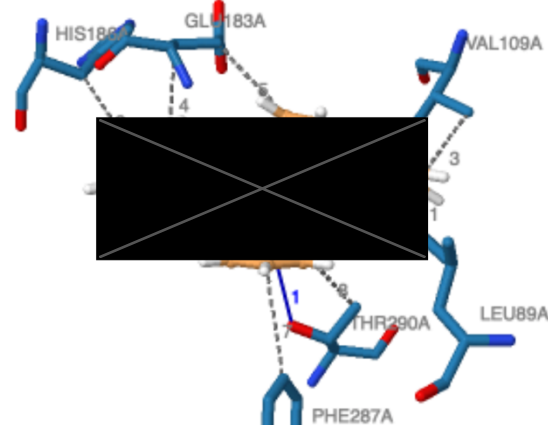


Figure 37 Analysis of the interactions occurring in the binding of GRA2 in model-5zhp

#### 4.2.4 Analogues docking

<sup>51</sup>Potency is an expression of the activity of a drug in terms of the concentration or amount of the drug required to produce a defined effect and it is strictly related to dissociation constant of the drug and its specific receptor. GRA2 was found to be effective in inhibiting GPR21's constituent activity but analogues are to be tested because of the high EC<sub>50</sub> of GRA2.

Compounds	Affinity mod-14	Hydrophobic interactions	Hydrogen bonds	Π-stacking
GRA2	-7.9	Leu89, Leu90, Phe179, Ala182, Trp185, Phe284, Phe287.		
-866	-8.3	Leu89, Leu90, Phe284	Ser184	
-041	-8.8	Leu89, Leu90, Ala182, Phe284, Phe287	Ala182	
-160	-10.9	Val109, Lys113, Glu183, Ile195, Met198, Leu199, Trp265, Tyr268, Ile269, Thr290, Ile294	Glu183	Phe272
-399	-9.3	Ile35, Leu90, Pro93, Phe284, Trp291	Phe284	Phe284, Trp291
-582	-9.7	Leu89, Leu90, Ala182, Phe284, Phe287	Ala182, Ser184	

*Figure 38 Table of the affinity values and interactions of GRA2 and analogues in model-2014*

From the analysis of the previous table, it is possible to see how there is a trend in increasing the affinity between the analogues of GRA2 and the model of GPR21. Given that the biggest problem of GRA2 is the high concentration needed in vitro to be effective the higher affinity of the analogues can be promising of a lower concentration required.

It can be immediately seen that the compound -160 has the best score and presents interactions in the expected regions but with some differences in the residues. By putting

these residues in the docking process, to produce a new grid, it is possible to dock GRA2 in the same position of compound 160 and find a higher affinity (-10.8). The same increase in affinity can be seen by docking GRA2 with MAESTRO Schrodinger using the new coordinates: from -6.59 to -7.92.

By superimposing the dockings (fig. 39) of -160 and GRA2, and verifying the residues



Figure 39 Superimposed dockings of -160 and GRA2 in model-2014

responsible for the interactions, it is possible to assess that the binding pocket is still the orthosteric one previously identified with PrankWeb and, even if presenting the residues identified in GPR52, here the binding site is in a slightly deeper portion of the receptor. The difference in binding site may be due to the steric space of antagonist molecules, higher than the one of the agonist studied in relation of GPR52. By performing the dockings with Schrodinger MAESTRO using the new coordinates almost all the compounds (-582 and -399 deviate from this trend) show a higher affinity.

The presence of a higher affinity site in GPR21 can be identified even by changing the coordinates of the grid in model-5zhp finding a new affinity score of -9.1 instead of -7.7.

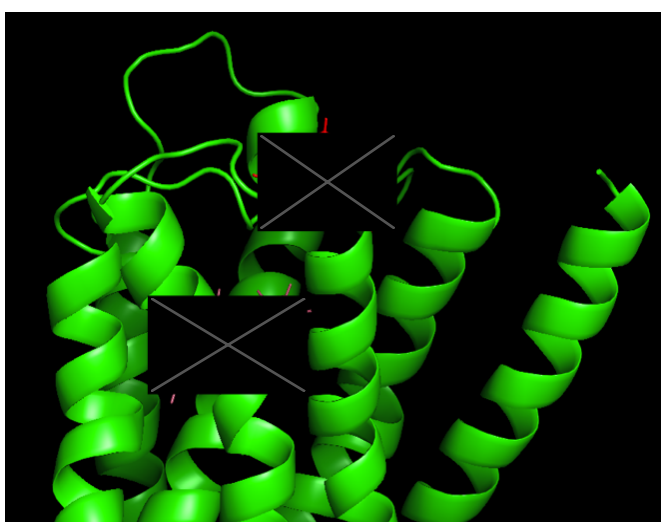


Figure 40 Different positions of GRA2 in model-2014's binding pocket

COMPOUNDS	AFFINITY MOD-2014 (NEW COORDINATES)
GRA2	-10.8
-866	-10.8
-041	-10.1
-160	-11.1
-399	-11.0
-582	-11.0

Figure 41 Resumptive table of the affinity values of GRA2 and analogues in model-2014 using the new coordinates

To better assess the trend of improving affinity showed by the analogues previously examined docking studies were performed on model-5zhp building a grid using the residues identified compound -160 in model-2014.

Compounds	Affinity mod-5zhp	Hydrophobic interactions	Hydrogen bonds	$\Pi$ -stacking and $\Pi$ -cation
GRA2	-9.1	Lys113, Ile195, Val196, Trp265, Tyr268, Phe272, Thr290, Ala293	Glu183, Tyr268	His186, Tyr268, Phe272, Ile113
-866	-9.6	His186, Thr192, Ile195, Val196, Leu199, Trp265, Ile269, Phe272, Ala293	Lys113, Glu183	Tyr268, Phe272
-041	-9.9	Val109, Lys113, Ile195, Val196, Leu199, Tyr268, Ile269, Phe272	Val109	
-160	-10.1	Leu89, Phe105, Val109, Trp265, Tyr268, Ile269, Thr290, Ala293	Glu183, Tyr268	
-399	-9.6	Val109, Lys113, His186, Thr192, Ile195, Val196, Leu199, Tyr268, Phe272, Ala293	Glu183, Tyr268	Trp265, Phe272, Lys113
-582	-9.5	Lys113, Phe161, Ile195, Val196, Leu199, Tyr200, Tyr268, Ile269, Phe272, Thr290, Ala293	Glu183, Tyr268	

*Figure 42* Resumptive table of the affinity values of GRA2 and analogues in model-5zhp using the new coordinates

As it is possible to see in the table the trend of increasing affinity is maintained in this model too and compound -160 is again the most affine.

#### 4.2.5 Tautomers docking

All of the six compounds analyzed present two tautomeric forms, in order to assess if the receptor presents a pattern of higher affinity for a specific tautomeric form, docking studies were performed for both the isoforms using Schrödinger MAESTRO.

Compound	Tautomer A	Tautomer B
GRA2	-6.59	-7.22
-866	-3.86	-4.04
-041	-4.72	-6.48
-160	-5.68	-5.50
-399	-6.06	-4.63
-582	-7.58	-6.48

Figure 43 Resumptive table of the affinity values of GRA2 and analogues in model-2014 using the new coordinates

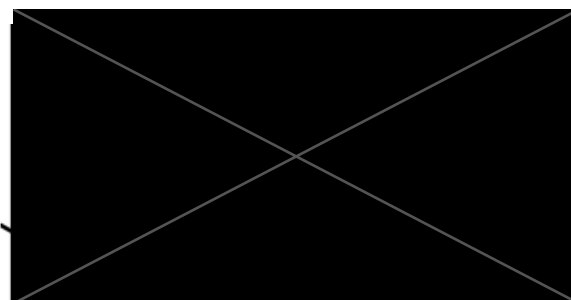
It is possible to find some differences in the affinity values of the two isoforms even if not particularly relevant in almost all the compounds. Nevertheless, is to be noted that performing the dockings with this program the trend of increasing affinity from GRA2 trough the different compound is not confirmed, requiring further *in vitro* studies to assess the potency of the different compounds.

#### 4.2.5 Compounds screening

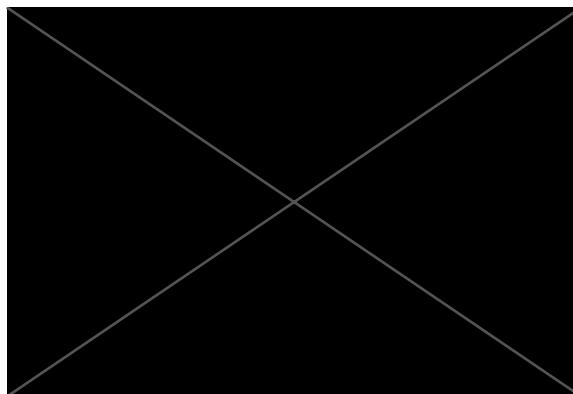
Using GRA2 and compound -160 a further screening of analogues compounds was performed to assess if a higher affinity can be obtained.

Starting with GRA2 structure, two considerations can be made:

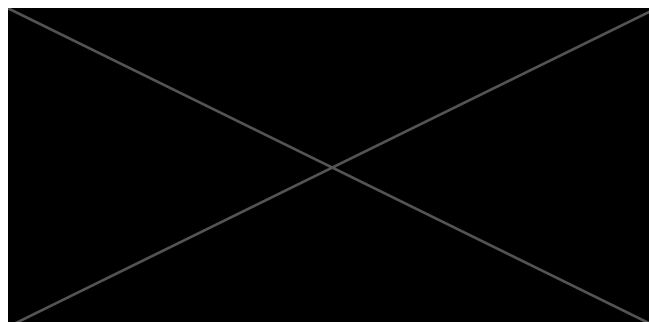
1. The fused rings system appears to be important for the affinity, when the second ring is removed the binding shows a lower affinity: -10.2.



2. It appears to be an available docking space near the fused aromatic rings, the introduction of little lipophilic substituents on the second rings improves the affinity of the GRA2's scaffold: -11.6.



The affinity gets even higher with a slightly bigger lipophilic substituent: -11.8.



Using compounds-160 scaffold it is possible to see the same affinity values adding two little lipophilic substituents on the other portion of the molecule, suggesting the presence of others binding possibilities little deeper in the pocket.

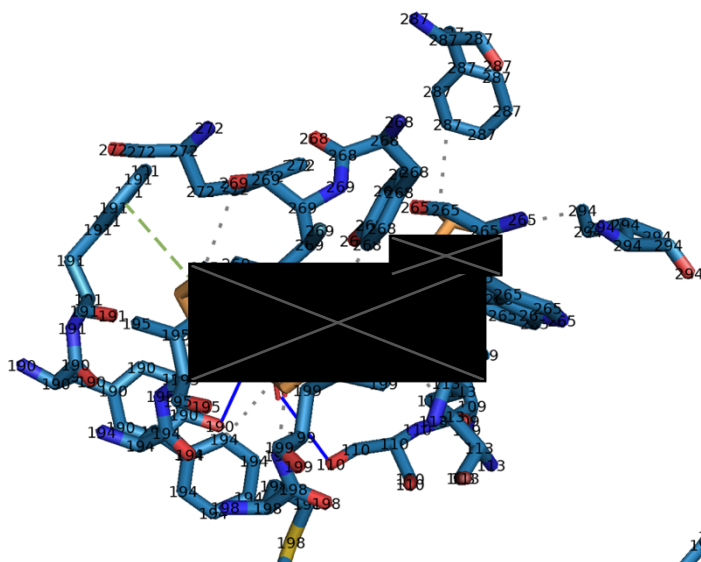


Figure 44 Analysis of the interactions occurring in the binding of the hypothesised compound1 in model-2014

interactions with residues in TM7. These residues were identified by X. Lin et al. and they were characteristic of the first region identified in this binding pocket.

Analyzing the new interactions responsible for the increase in the affinity is it possible to identify that this molecule presents again

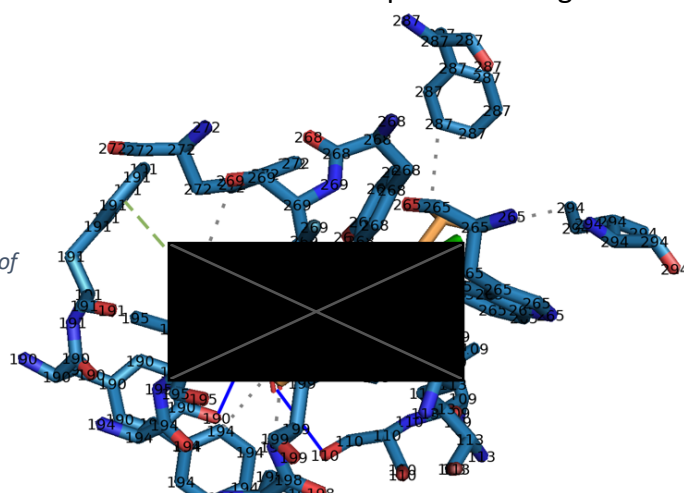
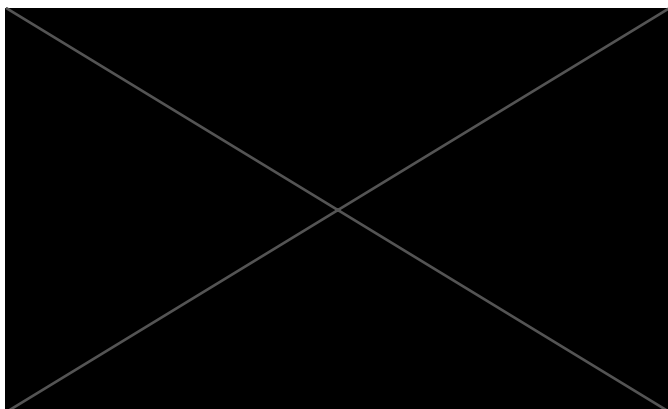


Figure 45 Analysis of the interactions occurring in the binding of the hypothesised compound2 in model-2014

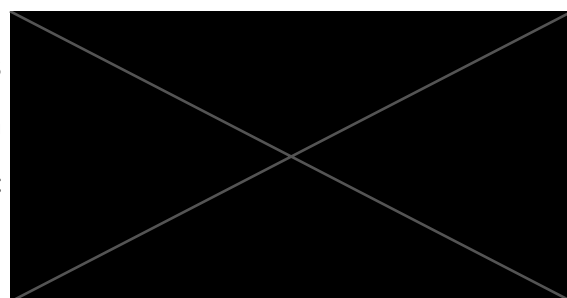


It appears that there are not interactions that directly require the presence of a fused cycles system but probably it is necessary to direct the substituent in the right position.






Merging the steric information from the modifications made to GRA2 and -160 structure it was possible to generate a compound that present added lipophilic substituents in both the ends of the GRA2 structure with an affinity value of -12.9.

The introduction of a small hydrophobic substituent is also possible in alpha of the amidic carbon, resulting in a slight increase in affinity (-11.4), or on the amidic nitrogen with a resultant affinity value of -11.6.



### 4.3 In vitro testing

The more promising compound -160 was tested alongside with   
-399 to assess their activity on HepG2 cells and better understand the possible role of the position of the fused rings system in determining affinity to GPR21.

### 4.4 MTT testing on HepG2 cells treated with -160 and -399

Before testing the activity of the described compounds their toxicity was assessed on HepG2 cells, cell line of election for the present work.

The chosen test is the MTT test, a colorimetric assay capable of measuring metabolic activity as indicator of cell viability, proliferation and cytotoxicity (*cf. Materials and methods 3.3*).

The assay was repeated different times (n=6) to guarantee repeatability and variability to the results.

The HepG2 cells were plated in a 96-wells culture plates and, after a period of 24 hours of settling, they were exposed to increasing concentrations of the two selected compounds: from 1  $\mu\text{M}$  to 100  $\mu\text{M}$ . The range chosen includes and ranges from the effective concentrations established for the lead compound, GRA2.

After treating the HepG2 cells with the compounds for 24 hours the medium was removed and the cells viability and health evaluated both morphologically, before adding the MTT solution, and then reading the absorbance of the following solubilized formazan solution.

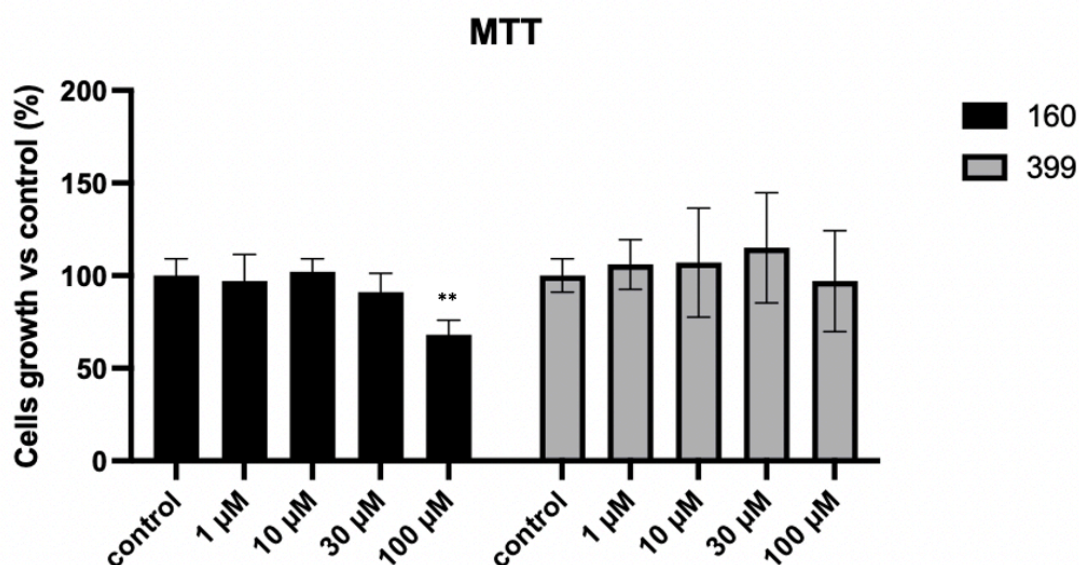




*Figure 46 Absorbance values of the MTT test performed after the administration of -160 and -399, on HepG2 cells under basal conditions, related to a non-treated control: the concentration of 100  $\mu\text{M}$  of -160 appears to be significantly toxic. \*\*= $P < 0.01$  vs control.*

For what concern the first compound analyzed, -160, the cells appeared healthy and presenting the usual morphology up to 30  $\mu\text{M}$ . Starting with the concentration of 100  $\mu\text{M}$  of the compound, signs of suffering appeared in form of spikes and residues of dead cell bodies. The observations were confirmed by the spectrophotometer lectures that showed absorbance values similar to the control ones, not stimulated with our compound, for all the wells presenting concentrations up to 30  $\mu\text{M}$ . The values of the wells containing the cells exposed to 100  $\mu\text{M}$  of AK-918/40762160 presented a clear trend of suffering with a decrease of the absorbance values over thirty percentage points.

Different trend was observed testing the second compound, -399, that again showed no signs of toxicity up to 30  $\mu\text{M}$  with absorbance values comparable to the control ones.

The toxicity on the higher concentration, 100  $\mu\text{M}$ , was not evident observing the cells with the microscope and the absorbance values did not reach significant values remaining over the 90% of the control.

#### 4.5 $\text{Ca}^{2+}$ release assay



This assay was performed to screen our compounds and, in this work, the evaluations about 160 and 399 are reported.

Before testing the compounds, a protocol for the assay was defined (*cf. Material and methods 3.6*) leading to plate 40000 cells per well in a black 96-wells culture plates without the use of pluronic.

As described in the previous section, the readings of the compounds were always reported to the ones following the cells exposure to a Triton X solution. The Triton X was used to normalize the results and granting homogeneity in the number of cells plated.

The readings were performed in kinetic mode in order to assess the timing of action of the compounds but only the best values for each compound and time are reported and normalized using the Triton X and control values.

All the compounds were administrated with a final concentration of 10  $\mu\text{M}$  and each experiment was repeated 3 times.

Compound	Compound/Triton X (A)	Control/Triton X (B)	A/B
 160	65%	84%	78%
	74%	90%	82%
	46%	63%	72%
 399	46%	63%	72%
	73%	90%	82%
	84%	84%	100%

**Figure 47** Resumptive table of the percentages of compound/triton (A), control/triton (B) and A/B deriving from the calcium release assay for -160 and -399

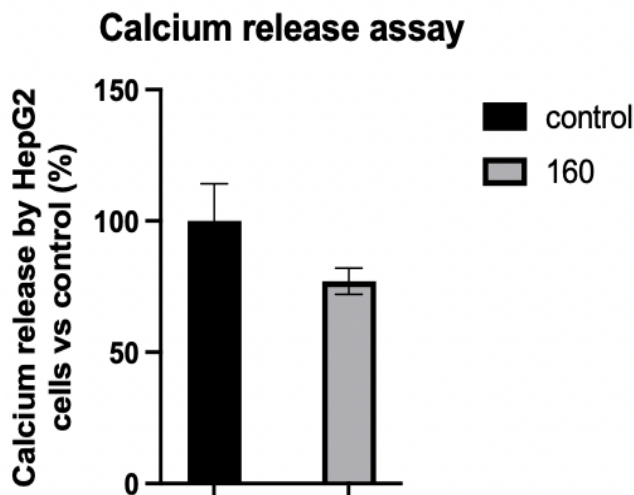


Figure 48 Graphic representation of the reduction in calcium release following administration of -160 vs control

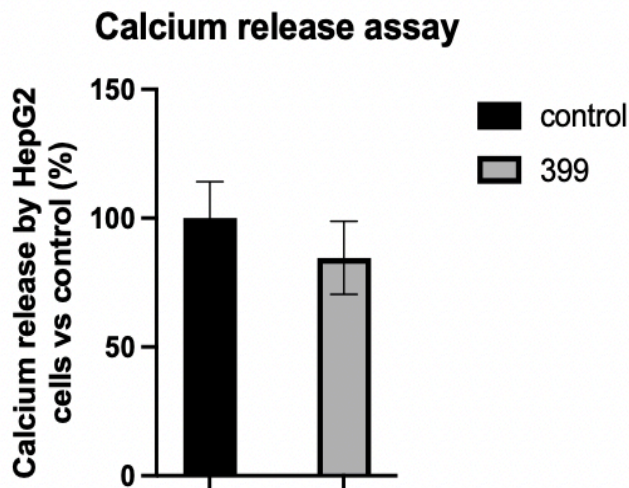


Figure 49 Graphic representation of the reduction in calcium release following administration of -399 vs control

	Type of test	P value	Significance (P < 0.05)
-160	Two-tailed t test	0.0569	No
-399	Two-tailed t test	0.2543	No

Figure 50 Table of the statistical analysis of the results deriving from the calcium release assay using -160 and -399

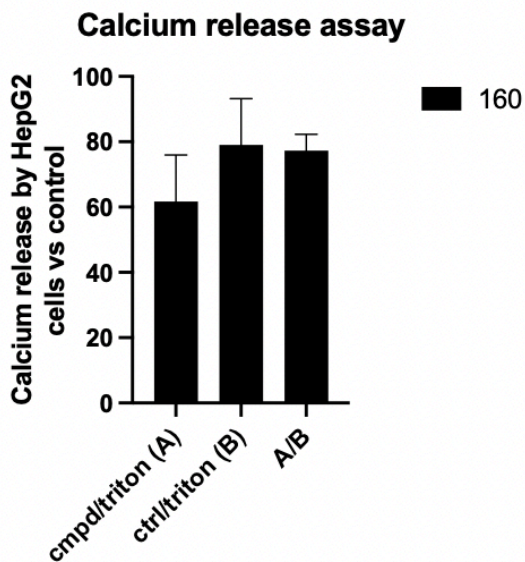


Figure 51 Graphic transposition of fig. 47 (-160)

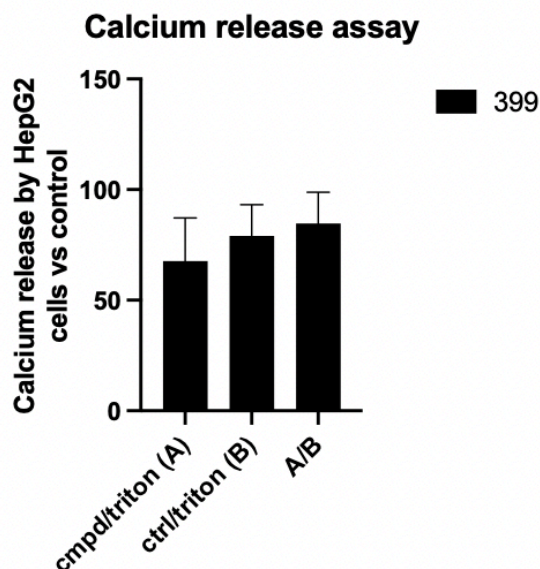


Figure 52 Graphic transposition of fig. 47 (-399)

The readings of the first compound, -160, are consistent with a reduction in the calcium release when compared to the control of basal conditions. The mean of the values obtained for this compound is 77% (+/- 5%) of the control values, indicating a reduction of the 23%.

As shown in *fig. 50* the reduction observed almost reaches the significance ( $p$  value  $< 0.05$ ) when compared to the control, scoring a  $p$  value of 0.0569 when analyzed with a t-test.

Less linear trend of values was observed for the compound -399 that showed a similar tendency (in relation to the first compound) in the first two experiments, not confirmed in the  $n=3$  in which seemed to have no effect in calcium release reduction.

Considering the triplet of readings this compound shows a mean reduction from the control's calcium release of 15% (+/- 14%).

In order to have a further reference for the analysis of these two compounds activity, the HepG2 cells were stimulated with the first effective concentration of GRA2: 10  $\mu$ M.

Compound	Compound/Triton X (A)	Control/Triton X (B)	A/B
GRA2	77%	90%	86%
	53%	63%	84%
	81%	82%	99%

Figure 53 Resumptive table of the percentages of compound/triton (A), control/triton (B) and A/B deriving from the calcium release assay for GRA2

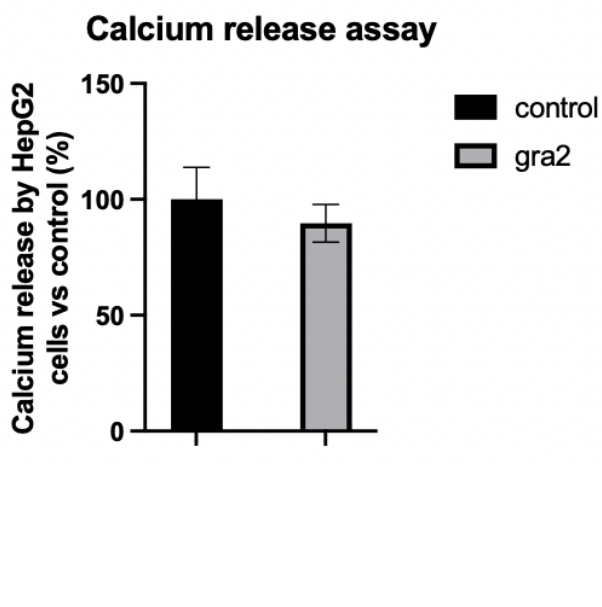


Figure 54 Graphic representation of the reduction in calcium release following administration of GRA2 vs control

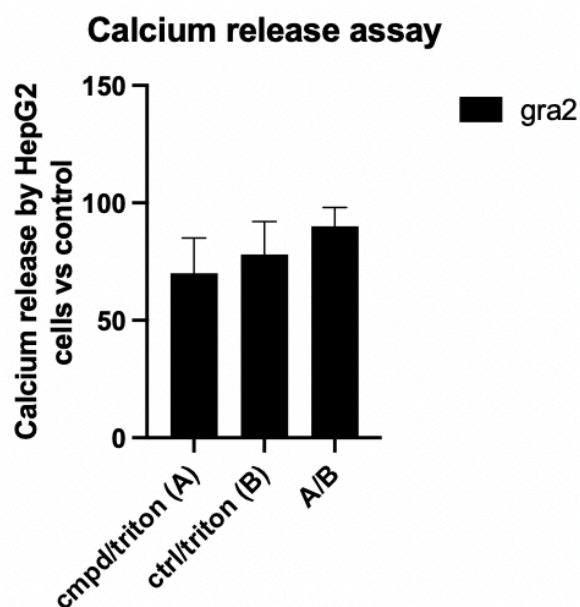


Figure 55 Graphic transposition of fig. 53

	Type of test	P value	Significance (P < 0.05)
GRA2	Two-tailed t test	0.3283	No

*Figure 56 Table of the statistical analysis of the results deriving from the calcium release assay using GRA2*

The same analysis performed for the two analogues, -160 and -399, is reported for the lead GRA2. As for -399 a trend in diminishing the calcium release was observed only for the first two experiments but no improvements were registered in the n=3.

Analyzing the three analyses the overall mean is of 90% (+/- 8%) out of the control of calcium release after GRA2 administration.

#### **4.6 Insulin resistance states generation: prolonged insulin exposure**

Following the methods described in the previous section (*cf. Material and methods 3.7*) and in order to evaluate the molecular consequences of insulin resistance states in HepG2 cells, those were induced with both high glucose medium exposure for different periods of time and with prolonged insulin exposure.

For the approach described in the present work the cells were treated with insulin 100 nM for 24 hours in both DMEM high glucose (HI) and DMEM low glucose (LI) and controls were used for both the high glucose condition (CH) and the low glucose one (CL).

##### **4.6.1 GPR21 expression in IR states**

As first assessment the protein extract was analyzed with a western blotting technique investigating the expression of GPR21 to determine if there were variations in IR states when compared to a control where no damage was induced.

All the data were normalized determining the presence of structural proteins, as the tubulin, that should be always present in a protein extract and not affected by treatments.

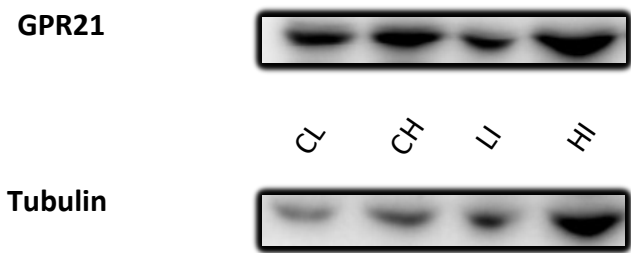


**Figure 57** Western blot results for GPR21 and tubulin CL, CH, LI and HI.

Each immunoblot is from a single experiment and is representative of three.

	n=1	n=2	n=3
HI/CL	61%	83%	57%
CH/CL	114%	100%	97%
LI/CL	73%	99%	59%

**Figure 58** Resumptive table of the percentages of the variation in GPR21 expression after 24 hours exposure to high glucose (CH), 100nM insulin (LI) and high glucose with 100nM insulin (HI). Densitometric analysis of the bands is expressed as relative optical density, corrected for the corresponding tubulin contents, and normalized using the related control band.

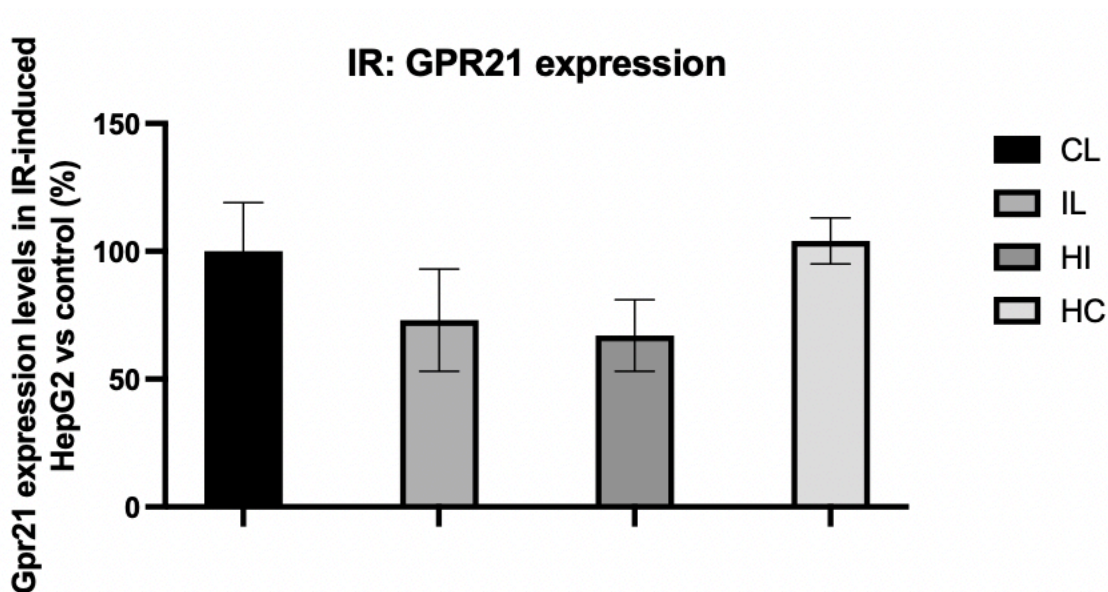


**Figure 59** Graphic transposition of fig. 58

After the analysis of the protein extract, deriving from HepG2 cells treated with insulin 100 nM for 24 hours, there was observed no increase in GPR21 expression.

From this analysis a mean value of 67% (+/- 14%) of GPR21 expression on the low glucose control was registered when the cells were exposed to insulin for 24 hours in DMEM high glucose.

#### 4.6.2 Insulin pathway activation in IR states

After exposing the HepG2 cells to the same conditions of high glucose and high insulin for 24 hours, the degree of activation of the insulin pathway was assessed investigating the levels of phosphorylated Akt (on Ser473) present in the extract. The suitability of HepG2 cells in investigating the insulin signaling pathway was previously assessed by *Sefried S. et al. (2018)*<sup>52</sup>. The experiment was repeated only two times (n=2) because the results were consistent and showed no signs of insulin pathway impairment.

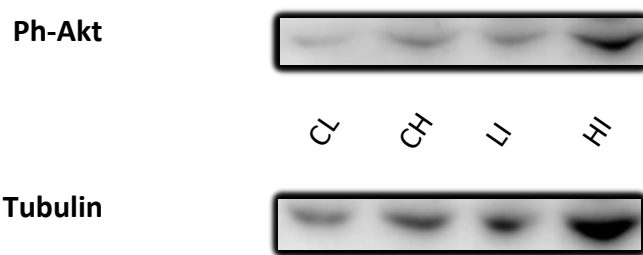


**Figure 60** Western blot results for Ph-Akt and tubulin CL, CH, LI and HI.

Each immunoblot is from a single experiment and is representative of two.

	CH/CL	LI/CL	HI/CL
Ph-Akt	121%	126%	125%

**Figure 61** Resumptive table of the mean percentages of the variation in Akt phosphorylation with different treatments (CH, LI and HI) versus CL control. Densitometric analysis of the bands is expressed as relative optical density, corrected for the corresponding tubulin contents, and normalized using the related control band.

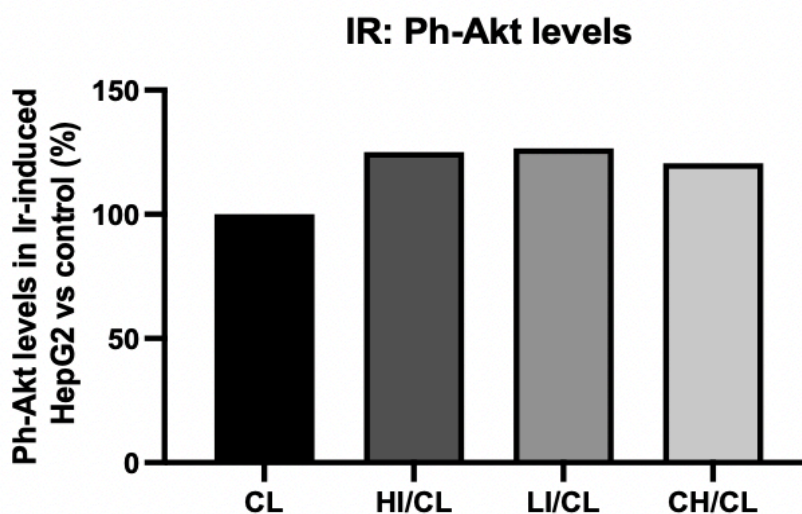


**Figure 62** Graphic transposition of fig. 61



From the analysis of the Ph-Akt presence in the extract, normalized using the tubulin values, it seemed to be slightly augmented compared to the control, indicating a trend towards an increase in the insulin pathway activation.

#### **4.7 Insulin pathway activation in IR states with 10 minutes insulin chase**

The analysis previously described (*cf.* 4.6.2) was repeated adding a final chase of insulin 100 nM before the extraction in order to better observe the effects of the IR model, 24 hours high glucose and high insulin medium, on the insulin pathway.

The insulin signaling pathway results relevantly activated after the chase amplifying the eventual differences between the damage model and the control.

As marker of election for the insulin signaling pathway activation Ph-GSK3 $\beta$  was chosen. As Ph-Akt the phosphorylation of this mediator indicates the activation of the insulin pathway (*cf.* 1.1.2 "Principal players") but, being in hepatic cells, Ph-GSK3 $\beta$  assumes an even greater significance for its role regarding the glycogen synthase (GS). The insulin pathway activation leads to the phosphorylation of the GSK3 $\beta$  (on Ser9) and its inactivation. Once phosphorylated this kinase stops blocking the action of the GS, which can synthesize glycogen from glucose, reducing its blood levels.

Ph-GSK3 $\beta$  levels were assessed after both the IR models: 72 hours of high glucose medium and 24 hours high glucose and high insulin medium.

The analysis was also performed after the stimulation with the chosen compounds, GRA2, -160 and -399, used at 10  $\mu$ M verifying if they showed a protective effect in terms of an increased phosphorylation of GSK3 $\beta$ .

Starting with the 24 hours high glucose and high insulin exposure the following mean values were found (n=2).

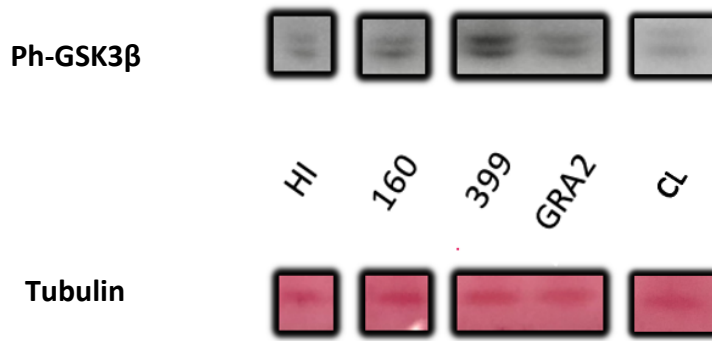


**Figure 63** Western blot results for Ph-GSK3 $\beta$  and tubulin HI and HI with 160, 399 and GRA2 administration.

Each immunoblot is from a single experiment and is representative of two.

	-160/HI	-399/HI	GRA2/HI	CL/HI
<b>Ph-GSK3<math>\beta</math></b>	1.12	1.16	1.03	0.89

**Figure 64** Resumptive table of the mean values (n=2) of the variation in GSK3 $\beta$  phosphorylation with different treatments (160, 399 and GRA2) versus HI control after 24 hours high glucose and high insulin exposure. Densitometric analysis of the bands is expressed as relative optical density, corrected for the corresponding tubulin contents, and normalized using the related control band

### IR w/ insulin chase: Ph-Gsk3 $\beta$ levels

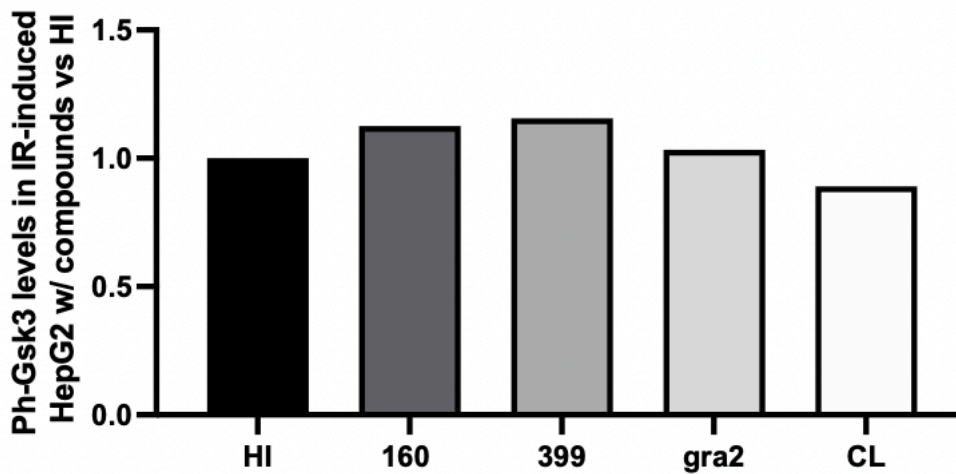


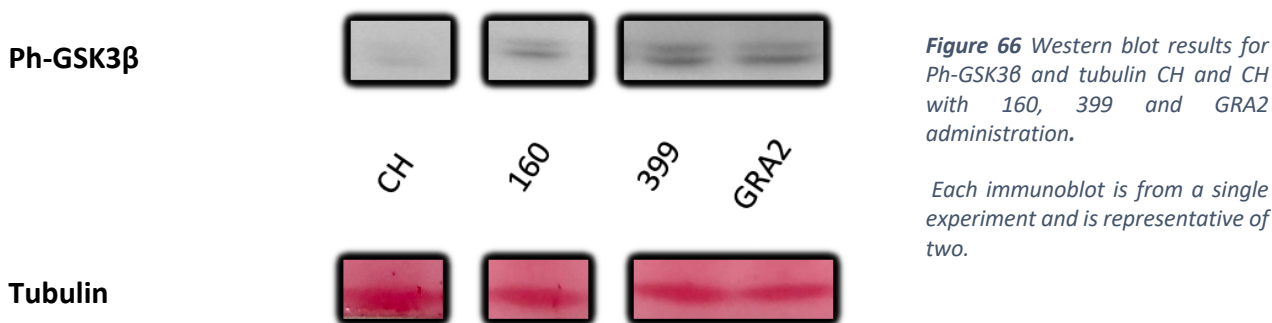
**Figure 65** Graphic transposition of fig. 64

From the analysis of the western blot results, the insulin chase confirmed the trend observed (cfr. 4.6.2) in which the model's protocol is not sufficient to impair the insulin pathway, which results almost equally activated after 24 hours in high glucose and high insulin medium (HI) and in the low glucose no insulin control (CL).

The compounds tested did not show a significant increase in activating the insulin pathway but compounds -160 and -399 still resulted in a slightly augmented phosphorylation of GSK3 $\beta$ . GRA2 showed moderately lower values, comparable to the HI condition ones.

The analysis just described was then repeated using the 72 hours high glucose exposure model, finding the following mean values (n=2).

For this analysis the treatments with the compounds were related to the high glucose control because, from studies performed by our research group, the 72 hours high glucose exposure showed an increment of GPR21 expression but no impairment of the insulin signaling pathway, rendering the high and low glucose controls comparable regarding the insulin cascade.



	-160/CH	-399/CH	GRA2/CH
<b>Ph-GSK3<math>\beta</math></b>	2.63	2.67	3.99

*Figure 67 Resumptive table of the mean values (n=2) of the variation in GSK3 $\beta$  phosphorylation with different treatments (160, 399 and GRA2) versus CH control after 72 hours high glucose DMEM exposure. Densitometric analysis of the bands is expressed as relative optical density, corrected for the corresponding tubulin contents, and normalized using the related control band.*

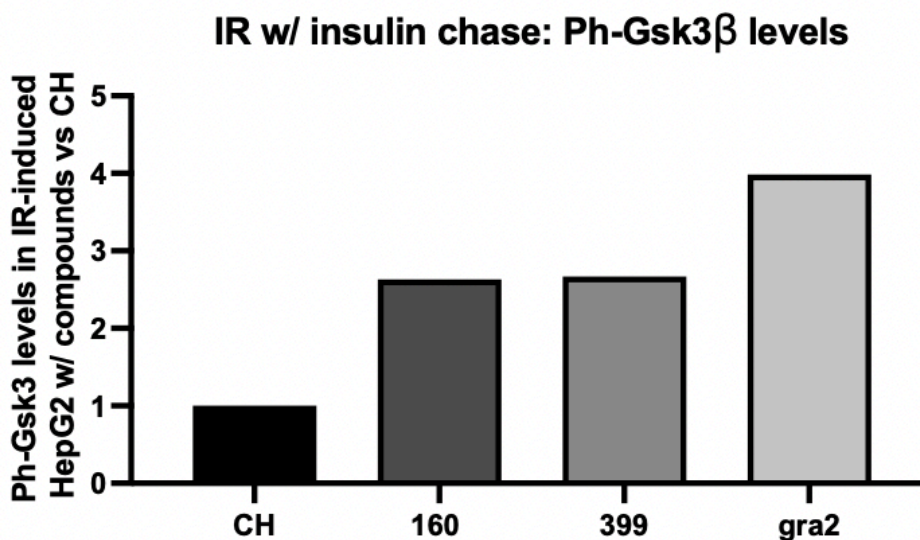


*Figure 68 Graphic transposition of figure 67*

From the analysis of the values reported, the treatment with all the three compounds considerably ameliorates the insulin pathway activation when compared with the control of cells exposed to a high glucose medium for 72 hours.

GRA2 reaches the best values of GSK3 $\beta$  phosphorylation almost quadruplicating its levels, the analogues -160 and -399 scores similar values over double the CH condition.

## 5. DISCUSSION

### 5.1 Preliminary remarks

Insulin signaling pathway comprehends several molecular mediators contributing to the ultimate function of maintaining the glucose homeostasis. Given its complexity this pathway can be impaired at different levels resulting in insulin resistance states, first among them the diabetes condition.

Diabetes is a disease characterized by high levels of glycaemia that entail, if not correctly treated, a wide range of acute and chronic complications<sup>3</sup>. Most common complications related to diabetes are due to an impaired micro and macro circulation leading, among others, to a significantly augmented risk of infarction or stroke<sup>2</sup>.

The diabetic pathology can have both autoimmune (type 1 diabetes, T1D) or diet-related (type 2 diabetes, T2D) causes. T1D has the exogenous administration of insulin as only available treatment whereas T2D, due to its more complex etiology, presents many possible pharmacological treatments targeting different steps of the pathway.

Despite the large number of therapeutic possibilities, almost half of the patients affected by T2D do not achieve treatment goals requiring further studies for the identification of new antidiabetic compounds.

The abundance of the GPCRs class members<sup>16</sup>, their recognized predisposition to be pharmacological targets and their proven presence in both islets of Langerhans and enteroendocrine cells<sup>21</sup> has rendered these receptors subject of numerous pharmacological studies.

Among the GPCRs one has started to attract particular attention due to its role in the onset and maintenance of insulin resistance states: GPR21<sup>5</sup>.

GPR21 is a constitutive active orphan receptor coupling a Gq protein that activates the PLC pathway promoting calcium release<sup>26</sup>. The activation of MAPK cascade following the calcium release, in particular JNK, is responsible for an impairment of the very first steps of the insulin signaling pathway<sup>27</sup> and for an HFD-induced accumulation of macrophages in mice adipose tissue<sup>5</sup>.

A knockout of GPR21's gene in mice revealed an improved tolerance from developing insulin resistance, a reduced macrophages chemotaxis following a high fat diet and a reduced secretion of inflammatory markers<sup>15</sup>.

*In vitro* studies showed also a direct correlation between GPR21 silencing or blockage, with the inverse agonist GRA2, and an augmented glucose uptake in HepG2 subsequent to an increased translocation of the glucose transporter GLUT-2, further confirmation of the insulin pathway restoration<sup>36</sup>.

In this work the tridimensional structure of GPR21 was investigated and, in particular, its supposed interactions with inverse agonist molecules. Following the analysis of the interactions the aim was to define the predicted affinity of different analogues of the lead compound GRA2, an effective inverse agonist to this receptor but characterized by low potency.

The compounds screened *in silico* were subsequently tested *in vitro* on HepG2 cells and compared to GRA2 to better define the affinity trend previously described and the following toxicological and molecular aspects.

## 5.2 *In silico* studies

Starting with selecting appropriate templates two useful models were built using an adenosine receptor (A2R, model-5mzj) and a muscarinic receptor (M3R, model-5zhp) in addition to the previous one based on two  $\beta$ 2-adrenergic receptors (model-2014). Being all the templates crystallized in association with an antagonist and representing different types of receptors, they can potentially describe a wide range of GPR21's aspects and reactivity.


These three templates all belong to the family A GPCRs (rhodopsin-like receptors) as GPR21, and in particular the M3 receptor couples with a  $G_q$  protein as GPR21 and it has been related to the onset of T2D (*Gautam D. et al., 2007*)<sup>53</sup>, therefore they can be considerate reliable predictive tools in generating models of GPR21 and simulating its activity.

Analysing the tridimensionality features of these models they all obtain quality scores over the 95% with few stereochemical warnings in portions that are supposedly far from the binding site and should not affect the predictive quality of the models.

The only known molecule binding GPR21 is GRA2, an inverse agonist which effectiveness has been proved at concentrations of 10 to 30  $\mu\text{M}$  (*cf.* *GPR21 overview 1.4*). Being the concentration needed to a drug to be a suitable candidate for *in vivo* studies in the range of the nanomolar, a series of analogues have been tested searching for higher potency, deriving from an increased affinity to GPR21 binding pocket. In this work the binding site of this receptor was investigated starting from previous work on similar receptors (specifically GPR52) by performing docking studies of GRA2 and five analogues using the three models generated and previously described.

From a first analysis the data reported in this work (*cf.* *binding pocket 4.2.2*) suggest the presence in GPR21 of a side pocket, compatible with the one previously observed in GPR52<sup>49</sup> (receptor with 71% of sequence homology with GPR21), with a non-negligible affinity for our compounds.

These data could indicate a competition between the orthosteric binding pocket and the side pocket for the binding of these ligands, and in particular could partially explain the high doses of GRA2 required in order to reach effectiveness. Molecules without significant difference in affinity values between these two sites may subdivide between the two pockets decreasing in potency. Further studies about the dissociation constant values may be required to assess if the side pocket could significantly affect compounds potency.

Once redefined the binding grid in order to allow the compounds to bind the orthosteric pocket, from a comparison between the affinity values of the analogues and GRA2, it appeared that all the five compounds had higher affinity than GRA2 for our receptor, in particular the compound 160.

By analyzing the interactions occurring between the different compounds and the aminoacidic residues in our models binding site, a different pattern of bonds was observed in the docking of -160, the compound with higher affinity.

A comparison in the position of the docked molecules showed two levels of interactions inside of the same orthosteric pocket previously defined: a higher one for almost all the compounds and a deeper one for -160.

Using the interactions occurring in -160 bonding as coordinates for a new binding grid, a portion of the binding pocket with higher affinity values was identified. Performing the docking of GRA2 and the other analogues in this position of the different models it was

possible to see a general improvement concerning the predicted affinity and an increased number of interactions.

Given the high homology between GPR21 and GPR52 (used as reference to define GPR21's binding site<sup>49</sup>) probably the differences observed in docking positions are not imputable to differences in the aminoacidic sequence but rather in the docked molecules. The work done on GPR52 was performed with an agonist whereas here inverse agonists are investigated.


Antagonistic molecules tend to be bigger than agonists, with more complex structures in order to efficiently compete with the physiological agonists, and in this receptor they tend to localize in a deeper portion of the receptor, tendency due to the possibility of establish a major number of interactions, with an increase in stability and decrease in free energy, in this portion.

As a further confirmation of the possibility, in the deeper portion of the binding pocket, to establish an even bigger number of interactions in this work different molecules were designed based on GRA2 and -160 structures. Increasing the presence of hydrophobic substituents in the lateral parts, a trend in increasing affinity was observed up to -12.9 of the best compound, being able to interact with both the higher and the deeper portions of the binding pocket.

A possible limit to the use of -160 is the identification of this compound as possible PAINS (Pan Assay INterference compounds) (*Baell J. et al., 2014*)<sup>54</sup> and presenting a structure similar to known colloidal aggregators (*McGovern SL et al., 2002*)<sup>55</sup> from a screening performed using Zinc15<sup>7</sup> online tools.

Being this just a summative screening in this work this compound was preliminarily tested given its supposed higher affinity for our target but, in order to continue the studies on this molecule, thorough dose-response curves, imperviousness to mild reductants and specificity versus counter-screening targets should be performed to assess the selectivity of this compound's activity<sup>56</sup>.

### 5.3 *In vitro* studies

The second part focused on two promising analogues of the lead compound GRA2: 

160 and 399.



From testing the toxicological aspects of these two molecules the first one, -160, confirmed the trend observed with the lead compound of cells suffering starting from the concentration of 100  $\mu$ M where not significant toxic effects were observed for the second one, -399.

Even if this first test indicated that -399 could represent a safer analogue, it should be noted that the described test only evaluated toxicity of these compounds on hepatic (cancer) cells and that toxicity at such high concentrations should not be relevant, because of the significantly lower concentrations for use of the drugs to be used *in vivo*.

To better assess the effects of these compounds on cells proliferation they should be tested in different cell types to reach a more comprehensive analysis.

The calcium release assay was performed on basal conditions of the HepG2 studied so the probe used detected the calcium released following the activation of all the constitutive active receptors, among them GPR21. The variations investigated with the administration of the compounds were minimal so a large number of cells per well were plated and a probe with high sensitivity was used, as a strategy to amplify the signal preserving its proportionality.

Reading such small variations was a complication and a limit of the screening performed and lead to difficulties in defining an appropriate protocol.

Even if the assay was repeated only for the minimum of times needed to confer representativity to the results, both the analogues not only showed a trend of reduction of the total amount of calcium released in the cells but they both reached better performances than GRA2 when used at the same concentration, a possible indication of higher potency.

Being noted that this was a preliminary test and it was only possible to define a trend of the activity of the compounds, the values obtained were consistent with the projections of affinity defined using the coordinates of the deeper portion of the binding pocket.

Furthermore compound -160 not only confirmed being the supposedly more potent analogue but nearly reached the significance threshold with just three experiments.

Another limit of this assay was the differences between the control/Triton X values deriving from the first two analyses and the last one, notably lower. We expected the control to

determine values close to a 50% of the maximum calcium release and lower values for the treatments, but this cell line showed notable resistance to the action of the Triton X. Only in the last analysis the concentration of Triton X used was higher and for longer period, determining values much closer to the expected ones. To the later adjustment of the protocol are imputable the high values of standard deviation and the notably high percentages of calcium release under the analysed condition versus the supposed maximum release.

It is worth noting that, even if the values of standard deviation of the readings, especially for GRA2 and -399, would require further measurements to be improved, this test was in this work used to screen the compounds in order to further investigate the more promising ones and that, for reasons of time and disposable material, additional readings were not possible.

Even if acknowledging the reported limits to the calcium assay the data described were sufficient not to exclude the compounds as potential more potent analogues of GRA2, especially -160.

The next step of the work was to define a model, or more than one, of insulin resistance in order to verify if those conditions could determine a variation of the GPR21 expression and then to test the compounds.

The establishment of insulin resistance conditions was related to the GPR21 expression and the insulin signalling pathway activation, nevertheless a glucose uptake assay was not performed and it could represent an interesting analysis to be conducted in future studies.

Of the two approaches tested by this research group only a 72 hours exposure to high glucose DMEM resulted in an significantly augmented GPR21 expression where the 24 hours treatment with high glucose and high insulin, reported in the present study, showed a trend towards a reduction of GPR21 levels.

Being GPR21 augmented expression supposedly a secondary adaptation mechanism in cells responding to an imbalanced glucose homeostasis, its reduction could be related to an ineffective approach in inducing insulin resistance. In order to assess if the insulin pathway was altered, despite the reduction in GPR21 expression, Ph-Akt levels were assessed as marker of this pathway's activation. The values deriving from the Ph-Akt evaluation after 24 hours

high insulin and high glucose versus a non-treated control showed a 25% increment suggesting a not-affected insulin pathway. The augmented phosphorylation of Akt observed is nevertheless consistent with the trend towards a decrement in GPR21 expression, here described when the same IR model was performed. This correlation could be a further confirmation of the detrimental role of GPR21 on the insulin signalling pathway.

A potential problem in assessing the degree of insulin pathway activation could be represented by the analysis of basal levels of activation, so the IR models were repeated adding a final 10 minutes chase with 100 nM insulin before the extraction as final booster to amplify the response. Furthermore to the cells where the IR models were induced, and the insulin chase performed, the activity of the compounds was tested to assess if they were able to restore the impaired pathway.

From this analysis, the 24 hours high glucose and high insulin model confirmed a not impaired insulin signalling pathway and the compounds had not relevant effects on the phosphorylation of its mediators.

Analyses conducted by this research group showed that even with the 72 hours high glucose exposure no reduction in phosphorylation of insulin pathway key mediators occurred. The latter observation seems to describe the 72 hours exposure to high glucose medium as a mere hyperglycaemic model rather than an IR one.

A protective and booster role on the activation of the insulin pathway was observed treating the cells exposed to 72 hours of high glucose with GRA2 and the analogues. Being that in this work and in the work of our team both the IR models showed no negative impact on the insulin pathway the only difference observed between the two models was the GPR21 expression. Starting from this consideration it could be hypothesized that an over expression of GPR21 occurs in borderline situations of pre-diabetes, in which the patients present higher glycaemia levels than normal but not yet belonging to a condition of overt diabetes. In this scenario the overexpression of GPR21 could facilitate the instauration of a more permanent state of insulin resistance, rendering the use of inverse agonists to this receptor potentially a relevant therapeutic tool to prevent the passage to a pre-diabetic condition to overt diabetes.

Regarding the effective potency of the compounds however further tests should be required to reach an eventual significance of the results, not achieved in this work because of technical limitations.

#### **5.4 Future studies**

Future studies could further investigate different aspects of this work to obtain a more comprehensive understating of GPR21 receptor and the best structure of inverse agonists to block its activity.

A good starting point could be to perform mutagenesis studies of the identified binding site<sup>57</sup> in order to evaluate if the inhibition is actually due to the interactions and binding pocket described in this work. This kind of studies should be able to definitely exclude a role of the side binding site as effective target of the compounds identified and to provide stronger basis to design and screen new compounds.

If the interactions identified were confirmed, the synthesis of the new compounds designed and reported in this work (*cf.* 4.2.6) could represents a valid tool in defining more affine and potent compounds.

Further studying compound -160, tests to exclude colloidal aggregation and PAIN behaviour should be performed such as thorough dose-response curves, imperviousness to mild reductants and specificity versus counter-screening targets.

As previously described, the 24 hours high glucose and high insulin model seems not to be sufficient to generate an insulin resistance in HepG2 cells appreciable at the signaling pathway level but it should be verified by performing a glucose uptake assay, more sensitive method than a western blot.

The evaluations regarding the signaling pathway and the influence of the compounds tested is only reported on Ph-Akt/Ph-GSK3 $\beta$  versus a structural protein but the analysis of the ratio of Ph-Akt/Ph-GSK3 $\beta$  levels versus total Akt ones could better describe the variations observed.

The evaluation of more affine compounds should also be investigated regarding macrophages migration and cytokines release following the most recent work on the matter<sup>38</sup>.

Noteworthy for further testing more potent compounds is also the correlation of GPR21 and CCR2 in expression and activity observed by *Riddy et al.*, suggesting GPR21's blockage as possible strategy in other diseases in which CCR2-driven inflammation is a cardinal feature.

To conclude, the discover of more affine inverse agonists to GPR21 could potentially not only represent a relevant therapeutic approach in treating pre-diabetic and diabetic patients but also lead to the acquisition of an additional tool in treating a wide range of inflammatory diseases.

## 6. BIBLIOGRAPHY

1. *International Diabetes Federation*:<https://www.idf.org/aboutdiabetes/what-is-diabetes/facts-figures.html>
2. *Sapra A, Bhandari P. Diabetes Mellitus. 2021 Sep 18. In: StatPearls [Internet]. Treasure Island (FL): StatPearls Publishing; 2022 Jan–. PMID: 31855345.*
3. *Cole JB, Florez JC. Genetics of diabetes mellitus and diabetes complications. Nat Rev Nephrol. 2020 Jul;16(7):377-390. doi: 10.1038/s41581-020-0278-5. Epub 2020 May 12. PMID: 32398868.*
4. *Riddy DM, Delerive P, Summers RJ, Sexton PM, Langmead CJ. G Protein-Coupled Receptors Targeting Insulin Resistance, Obesity, and Type 2 Diabetes Mellitus. Pharmacol Rev. 2018 Jan;70(1):39-67. doi: 10.1124/pr.117.014373. PMID: 29233848.*
5. *Osborn O, Oh DY, McNelis J, Sanchez-Alavez M, Talukdar S, Lu M, Li P, Thiede L, Morinaga H, Kim JJ, Heinrichsdorff J, Nalbandian S, Ofrecio JM, Scadeng M, Schenk S, Hadcock J, Bartfai T, Olefsky JM. G protein-coupled receptor 21 deletion improves insulin sensitivity in diet-induced obese mice. J Clin Invest. 2012 Jul;122(7):2444-53. doi: 10.1172/JCI61953. Epub 2012 Jun 1. PMID: 22653059; PMCID: PMC3386820.*
6. *Charles A. Stuart, Melanie P. McCurry, Anna Marino, Mark A. South, Mary E. A. Howell, Andrew S. Layne, Michael W. Ramsey, Michael H. Stone, Slow-Twitch Fiber Proportion in Skeletal Muscle Correlates With Insulin Responsiveness, The Journal of Clinical Endocrinology & Metabolism, Volume 98, Issue 5, 1 May 2013, Pages 2027–2036, <https://doi.org/10.1210/jc.2012-3876>*
7. *De Meyts P. The Insulin Receptor and Its Signal Transduction Network. 2016 Apr 27. In: Feingold KR, Anawalt B, Boyce A, Chrousos G, de Herder WW, Dhatariya K, Dungan K, Hershman JM, Hofland J, Kalra S, Kaltsas G, Koch C, Kopp P, Korbonits M, Kovacs CS, Kuohung W, Laferrère B, Levy M, McGee EA, McLachlan R, Morley JE, New M, Purnell J, Sahay R, Singer F, Sperling MA, Stratakis CA, Trencle DL, Wilson DP, editors. Endotext [Internet]. South Dartmouth (MA): MDText.com, Inc.; 2000–. PMID: 27512793.*
8. *Katzung B.G., Masters S.B., Trevor A.J., Farmacologia generale e clinica, IX Edition , Italian edition cured by Preziosi P., pages 835-836, 839*
9. *White MF. Insulin signaling in health and disease. Science. 2003 Dec 5;302(5651):1710-1. doi: 10.1126/science.1092952. PMID: 14657487.*
10. *Akhtar A, Sah SP. Insulin signaling pathway and related molecules: Role in neurodegeneration and Alzheimer's disease. Neurochem Int. 2020 May;135:104707. doi: 10.1016/j.neuint.2020.104707. Epub 2020 Feb 21. PMID: 32092326.*
11. *Miinea CP, Sano H, Kane S, Sano E, Fukuda M, Peränen J, Lane WS, Lienhard GE. AS160, the Akt substrate regulating GLUT4 translocation, has a functional Rab GTPase-activating protein domain. Biochem J. 2005 Oct 1;391(Pt 1):87-93. doi: 10.1042/BJ20050887. PMID: 15971998; PMCID: PMC1237142*

12. Moller DE. Potential role of TNF-alpha in the pathogenesis of insulin resistance and type 2 diabetes. *Trends Endocrinol Metab.* 2000 Aug;11(6):212-7. doi: 10.1016/s1043-2760(00)00272-1. PMID: 10878750
13. Leibowitz G, Cerasi E, Ketzinel-Gilad M. The role of mTOR in the adaptation and failure of beta-cells in type 2 diabetes. *Diabetes Obes Metab.* 2008 Nov;10 Suppl 4:157-69. doi: 10.1111/j.1463-1326.2008.00952.x. PMID: 18834443.
14. Qu CK. The SHP-2 tyrosine phosphatase: signaling mechanisms and biological functions. *Cell Res.* 2000 Dec;10(4):279-88. doi: 10.1038/sj.cr.7290055. PMID: 11191350.
15. Gardner J., et al. G-protein-coupled receptor GPR21 knockout mice display improved glucose tolerance and increased insulin response. *Biochem Biophys Res Commun.* 2012, 418, 1-5. PubMed ID: 22155242
- 16 Yang D, Zhou Q, Labroska V, Qin S, Darbalaei S, Wu Y, Yuliantie E, Xie L, Tao H, Cheng J, Liu Q, Zhao S, Shui W, Jiang Y, Wang MW. G protein-coupled receptors: structure- and function-based drug discovery. *Signal Transduct Target Ther.* 2021 Jan 8;6(1):7. doi: 10.1038/s41392-020-00435-w. PMID: 33414387; PMCID: PMC7790836
- 17 <https://www.nature.com/scitable/topicpage/gpcr-14047471/>
- 18 Hoque M, Ali S, Hoda M. Current status of G-protein coupled receptors as potential targets against type 2 diabetes mellitus. *Int J Biol Macromol.* 2018 Oct 15;118(Pt B):2237-2244. doi: 10.1016/j.ijbiomac.2018.07.091. Epub 2018 Jul 17. PMID: 30030074.
- 19 Barella LF, Jain S, Kimura T, Pydi SP. Metabolic roles of G protein-coupled receptor signaling in obesity and type 2 diabetes. *FEBS J.* 2021 Apr;288(8):2622-2644. doi: 10.1111/febs.15800. Epub 2021 Mar 22. PMID: 33682344.
- 20 Jean-Charles PY, Kaur S, Shenoy SK. G Protein-Coupled Receptor Signaling Through  $\beta$ -Arrestin-Dependent Mechanisms. *J Cardiovasc Pharmacol.* 2017 Sep;70(3):142-158. doi: 10.1097/FJC.0000000000000482. PMID: 28328745; PMCID: PMC5591062.
- 21 Ghislain J, Poitout V. Targeting lipid GPCRs to treat type 2 diabetes mellitus - progress and challenges. *Nat Rev Endocrinol.* 2021 Mar;17(3):162-175. doi: 10.1038/s41574-020-00459-w. Epub 2021 Jan 25. PMID: 33495605.
- 22 Li, J.H.; Jain, S.; McMillin, S.M.; Cui, Y.; Gautam, D.; Sakamoto, W.; Lu, H.; Jou, W.; McGuinness, O.P.; Gavrilova, O.; et al. A novel experimental strategy to assess the metabolic effects of selective activation of a G(q)-coupled receptor in hepatocytes in vivo. *Endocrinology* 2013, 154, 3539–3551
- 23 O'Dowd BF, Nguyen T, Jung BP, Marchese A, Cheng R, Heng HH, Kolakowski LF Jr, Lynch KR, George SR. Cloning and chromosomal mapping of four putative novel human G-protein-coupled receptor genes. *Gene.* 1997 Mar 10;187(1):75-81. doi: 10.1016/s0378-1119(96)00722-6. PMID: 9073069.
- 24 Kakarala KK, Jamil K. Sequence-structure based phylogeny of GPCR Class A Rhodopsin receptors. *Mol Phylogenet Evol.* 2014 May;74:66-96. doi: 10.1016/j.ympev.2014.01.022. Epub 2014 Feb 3. Erratum in: *Mol Phylogenet Evol.* 2014 Jul;76:293-7. PMID: 24503482.

- 25 Bresnick JN, Skynner HA, Chapman KL, Jack AD, Zamiara E, Negulescu P, Beaumont K, Patel S, McAllister G. Identification of signal transduction pathways used by orphan g protein-coupled receptors. *Assay Drug Dev Technol.* 2003 Apr;1(2):239-49. doi: 10.1089/15406580360545053. PMID: 15090189.
- 26 Xiao SH, Reagan JD, Lee PH, Fu A, Schwandner R, Zhao X, Knop J, Beckmann H, Young SW. High throughput screening for orphan and liganded GPCRs. *Comb Chem High Throughput Screen.* 2008 Mar;11(3):195-215. doi: 10.2174/138620708783877762. PMID: 18336213.
- 27 Leonard S., et al. Regulating the effects of GPR21, a novel target for type 2 diabetes. *Scientific Reports.* 2016, 6: 27002. PubMed ID: 27243589
- 28 Martin AL, Steurer MA, Aronstam RS. Constitutive Activity among Orphan Class-A G Protein Coupled Receptors. *PLoS One.* 2015 Sep 18;10(9):e0138463. doi: 10.1371/journal.pone.0138463. PMID: 26384023; PMCID: PMC4575141.
- 29 Alex White, Frédéric Jean-Alphonse, Fei Fang, Karina Pena, Shi Liu, et al.. G q/11 -dependent regulation of endosomal cAMP generation by parathyroid hormone class B GPCR. *Proceedings of the National Academy of Sciences of the United States of America , National Academy of Sciences, 2020, 117 (13), pp.7455-7460*
- 30 Lumeng CN, Saltiel AR. Inflammatory links between obesity and metabolic disease. *J Clin Invest.* 2011;121(6):2111–2117.
- 31 Olefsky JM, Glass CK. Macrophages, inflammation, and insulin resistance. *Annu Rev Physiol.* 2010;72:219-46. doi: 10.1146/annurev-physiol-021909-135846. PMID: 20148674.
- 32 Schenk S, Saberi M, Olefsky JM. Insulin sensitivity: modulation by nutrients and inflammation. *J Clin Invest.* 2008 Sep;118(9):2992-3002. doi: 10.1172/JCI34260. PMID: 18769626; PMCID: PMC2522344.
- 33 Wang J., et al. GPR21 KO mice demonstrate no resistance to high fat diet induced obesity or improved glucose tolerance. *F1000Research.* 2016, 5, 136-142. PubMed ID: 27081476
- 34 Samarelli AV, Ziegler T, Meves A, Fässler R, Böttcher RT. Rabgap1 promotes recycling of active  $\beta 1$  integrins to support effective cell migration. *J Cell Sci.* 2020 Sep 23;133(18):jcs243683. doi: 10.1242/jcs.243683. PMID: 32843574; PMCID: PMC7522031.
- 35 Brown E.J. (2003) Integrins of Macrophages and Macrophage-Like Cells. In: Gordon S. (eds) *The Macrophage as Therapeutic Target. Handbook of Experimental Pharmacology, vol 158.* Springer, Berlin, Heidelberg. [https://doi.org/10.1007/978-3-642-55742-2\\_7](https://doi.org/10.1007/978-3-642-55742-2_7)
- 36 Kinsella GK, Cannito S, Bordano V, Stephens JC, Rosa AC, Miglio G, Guaschino V, Iannaccone V, Findlay JBC, Benetti E. GPR21 Inhibition Increases Glucose-Uptake in HepG2 Cells. *Int J Mol Sci.* 2021 Oct 5;22(19):10784. doi: 10.3390/ijms221910784. PMID: 34639123; PMCID: PMC8509304
- 37 Seyer et al., Hepatic glucose sensing is required to preserve  $\beta$  cell glucose competence Published March 15, 2013 Citation Information: *J Clin Invest.* 2013;123(4):1662-1676. <https://doi.org/10.1172/JCI65538>.
- 38 Valentina Bordano, Gemma K. Kinsella, Stefania Cannito, Chiara Dianzani, Casimiro Luca Gigliotti, John C. Stephens, Chiara Monge, Claudia Bocca, Arianna C. Rosa, Gianluca Miglio, Umberto Dianzani, John



- B.C. Findlay, Elisa Benetti, *G protein-coupled receptor 21 in macrophages: An in vitro study*, *European Journal of Pharmacology*, 2022, 175018, ISSN 0014-2999, DOI: 10.1016/j.ejphar.2022.175018.
- 39 Riddy DM, Kammoun HL, Murphy AJ, Bosnyak-Gladovic S, De la Fuente Gonzalez R, Merlin J, Ziemann M, Fabb S, Pierce TL, Diepenhorst N, Rueda P, El-Osta A, Gautier JF, Venteclef N, Charman WN, Christopoulos A, Sexton PM, Summers RJ, Febbraio MA, Delerive P, Langmead CJ. Deletion of GPR21 improves glucose homeostasis and inhibits the CCL2-CCR2 axis by divergent mechanisms. *BMJ Open Diabetes Res Care*. 2021 Nov;9(2):e002285. doi: 10.1136/bmjdr-2021-002285. PMID: 34782333; PMCID: PMC8593704.
- 40 Hossain MS, Mineno K, Katafuchi T. Neuronal Orphan G-Protein Coupled Receptor Proteins Mediate Plasmalogens-Induced Activation of ERK and Akt Signaling. *PLoS One*. 2016 Mar 2;11(3):e0150846. doi: 10.1371/journal.pone.0150846. PMID: 26934370; PMCID: PMC4775022.
- 41 Romero-Nava, R., García, N., Aguayo-Cerón, K. A., Sánchez Muñoz, F., Huang, F., Hong, E., & Villafaña, S. (2020). Modifications in GPR21 and GPR82 genes expression as a consequence of metabolic syndrome etiology. *Journal of Receptors and Signal Transduction*. <https://doi.org/10.1080/10799893.2020.1784228>
- 42 ATCC (American Type Culture Collection), <https://www.atcc.org/products/hb-8065>
- 43 MTT Assay Protocol for Cell Viability and Proliferation, <https://www.sigmaaldrich.com/IT/it/technical-documents/protocol/cell-culture-and-cell-culture-analysis/cell-counting-and-health-analysis/cell-proliferation-kit-i-mtt>
- 44 <https://www.nature.com/scitable/definition/western-blot-288>
- 45 Cordero-Herrera I, Martín MÁ, Goya L, Ramos S. Cocoa flavonoids attenuate high glucose-induced insulin signalling blockade and modulate glucose uptake and production in human HepG2 cells. *Food Chem Toxicol*. 2014 Feb;64:10-9. doi: 10.1016/j.fct.2013.11.014. Epub 2013 Nov 19. PMID: 24262486.
- 46 Qun Huang, Lei Chen, Hui Teng, Hongbo Song, Xiaoqi Wu, Meiyu Xu, Phenolic compounds ameliorate the glucose uptake in HepG2 cells' insulin resistance via activating AMPK: Anti-diabetic effect of phenolic compounds in HepG2 cells, *Journal of Functional Foods*, Volume 19, Part A, 2015, Pages 487-494, ISSN 1756-4646, <https://doi.org/10.1016/j.jff.2015.09.020>.
- 47 Jumper, J et al. Highly accurate protein structure prediction with AlphaFold. *Nature* (2021).
- 48 Varadi, M et al. AlphaFold Protein Structure Database: massively expanding the structural coverage of protein-sequence space with high-accuracy models. *Nucleic Acids Research* (2021).
- 49 Lin, X., Li, M., Wang, N. et al. Structural basis of ligand recognition and self-activation of orphan GPR52. *Nature* 579, 152–157 (2020). <https://doi.org/10.1038/s41586-020-2019-0>
- 50 Daina, A., Michielin, O. & Zoete, V. SwissADME: a free web tool to evaluate pharmacokinetics, drug-likeness and medicinal chemistry friendliness of small molecules. *Sci Rep* 7, 42717 (2017). <https://doi.org/10.1038/srep42717>

51 Waldman SA. Does potency predict clinical efficacy? Illustration through an antihistamine model. *Ann Allergy Asthma Immunol.* 2002 Jul;89(1):7-11; quiz 11-2, 77. doi: 10.1016/S1081-1206(10)61904-7. PMID: 12141724.

52 Sefried, S.; Haring, H.U.; Weigert, C.; Eckstein, S.S. Suitability of hepatocyte cell lines HepG2, AML12 and THLE-2 for investigation of insulin signalling and hepatokine gene expression. *Open Biol.* 2018, 8.

53 Gautam D, Han SJ, Duttaroy A, Mears D, Hamdan FF, Li JH, Cui Y, Jeon J, Wess J. Role of the M3 muscarinic acetylcholine receptor in beta-cell function and glucose homeostasis. *Diabetes Obes Metab.* 2007 Nov;9 Suppl 2:158-69. doi: 10.1111/j.1463-1326.2007.00781.x. PMID: 17919190.

54 Baell, J.; Walters, M. A. Chemistry: Chemical con artists foil drug discovery. *Nature* 2014, 513, 481–483.

55 McGovern, S. L.; Caselli, E.; Grigorieff, N.; Shoichet, B. K. A common mechanism underlying promiscuous inhibitors from virtual and high-throughput screening. *J. Med. Chem.* 2002, 45, 1712–1722

56 ACS Cent. Sci. 2017, 3, 3, 143–147, Publication Date:February 28, 2017, <https://doi.org/10.1021/acscentsci.7b00069>

57 Conner A.C., Barwell J., Poyner D.R., Wheatley M. (2011) The Use of Site-Directed Mutagenesis to Study GPCRs. In: Willars G., Challiss R. (eds) Receptor Signal Transduction Protocols. Methods in Molecular Biology (Methods and Protocols), vol 746. Humana Press, Totowa, NJ. [https://doi.org/10.1007/978-1-61779-126-0\\_5](https://doi.org/10.1007/978-1-61779-126-0_5)

## IMAGES

<b>Figure 1</b> Glycaemia values of reference in healthy subjects and diabetic patients ( <a href="https://www.insider.com/normal-blood-sugar-levels">https://www.insider.com/normal-blood-sugar-levels</a> ) .....	1
<b>Figure 2</b> Cytokines and free fatty acids molecular pathway associated to insulin resistance onset (Feng et al. “The Role of JNK Signaling Pathway in Obesity-Driven Insulin Resistance”. <i>Diabetes Metab Syndr Obes.</i> 2020;13:1399-1406 .....	3
<b>Figure 3</b> Insulin signalling pathway ( <a href="https://www.tocris.com/pathways/insulin-signaling-pathway">https://www.tocris.com/pathways/insulin-signaling-pathway</a> ).....	4
<b>Figure 4</b> GPCRs associated G-proteins subunits and the different pathways activated by the alpha-subunits (Jo, M. Jung, S. Engineering therapeutic antibodies targeting G-protein–coupled receptors. <i>Exp Mol Med</i> 48, e207, 2016) .....	11
<b>Figure 5</b> Multifaceted functions of beta-arrestins: desensitization, endocytosis and signalling (S.K.Shenoy et al., REVIEW  VOLUME 32, ISSUE 9, P521-533, SEPTEMBER 01, 2011“β-arrestin-mediated receptor trafficking and signal transduction”, Published:June 15, 2011 ..	12
<b>Figure 6</b> GPR21 signalling pathway activation when coupled with different types of alpha subunits (Xiao et al., High throughput screening for orphan and liganded GPCRs. <i>Comb Chem High Throughput Screen.</i> 2008 Mar;11(3):195-215) .....	15
<b>Figure 7</b> GPCRs comparison for constitutive activity assessment vs control (Martin AL et al., Constitutive Activity among Orphan Class-A G Protein Coupled Receptors. <i>PLoS One.</i> 2015 Sep 18) .....	16

<b>Figure 8</b> GPR21 signalling pathway: PLC activation, calcium release and IRS1 inactivation (Leonard S., et al. Regulating the effects of GPR21, a novel target for type 2 diabetes. Scientific Reports. 2016, 6: 27002. PubMed ID: 27243589).....	16
<b>Figure 9</b> Bürker chamber.....	26
<b>Figure 10</b> Secondary antibody coupled with horseradish peroxidase and luminol oxidation (Characterization of potential modulators of the intestinal peptide transporter PEPT1 in Caenorhabditis elegans and human colon carcinoma cells - Scientific Figure on ResearchGate).....	32
<b>Figure 11</b> Schematic refiguration of the plate used to assess the method and the basal conditions of the calcium release assay.....	35
<b>Figure 12</b> Insulin concentration and glucose uptake in HepG2 cells (Huang et al., Phenolic compounds ameliorate the glucose uptake in HepG2 cells' insulin resistance via activating AMPK: Anti-diabetic effect of phenolic compounds in HepG2 cells, Journal of Functional Foods, Volume 19, Part A, 2015, Pages 487-494) .....	38
<b>Figure 13</b> GPRs 20,21,22 and 23 FASTA sequences alignment and transmembrane segments identification (B.F. O'Dowd et al. Gene 187 (1997) 75-91) .....	42
<b>Figure 14</b> Resumptive table the template used to create a GPR21 tridimensional model and their main parameters .....	43
<b>Figure 15</b> Model-5mzj .....	43
<b>Figure 16</b> Model-4gbr .....	44
<b>Figure 17</b> Model-5zhp .....	44
<b>Figure 18</b> Table of GPR21 models evaluation .....	45
<b>Figure 19</b> Multiple alignment: GPR21, model-mzj, model-5zhp, model-4gbr, 5zhp, 4gbr and 5mzj (performed using Clustalw online tools: <a href="https://www.genome.jp/tools-bin/clustalw">https://www.genome.jp/tools-bin/clustalw</a> ) .	45
<b>Figure 20</b> Model-5mzj and model-AlphaFold structures alignment; affinity of 1.39.....	46
<b>Figure 21</b> Model-5zhp and model-2014 structures alignment; affinity of 1.27 .....	46
<b>Figure 22</b> Amminoacids responsible for c17, a surrogate agonist, docking in GPR52 (X. Lin et al., Structural basis of ligand recognition and self-activation of orphan GPR52. Nature 579, 152–157 (2020) .....	47
<b>Figure 23</b> Alignment between GPR52 and GPR21 with the identification of main secondary and tertiary structure features (X. Lin et al., Structural basis of ligand recognition and self-activation of orphan GPR52. Nature 579, 152–157 (2020) .....	47
<b>Figure 24</b> GRA2 and analogues ADME analysis summary table.....	50
<b>Figure 25</b> GRA2 docked in model-2014; grid: -7.91, -9.44 and 17.6. ....	50
<b>Figure 26</b> GRA2 docked in model-5mzj; grid: -25.28, 9.51 and 13.74.....	50
<b>Figure 27</b> Model-5mzj's binding pocket defined with PrankWeb.....	51
<b>Figure 28</b> First model-2014 binding site identified with PrakWeb.....	51
<b>Figure 29</b> Schematic representation of fig. 28 binding pocket on GPR21 sequence .....	52
<b>Figure 30</b> Schematic representation of fig. 31 binding pocket on GPR21 sequence .....	52
<b>Figure 31</b> Second model-2014 binding site identified with PrakWeb.....	52
<b>Figure 32</b> Analysis of the interactions occurring in the binding of GRA2 in model-5mzj.....	53
<b>Figure 33</b> Analysis of the interactions occurring in the binding of GRA2 in model-2014 .....	53
<b>Figure 34</b> Binding of GRA2 in model-2014; grid -5.45, -9.0 and 17.57.....	53
<b>Figure 35</b> Analysis of the interactions occurring in the binding of GRA2 in model-2014; grid - 5.45, -9.0 and 17.57 .....	54
<b>Figure 36</b> Binding of GRA2 in model-5zhp .....	54
<b>Figure 37</b> Analysis of the interactions occurring in the binding of GRA2 in model-5zhp.....	54

<b>Figure 38</b> Table of the affinity values and interactions of GRA2 and analogues in model-2014 .....	55
<b>Figure 39</b> Superimposed dockings of -160 and GRA2 in model-2014 .....	56
<b>Figure 40</b> Different positions of GRA2 in model-2014's binding pocket.....	56
<b>Figure 41</b> Resumptive table of the affinity values of GRA2 and analogues in model-2014 using the new coordinates.....	56
<b>Figure 42</b> Resumptive table of the affinity values of GRA2 and analogues in model-5zhp using the new coordinates .....	57
<b>Figure 43</b> Resumptive table of the affinity values of GRA2 and analogues in model-2014 using the new coordinates.....	58
<b>Figure 44</b> Analysis of the interactions occurring in the binding of the hypothesised compound1 in model-2014.....	59
<b>Figure 45</b> Analysis of the interactions occurring in the binding of the hypothesised compound2 in model-2014.....	59
<b>Figure 46</b> Absorbance values of the MTT test performed after the administration of -160 and -399, on HepG2 cells under basal conditions, related to a non-treated control: the concentration of 100 $\mu$ M of -160 appears to be significantly toxic. **= $P < 0.01$ vs control.....	61
<b>Figure 47</b> Resumptive table of the percentages of compound/triton (A), control/triton (B) and A/B deriving from the calcium release assay for -160 and -399 .....	62
<b>Figure 48</b> Graphic representation of the reduction in calcium release following administration of -160 vs control.....	63
<b>Figure 49</b> Graphic representation of the reduction in calcium release following administration of -399 vs control.....	63
<b>Figure 50</b> Table of the statistical analysis of the results deriving from the calcium release assay using -160 and -399 .....	63
<b>Figure 51</b> Graphic transposition of fig. 47 (-160) .....	63
<b>Figure 52</b> Graphic transposition of fig. 47 (-399) .....	63
<b>Figure 53</b> Resumptive table of the percentages of compound/triton (A), control/triton (B) and A/B deriving from the calcium release assay for GRA2.....	64
<b>Figure 54</b> Graphic representation of the reduction in calcium release following administration of GRA2 vs control .....	64
<b>Figure 55</b> Graphic transposition of fig. 53.....	64
<b>Figure 56</b> Table of the statistical analysis of the results deriving from the calcium release assay using GRA2.....	65
<b>Figure 57</b> Western blot results for GPR21 and tubulin CL, CH, LI and HI .....	66
<b>Figure 58</b> Resumptive table of the percentages of the variation in GPR21 expression after 24 hours exposure to high glucose (CH), 100nM insulin (LI) and high glucose with 100nM insulin (HI).....	66
<b>Figure 59</b> Graphic transposition of fig. 58.....	66
<b>Figure 60</b> Western blot results for Ph-Akt and tubulin CL, CH, LI and HI .....	67
<b>Figure 61</b> Resumptive table of the mean percentages of the variation in Akt phosphorylation with different treatments (CH, LI and HI) versus CL control .....	67
<b>Figure 62</b> Graphic transposition of fig. 61.....	67
<b>Figure 63</b> Western blot results for Ph-GSK3 $\beta$ and tubulin HI and HI with 160, 399 and GRA2 administration.....	69
<b>Figure 64</b> Resumptive table of the mean values (n=2) of the variation in GSK3 $\beta$ phosphorylation with different treatments (160, 399 and GRA2) versus HI control after 24 hours high glucose and high insulin exposure .....	69

<b>Figure 65</b> Graphic transposition of fig. 64.....	69
<b>Figure 66</b> Western blot results for Ph-GSK3 $\beta$ and tubulin CH and CH with 160, 399 and GRA2 administration.....	70
<b>Figure 67</b> Resumptive table of the mean values (n=2) of the variation in GSK3 $\beta$ phosphorylation with different treatments (160, 399 and GRA2) versus CH control after 72 hours high glucose DMEM exposure.....	70
<b>Figure 68</b> Graphic transposition of figure 67 .....	70

## SITOGRAPHY

- α) <https://swissmodel.expasy.org/interactive>*
- β) <https://saves.mbi.ucla.edu>*
- γ) <https://www.schrodinger.com/products/maestro>*
- δ) <https://pymol.org/2/>*
- ε) <https://mcule.com/apps/1-click-docking/>*
- ζ) <https://prankweb.cz>*
- η) <http://zinc15.docking.org/patterns/home>*